Regional Three-Dimensional Deformation of Healthy and Tendinopathic Human Achilles Tendon During Isometric Plantarflexion Contraction

Author

Nuri, Leila

Published

2017

Thesis Type

Thesis (PhD Doctorate)

School

School of Allied Health

DOI

10.25904/1912/1954

Regional three-dimensional deformation of healthy and tendinopathic human Achilles tendon during isometric plantarflexion contraction

Leila Nuri

B.Sc. (*Hons, Physiotherapy*), M.Sc. (*Sport Physiotherapy*)

School of Allied Health Sciences

Menzies Health Institute Queensland, Griffith University

Submitted in fulfilment of the requirements of the degree of Doctor of Philosophy

March 2017

Abstract

Understanding how healthy and tendinopathic human Achilles tendon (AT) deforms at the regional level in three-dimensional (3D) space under load could provide better insight into *in vivo* AT mechanobiology, physiology, recovery, pathophysiology, injury, and function. This thesis investigated the 3D morphology of the healthy and tendinopathic human AT at the level of whole AT (e.g., gastrocnemius muscle-tendon junction (MTJ) to calcaneus), free AT (e.g., soleus MTJ to calcaneus), and proximal AT (e.g., gastrocnemius MTJ to soleus MTJ) under load using freehand 3D ultrasound.

In studies 1 and 2, the regional 3D deformation of healthy AT was investigated during and immediately following 10 successive 25-second (s) plantarflexion contractions at 50% maximal voluntary isometric contraction (MVIC), and at 5 further time points [15, 30, 60, 90, and 120 minutes (min)] during recovery. The longitudinal creep response of whole AT during repeated loading was found to be primarily driven from free AT and was accompanied by a corresponding transverse creep response of free AT that was most pronounced within the mid-portion. Further, the longitudinal and transverse creep of AT reached steady state simultaneously following three contractions. During recovery, the whole and free AT longitudinal strains and the free AT transverse strain remained at the steady state for 60 min and achieved full recovery after 2 hours (h). The finding that AT creep response is more pronounced at the level of free AT mid-portion further highlights the vulnerable nature of this region of AT to the exercise-induced tendon creep or early stage mechanical fatigue effects and may explain why free AT mid-portion is more susceptible to strain-related injuries (e.g., tendinopathy and rupture) when it is subjected to the repeated loads. Further, the time-frame in which the whole and free AT longitudinal

strains and the free AT transverse strain could be achieved without large confounding effects of creep recovery is approximately 60 min and should be considered when conducting *in vivo* AT mechanical testing.

In studies 3 and 4, the regional 3D morphology of AT at rest, during a single tensile load (plantarflexion contraction at 50% MVIC), and during repeated loads (10 successive 25-s plantarflexion contractions at 50% MVIC) in individuals with unilateral mid-portion Achilles tendinopathy (MAT) and healthy control matched tendons was investigated. At rest, MAT was associated with larger resting tendon cross-sectional area (CSA) than healthy control tendons throughout the entire tendon length, which was mainly driven by a greater tendon antero-posterior (AP) diameter. During application of a single load, the MAT experienced a reduction in tendon CSA, AP diameter, and medio-lateral (ML) diameter, and volume. In contrast, the healthy control tendon remained iso-volumetric and experienced a reduction in tendon CSA and ML diameter and an increase in tendon AP diameter. Further, the MAT experienced greater longitudinal and transverse strains than healthy control tendon across all the tendon regions. During repeated loading, the whole and free AT longitudinal strains and free AT CSA and volume strains experienced a greater magnitude of creep and reached steady state following a greater number of contractions in MAT (five contractions) compared to control tendon (three contractions). Further, the MAT experienced a substantial CSA and volume reduction from the onset of loading, which preceded a pronounced longitudinal strain response of the whole and free AT. These findings suggest that MAT alters the magnitude of whole and free AT longitudinal strains, the magnitude and direction of free AT transverse strain, and the magnitude of free AT volume change compared to healthy control tendons during a single

load and repeated loads. This observation is indicative of fundamental alterations in the normal solid-fluid interactions and local mechanical environment in MAT, which likely compromise the ability of MAT to support external loading and have possible implications for injury risk, tendon repair and rehabilitation in MAT.

Acknowledgements

I'm writing my fourth thesis after 11 years of heavy academic studies: 4 years and 6 months Bachelor's Degree (Patellofemoral pain syndrome), 3 years Master's Degree (two thesis including Ankle sprain and Physiotherapy in diabetes), and 3 years and 6 months Ph.D. (Achilles tendinopathy). Eleven Years!!! I feel like I've been living in different schools and universities all of my life.

First of all, I would like to thank my Mom (S.Movarekh), Dad (M.Nuri), and my two sisters (Fatemeh and Soghra) for encouraging and supporting me through my many times of stress, excitement, frustration, and celebration. I wouldn't be here without you.

Special note to my Dad: I've missed the following words for 11 years throughout my academic studies (Dad, 4am, Home, Running, -25°C, Breakfast, Kitchen, Persian tea, Singing for Leila, Dad: Judgement, Justice, Court, Public Speaking, Today, this case will be….., Dad: Organized, Law, Law, Law, and again Law, Dad: How much I miss talking about law with you, Dad: Everything to me).

I would like to express my deepest gratitude to my Ph.D. supervisors **Professor Rod Barrett, Dr Richard Newsham-West, and Dr Steven Obst** for their constant guidance, encouragement, unwavering support, and mentorship throughout this project.

Special note to Rod: I will miss the following words for the rest of my life (Rod, Rod=My Ph.D., Rod: Matlab, Rod: Graphs and Figures, Rod: Manuscripts, Rod: Revisions, Rod: I'm stressed, Rod: What should I do now? I don't have anything to do, I finished, Rod: Kindness, Rod: My supervisor).

Special note to Richard: Richard can you remember the first day I came to Griffith I couldn't understand your accent? Now, I can Richard. Thanks for accepting me as your student and giving me the opportunity to do my Ph.D. in Griffith University. It has been my honor to be your student.

I would also like to extend my thanks to those who offered guidance and support in my Ph.D: Ali Moeini (Thanks for supporting me through Skype), Josephine Carreon (Thanks for making Australia like home for me), Nina Hopmeier (Thanks for the support), Guillermo Jacuinde (Memo, without you, I couldn't have collected any data), and my officemates: David Lee, Pavan Teja Devanaboyina, Nagarajan Manickaraj, and Vijey Palaniswamy.

Statement of Originality

This work has not previously been submitted for a degree or diploma in any university. To the best of my knowledge and belief, the thesis contains no material previously published or written by another person except where due reference is made in the thesis itself.

Leila Nuri, 10/03/2017

Table of Contents

List of Figures

List of Tables

List of Abbreviations

ADC	Apparent diffusion coefficient
AP	Antero-posterior
AT	Achilles tendon
B-mode	Brightness mode
Cal	Calcaneus
CSA	Cross-sectional area
CV	Coefficient of variation
EMG	Electromyography
GAG	Glycosaminoglycan
ICC	Intraclass Correlation Coefficient
LG	Lateral Gastrocnemius
MAT	Mid-portion Achilles tendinopathy
MG	Medial Gastrocnemius
ML	Medio-lateral
MRI	Magnetic Resonance Imaging
MTJ	Muscle-tendon junction
MVIC	Maximal voluntary isometric contraction
RMS	Root mean square
SEM	Standard error of mean
SD	Standard deviation
SOL	Soleus
TA	Tibialis anterior
TS	Triceps surae
VAS	Visual analogue scale
VISA-A	Victorian Institute of Sports Assessment-Achilles tendon

3D	Three-dimensional
2D	Two-dimensional
3DUS	Three dimensional ultrasound
2DUS	Two dimensional ultrasound

List of Original Articles

Chapter 3-6 of this thesis are based on published or submitted co-authored papers. My contribution to each co-authored paper is outlined at the beginning of each relevant chapter. The bibliographic details for each paper are as follows:

Chapter 3

Nuri, L., Obst, S., Newsham-West, R. and Barrett, R. (2016). Regional three-dimensional deformation of human Achilles tendon during conditioning. *Scandinavian Journal of Medicine & Science in Sports*. DOI: 10.1111/sms.12742.

Chapter 4

Nuri, L., Obst, S., Newsham-West, R. and Barrett, R. (2017). Recovery of human Achilles tendon three-dimensional deformation following conditioning. (Under Review).

Chapter 5

Nuri, L., Obst, S., Newsham-West, R. and Barrett, R. (2017). Three-dimensional morphology and volume of the free Achilles tendon at rest and under load in people with unilateral mid-portion Achilles tendinopathy. (Under Review).

Chapter 6

Nuri, L., Obst, S., Newsham-West, R. and Barrett, R. (2017). The tendinopathic Achilles tendon does not remain iso-volumetric upon repeated loading: insights from 3D ultrasound". *Journal of Experimental Biology*. DOI: 10.1242/jeb.159764.

List of Conference Presentations

Nominated for the New Investigator Award in five conferences

10th Australasian Biomechanics Conferences, The University of Melbourne, Woodward Conference Centre, Melbourne, Australia, 4th-6th December, 2016. Three dimensional morphology of the Achilles tendon at rest and under load in people with unilateral mid-portion Achilles tendinopathy. **Nuri L,** Obst S, Newsham-West R, Barrett R. **Podium.**

Sport Medicine Australia Conference, Melbourne Cricket Ground, Melbourne, Australia, 12th-15th October, 2016. Three dimensional morphology of the Achilles tendon at rest and under load in people with unilateral mid-portion Achilles tendinopathy**. Nuri L,** Obst S, Newsham-West R, Barrett R**. Podium.**

Sport Medicine Australia Conference, Gold Coast, Queensland, Australia, 21th -24th October, 2015. Achilles tendon is not a single elastic structure. **Nuri L**, Obst S, Newsham-West R, Barrett R. **Podium.**

Gold Coast Health and Medical Research Conference, Mercure Resort Gold Coast, Australia, 4th-5th December, 2015. Achilles tendon mechanical properties during preconditioning. **Nuri L**, Newsham-West R, Barrett R. **Podium.**

Gold Coast Health and Medical Research Conference, Mercure Resort Gold Coast, Australia, 4th-5th December, 2014. Acute effect of exercise on Achilles tendon strain: a systematic review. **Nuri L**, Newsham-West R, Barrett R. **Podium.**

Student conferences

HMNS Postgraduate Student Conference, Stradbroke Island, Brisbane, Australia, 8th-10th April, 2015. Preconditioning of Achilles tendon. **Nuri L,** Newsham-West R, Barrett R. **Podium.**

Sensorimotor Control Meeting, The University of Queensland, Brisbane, Australia, 20th-21st February, 2015. **Attendee.**

Tendon research Australia and New Zeland (TRANZ meeting), Griffith University, Gold Coast, 8th-9th December 2014. **Attendee.**

Awards

2016 Sport Medicine Australia Conference, **John Sutton Award for Best New Investigator (Exercise and Sports Science)**, Three dimensional morphology of the Achilles tendon at rest and under load in people with unilateral mid-portion Achilles tendinopathy, Melbourne Cricket Ground, Melbourne, Australia, 12th-15th October, 2016.

Best Three-Minute Thesis Presentation Award, Centre for Musculoskeletal Research (CMR), Sharks Events Centre, Gold Coast, Australia, 15th December, 2014.

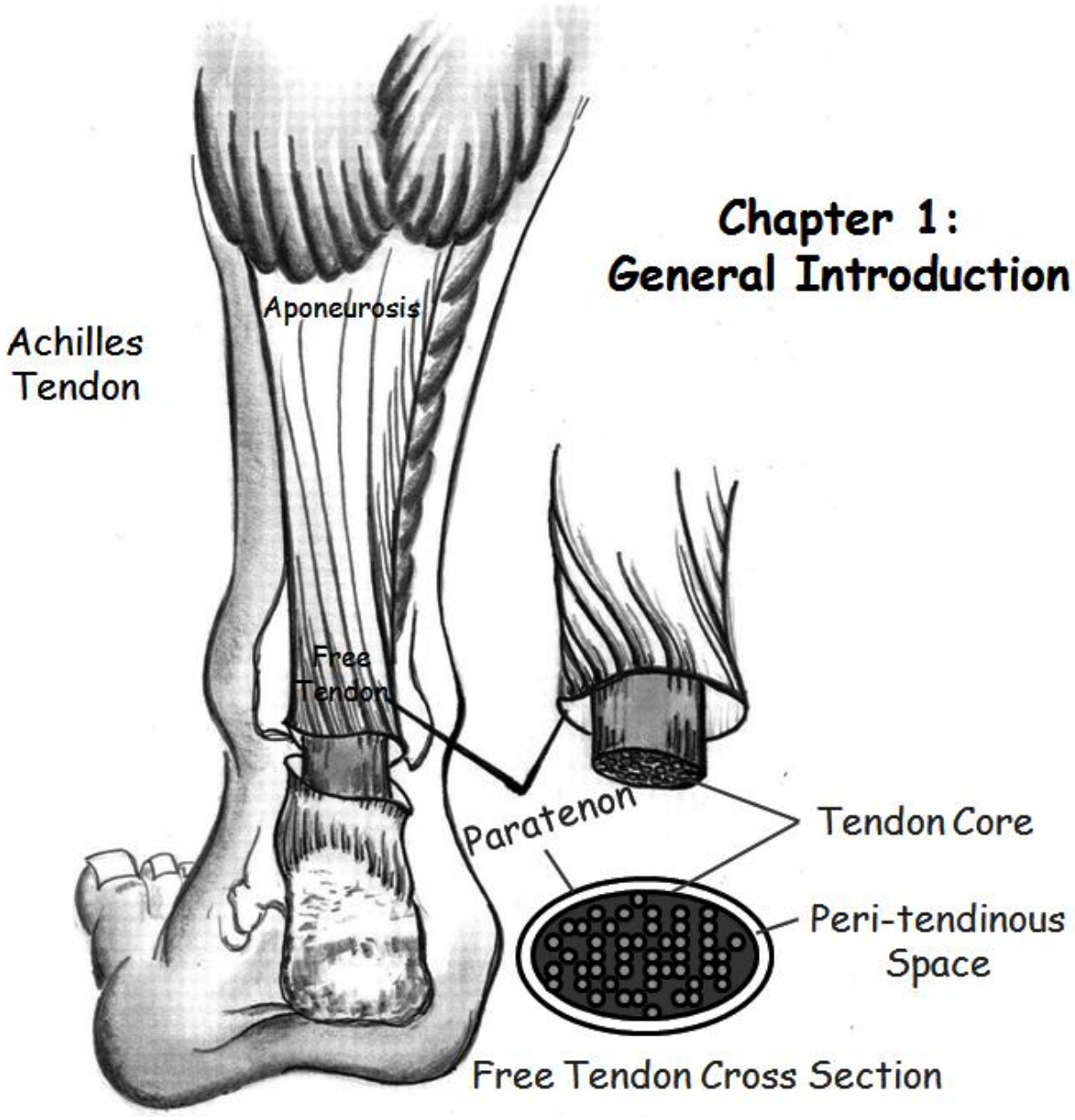
Chapter 1:
General Introduction
Achilles
Tendon
Aponeurosis
Free
Tendon
Paratenon
Tendon Core
Peri-tendinous
Space
Free Tendon Cross Section

Chapter 1. General Introduction

1.1 General Background

1.1.1 Achilles tendon structure and function

The human Achilles tendon (AT) is the conjoint tendon of the gastrocnemius and soleus muscles (i.e., triceps surae muscles) and is known as the strongest and largest tendon in the body (Doral et al., 2010; Pierre-Jerome et al., 2010). The AT plays an important role in force transmission and energy storage and return during functional activities such as walking and running and improves the economy and performance of motion by reducing muscle work and allowing muscle fascicles to act at lengths and speeds more favourable for power production (Lichtwark et al., 2007; Lichtwark and Wilson, 2006). The human AT is frequently subjected to appreciable loads during locomotion such as running (Komi et al., 1992), walking (Giddings et al., 2000), counter movement jump (Fukashiro et al., 1995), and hopping (Lichtwark and Wilson, 2007) despite exhibiting the strain rate sensitivity and material properties similar to other tendons (Ker et al., 1988; Wren et al., 2001). Structurally, the whole AT [e.g., gastrocnemius muscle-tendon junction (MTJ) to calcaneus] is comprised of two distinct parts, including the proximal AT (e.g., gastrocnemius MTJ to soleus MTJ) and free AT (e.g., soleus MTJ to calcaneus). Previous *in vivo* studies have demonstrated that the free AT strains more than the proximal AT in the longitudinal direction during the same tensile load both before (Farris et al., 2013a; Finni et al., 2003; Magnusson et al., 2003) and after fatigue exercise (Lichtwark et al., 2013a; Obst et al., 2015a). This indicates that the AT aponeurotic sheath and free tendon may have different mechanical demands and functional roles during force transmission *in*

vivo and highlights the vulnerable nature of the free AT to the exercise-induced tendon creep or early stage mechanical fatigue effects, a property that predispose the free tendon to strain-related injuries.

1.1.2 Three-dimensional morphology of the healthy AT at rest and under load

The healthy free AT three-dimensional (3D) morphology at rest and during tensile loading has been well characterized in previous *in vivo* studies. It has been demonstrated that free tendon has a variable cross-sectional area (CSA) (Magnusson and Kjaer, 2003; Muraoka et al., 2005; Obst et al., 2015b; Obst et al., 2014b), antero-posterior (AP) diameter (Fredberg et al., 2008; Leung and Griffith, 2008; O'Reilly and Massouh, 1993; Obst et al., 2015b; Obst et al., 2014b), and medio-lateral (ML) diameter (Gatt et al., 2015; Iwanuma et al., 2011; Obst et al., 2015b; Obst et al., 2014b) along its length, with the minimum free AT CSA reported to be at around 50-70% of the tendon length (Obst et al., 2014b). This suggests that the stress (i.e., force/CSA) experienced by tendon during load may vary between different regions of free AT. During tensile loading, it has been shown that free AT undergoes a longitudinal strain (Farris et al., 2013a; Finni et al., 2003; Iwanuma et al., 2011; Lichtwark et al., 2013a; Magnusson et al., 2003; Obst et al., 2015a; Obst et al., 2014b) that is coupled to a corresponding reduction in tendon CSA (Obst et al., 2015b; Obst et al., 2014b; Reeves and Cooper, 2014), a reduction in tendon ML diameter (Iwanuma et al., 2011; Obst et al., 2015b; Obst et al., 2014b), and an increase in tendon AP diameter (Obst et al., 2015b; Obst et al., 2014b) throughout the entire tendon length, with the tendon volume remaining unaltered (Iwanuma et al., 2011; Nuri et al., 2016; Obst et al., 2015b; Obst et al., 2014b). The relationship between the longitudinal and transverse

morphologies of the healthy free AT during load is suggestive of fundamental reorganization of the tendon collagen fascicles and fibers (Obst et al., 2014b). Furthermore, the load-induced alterations in free tendon transverse morphology (i.e., CSA, AP diameter, and ML diameter) have been shown to be region-specific along the tendon length, with the tendon mid-portion undergoing greater transverse strain relative to the proximal and distal portions (Iwanuma et al., 2011; Obst et al., 2015b; Obst et al., 2014b; Reeves and Cooper, 2014).

1.1.3 Conditioning of tendon

Tendons, like most other biological tissues, exhibit time- and history-dependent viscoelastic behavior during mechanical testing. For example when tendons are exposed to cyclic tensile loading after a period of unloading, they experience a gradual increase in length (i.e., creep) and/or a loss of tension (i.e., stress relaxation) for the same level of tensile load until a point of steady state mechanical behavior is reached (Elliott et al., 2003; Fung, 2013). Conditioning is a process whereby successive standardized sub-failure loading is applied to the tendon in order to minimize the effect of tendon time- and history-dependent viscoelastic properties and thus establishes consistent and repeatable mechanical results (Carew et al., 2000; Graf et al., 1994; Hawkins et al., 2009; Hosseini et al., 2014; Maganaris, 2003; Schatzmann et al., 1998; Sopakayang, 2013). Although the underlying mechanism accounting for the conditioning effect of tendon is not completely understood, it is likely related to the progressive microstructural changes such as collagen fibre recruitment, re-alignment, un-crimping, sliding, and interstitial fluid movement during conditioning (Hosseini et al., 2014; Houssen et al., 2011; Miller et al., 2012a; Miller et al.,

2012b; Quinn and Winkelstein, 2011; Schatzmann et al., 1998; Thorpe et al., 2014). Tendon conditioning has the potential to be a source of variability during *in vivo* measurement of tendon mechanical properties such as strain, stiffness, Young's modulus and hysteresis if steady-state behavior of the tendon is yet to be reached prior to testing. Conditioning of the tendon is therefore recognised as an important countermeasure against the confounding effects of time- and history-dependent tendon viscoelastic properties prior to mechanical testing (Lichtwark et al., 2013a; Obst et al., 2015a; Seynnes et al., 2015).

1.1.4 Conditioning of healthy Achilles tendon

Our understanding of healthy human AT conditioning is limited to two-dimensional (2D) measures of whole AT longitudinal elongation and strain. For example, Maganaris (2003) examined the effect of 10 × 4-s isometric plantarflexion contractions at 80% maximum voluntary isometric contraction (MVIC) on whole AT longitudinal elongation using 2D ultrasound. The loading protocol caused tendon elongation to increase by 5 mm from the first contraction to the tenth contraction, with no significant changes in tendon length obtained after the fifth contraction. Similarly, Hawkins et al. (2009) investigated the effect of 7-min of cyclic isometric ankle plantarflexion contractions (315 cycles) at 25-35% of MVIC on whole AT longitudinal strain using 2D ultrasound. Whole AT longitudinal strain experienced a total dynamic creep of 3% and reached steady state after 270 loading cycles. It was recommended that a minimum of 270 loading cycles or a 6-min warm-up is required for the whole AT to reach a relatively steady state behavior. Because the longitudinal strain of whole AT varies between the proximal AT and free AT during load and the free AT longitudinal deformation is accompanied by a corresponding region-specific alteration in

tendon transverse morphology, the whole AT conditioning effects may not reflect the 3D deformation of AT at the regional level. Therefore, further study is warranted to evaluate the regional 3D deformation of healthy human AT during conditioning.

1.1.5 Recovery of the Achilles tendon following conditioning

Conditioning effects on tendon mechanical and morphological properties are non-damaging, transient, and recoverable (Fung, 2013; Graf et al., 1994; McPherson et al., 1992; O'Brien et al., 1989; Thorpe et al., 2014). Understanding the time course of tendon recovery following conditioning is crucial for understanding the unloaded tendon mechanics, tendon behavior in response to subsequent mechanical loads, and the design of optimal tendon load-rest periods in activities that expose the tendon to cyclic and repeated tensile loadings. The time course of recovery of human AT thickness, volume and hydration state, and structural integrity following fatiguing exercise has been reported in previous *in vivo* studies (Grigg et al., 2009; Grigg et al., 2012; Grosse et al., 2015; Rosengarten et al., 2014; Wearing et al., 2013). However, because tendon conditioning and fatigue loading protocols are characterized with early stage of fatigue (e.g. creep) and initiation of microstructural damage, respectively (Fung et al., 2010; Fung et al., 2009; Thorpe et al., 2014), the time course of recovery from fatigue loading may not represent the recovery process from only a conditioning protocol. Further, the measurement of tendon parameters used to quantify tendon recovery in the aforementioned studies (e.g., thickness, water content, and structural integrity) is confined to a single site of the free tendon with tendon in an unloaded state using 2D ultrasound (Grigg et al., 2009; Grigg et al., 2012; Grosse et al., 2015; Rosengarten et al., 2014; Wearing et al., 2013). Therefore,

further study is needed to investigate the time course of recovery of AT 3D deformation (longitudinal and transverse deformation and strain) during load following a standardized conditioning protocol at the global and regional AT level.

1.1.6 Achilles tendinopathy and three-dimensional morphology of the tendinopathic AT at rest and under load

Mid-portion Achilles tendinopathy (MAT) is a degenerative disorder of the AT involving adaptation failures in the tendon cell matrix to excessive load changes (Paavola et al., 2002). The stereotypical signs and symptoms of MAT include swelling and thickening of the tendon, morning stiffness, and pain during functional activities and palpation in tendon mid-portion (Maffulli, 1998; Van Dijk et al., 2011). It has been reported that MAT causes considerable morbidity and functional impairment among the athletic and general populations (de Jonge et al., 2011; Emerson et al., 2010; Kvist, 1994). Various pathological changes within the tendinopathic tendon have been documented, including degeneration and disorganization of the collagen fibers (Pingel et al., 2014), increased number of tendon cells (Andersson et al., 2011a; Åström and Rausing, 1995), increased water content (de Mos et al., 2007), neovascularisation (De Jonge et al., 2014; Yang et al., 2012), elevated sulfated glycosaminoglycan content (Corps et al., 2006), increase in the ratio of collagen type III to type I collagen (Maffulli et al., 2000; Pingel et al., 2014), and increase in tendon thickness, CSA, and volume (Arya and Kulig, 2010; Gärdin et al., 2010; Grigg et al., 2012; Leung and Griffith, 2008; Shalabi et al., 2004b). These changes in tendon structure, composition, and histology have been shown to impair the whole AT normal mechanical and material properties, with the tendinopathic tendon showing greater

longitudinal strain, lower stiffness, lower Young's modulus, and greater hysteresis compared to healthy matched control tendons under the same external ankle torque (Arya and Kulig, 2010; Chang and Kulig, 2015; Child et al., 2010; Kulig et al., 2016; Wang et al., 2012). Such pathological alterations associated with MAT may change the normal morphology of AT throughout the entire tendon length at rest, under a single load, and during repetitive loading. However, our current knowledge regarding the alterations in morphology of tendinopathic AT are only limited to changes in tendon morphology (e.g., CSA and AP diameter) at a single site of tendon mid-portion at rest (Arya and Kulig, 2010; Grigg et al., 2012; Leung and Griffith, 2008) and short-term alterations in tendon morphology (e.g., AP diameter, water content, and volume) following exercise (Fahlström and Alfredson, 2010; Grigg et al., 2012; Ho and Kulig, 2016b; Shalabi et al., 2004b; Wearing et al., 2015). Further, given that free AT is mainly affected by MAT (Maffulli, 1998) and AT deformation during load is region-specific and occurs in 3D space (Obst et al., 2014b), there is a need to investigate the regional 3D morphology of tendinopathic tendon at rest, under a single tensile load, and during repeated loading. Such information could have important implications for our understanding of tendinopathic tendon physiology, mechanobiology, and potential mechanisms associated with tendinopathic tendon injury risk and function.

1.1.7 Use of freehand three-dimensional ultrasound to study human Achilles tendon morphology and mechanics

Two-dimensional ultrasound (2DUS) has been extensively used in investigation of the human AT morphological (e.g., length, thickness, and CSA) and mechanical (e.g., strain,

stiffness, and Young's modulus) properties. However, there are a number of inherent limitations associated with the use of 2DUS. The 2D scanning methods to capture the AT morphology at rest and during load is confined to single longitudinal or transverse plane images at the predefined locations along the tendon length. Because the shape and elongation of AT is encompassed in 3D space and the line of action of AT does not follow a linear path (Obst et al., 2014a; Obst et al., 2014b), the narrow field of view in 2DUS does not provide the 3D representation of tendon morphology and introduces a systematic underestimation/overestimation of tendon morphology at rest and under load (Lichtwark et al., 2013b; Obst et al., 2014a; Seynnes et al., 2015). The image plane is also highly sensitive to probe position and orientation, which can be difficult to control. Further, the anatomical structures, landmark of interest, and tendon line of action may also shift away from their original positions and move out of the image plane during muscular contraction. Such changes are unaccounted for during 2DUS imaging (Cronin et al., 2011; Cronin and Lichtwark, 2013; Obst et al., 2014b; Seynnes et al., 2015). MRI overcomes some of the limitations associate with 2DUS and provides a complete 3D reconstruction of the AT for the measurement of tendon diameter and cross-sectional area along the whole length of AT as well as the tendon volumetric data. However, MRI is expensive, immobile, requires a long examination time, relatively less available, and has limited application to the measurement of tendon morphology under load. These limitations can be overcome by freehand three-dimensional ultrasound (3DUS), which involves combining 2DUS imaging and 3D motion analysis to generate 3D reconstruction of tissue morphology in a fixed coordinate system (Prager et al., 1998; Treece et al., 2003). The freehand 3DUS has been shown to provide accurate measures of human free AT volume and length compared with

phantoms similar in size (0.05 mL and 0.2 mm, respectively), and repeatable measures of free AT volume, length, and average CSA *in vivo* at rest and during different ankle loading conditions (Obst et al., 2014a). The 3DUS system has been used in recent biomechanical studies for measurement of the 3D morphology (i.e., tendon length, CSA, AP diameter, ML diameter) and volume of the AT at rest and during a single isometric contraction before (Farris et al., 2013a; Obst et al., 2014b) and after an acute bout of exercise (Lichtwark et al., 2013b; Obst et al., 2015a). Freehand 3DUS was used throughout this thesis to investigate the specific purposes outlined in the following section.

1.2 Purpose

The specific purposes of this thesis were to determine:

1): The effect of a conditioning protocol consisting of 10 × 25-s successive submaximal (50%) voluntary isometric plantarflexion contractions on the longitudinal deformation of the whole AT, proximal AT, and free AT and the transverse deformation (i.e., CSA) of the proximal-, mid-, and distal portions of the free AT, and the corresponding free tendon volume (Chapter 3).

2): The time course of the recovery of the longitudinal deformation of the whole AT, proximal AT, and free AT and the transverse deformation (i.e., CSA) of the free AT mid-portion following a conditioning protocol consisting of 10 × 25-s successive submaximal (50%) voluntary isometric plantarflexion contractions at up to 2 h (Chapter 4).

3): The effect of unilateral MAT on free AT 3D morphology (length, CSA, AP diameter, and ML diameter) and volume at rest and during a submaximal (50%) voluntary isometric

plantarflexion contraction in tendinopathy and contralateral legs in individuals with unilateral MAT compared to those of the control healthy matched leg (Chapter 5).

4): The effect of unilateral MAT on longitudinal deformation of the whole AT, proximal AT, and free AT and the corresponding free tendon transverse (i.e., CSA) and volume deformation during repeated loading consisting of 10 × 25-s successive submaximal (50%) voluntary isometric plantarflexion contractions in tendinopathy leg relative to those of the contralateral leg in individuals with unilateral MAT (Chapter 6).

1.3 Thesis organisation

This thesis is comprised of seven chapters. The main experimental chapters 3-6 are presented in the format of a journal article.

Chapter 1 provides a general introduction to the thesis.

Chapter 2 is a review of the literature that provides an overview of the relevant literature on tendon normal structure, function, and mechanical and material properties, the human AT anatomy and function and its 3D morphology at rest and under load, tendon conditioning and its effects on tendon viscoelastic properties, recovery from tendon conditioning effects, pathological findings in tendinopathic tendon, alterations in tendon mechanical and material properties and muscle activities of the plantarflexors and dorsiflexors in chronic Achilles tendinopathy.

Chapter 3 describes the findings from a study that examined the regional 3D deformation of the healthy AT during conditioning (specific purpose 1).

Chapter 4 describes the findings from a study that examined the time course of recovery of the regional 3D deformation of the healthy AT following conditioning (specific purpose 2).

Chapter 5 describes the findings from a study that examined the 3D morphology and volume of the free AT at rest and under load in people with unilateral mid-portion Achilles tendinopathy (specific purpose 3).

Chapter 6 describes the findings from a study that examined the regional 3D morphology and volume of the AT during repeated loads in people with unilateral mid-portion Achilles tendinopathy (specific purpose 4).

Chapter 7 summarises the results of all studies included in this thesis and highlights the unique contribution and significance of the findings within the context of the relevant literature. The main limitations of the studies conducted and the general conclusion of the thesis are also presented.

Chapter 2: Literature Review

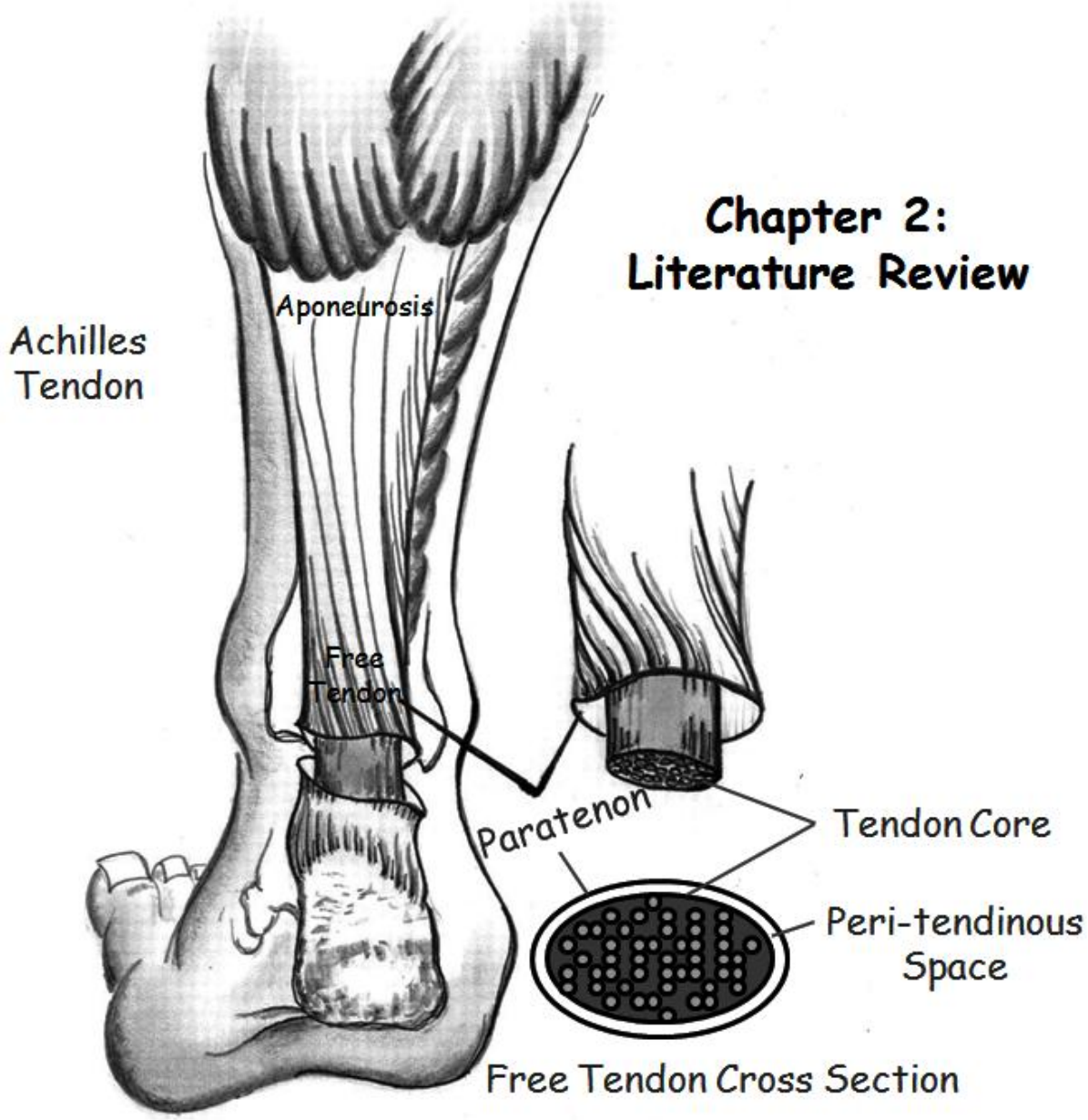

Chapter 2. Literature Review

2.1 Tendon function, composition, and structure

Tendons are dense connective tissue structures interposed between muscles and bones in the body. Their primary function is transmitting the forces generated by muscle contraction directly to the bone with a minimal dispersion of energy, resulting in stabilization or movement across joints (Gupta and Screen, 2017; Józsa and Kannus, 1997; Screen et al., 2004). However, energy-storing tendons such as the human Achilles tendon and the equine superficial digital flexor tendon have an additional important role in reducing the energetic cost of locomotion by stretching and recoiling with each stride to store and return the energy to the system (Lichtwark and Wilson, 2007; Thorpe et al., 2013b; Thorpe et al., 2016). This tendon elastic action serves a diverse set of functions, including metabolic energy conservation, amplification of muscle power output, attenuation of muscle power input, and rapid mechanical feedback that may aid in stability (Alexander et al., 1991).

Like other connective tissues, tendon is mainly composed of water, which makes up 55-70% of the total tendon weight (Dourte et al., 2013; Franchi et al., 2010). Tendon extracellular matrix is composed predominantly of collagen, which accounts for 60-85% of the tendon dry weight. Approximately 95% of the collagen is type I with small amounts of collagen type III, V, XII, and XIV (Connizzo et al., 2016; Young et al., 2016). The remainder of the tendon matrix structure consists of elastin, tenocytes and tenoblasts between collagens and ground substance surrounding the collagen including proteoglycans, glycosaminoglycans, structural glycoproteins, and other small molecules (Pang et al., 2016; Ryan et al., 2015).

Structurally, the collagen fibril is the smallest unit of the tendon. An aggregate of collagen fibrils form a collagen fiber. Collagen fibers are bound together by the endotenon to form the primary fiber bundles (sub-fascicle). A group of primary fiber bundles constitutes a secondary fiber bundle (fascicle) and a group of secondary fiber bundles forms a tertiary fiber bundle. Finally, the tertiary fiber bundles form the whole tendon. The tendon is enveloped by a well-defined layer of connective tissue, the epitenon, which is in direct contact with the endotenon (Figure 1) (Khan et al., 1999; Santos et al., 2017). The epitenon is surrounded by the paratenon, a layer of loose areolar connective tissue, which serves as an elastic sleeve to allow gliding of the tendon within the surrounding tissues. Together these two layers (i.e., epitenon and paratenon) are known as the peri-tendon and the space between them is called peri-tendinous space (Benjamin et al., 2008; Kannus, 2000; Khan et al., 1999; Sellon et al., 2014; Skirven et al., 2011).

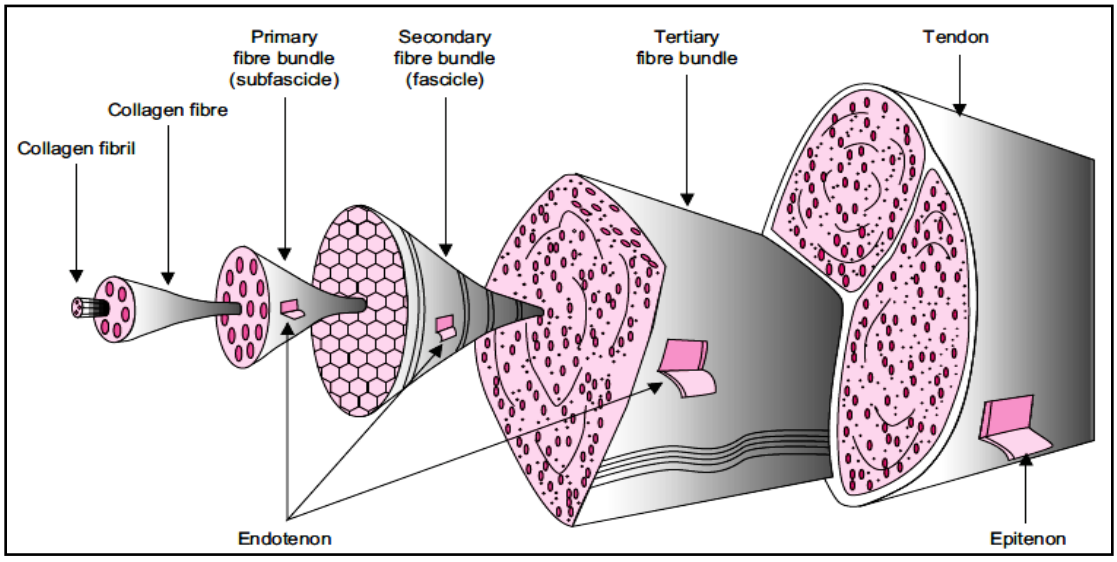

Figure 1: *The structural organization of tendon tissue. Adapted from Khan et al. (1999).*

2.2 Tendon mechanotransduction

Tendon resident cells respond to the externally applied physical loads by the process of mechanotransduction, which involves the assessment of the mechanics of the tendon extracellular matrix by the cells through their cytoskeletons (Wang, 2006). The deformation of the tendon cell cytoskeletons, via membrane anchored attachment proteins (integrins), or stimulation of other transmembrane cell proteins (G-protein receptors, receptor kinases, mitogen-activated protein kinases) initiates a cascade of gene expressions activating catabolic and/or anabolic cell responses, resulting in deposition, rearrangement or removal of the extracellular matrix to maintain overall tendon form and function (Nourissat et al., 2015; Wang, 2006). Tendon mechanotransduction process is a fundamental biologic response for tendon tissue development, homeostasis, disease, and repair (Arnoczky et al., 2004; Humphrey et al., 2014; Lavagnino et al., 2015).

2.3 The human Achilles tendon

The Achilles tendon (AT) is the thickest, largest, and strongest tendon in the human body (Doral et al., 2010; Pierre-Jerome et al., 2010). AT is the combination of tendons of gastrocnemius and soleus muscles. The gastrocnemius is a fusiform muscle, with two heads, medial and lateral, originating from the posterior surface of the femoral condyles and inserting onto the calcaneus. The medial and lateral bellies of the gastrocnemius muscle fuse in a single muscle belly occupying the posterior superficial compartment of the lower leg. The soleus muscle, a large flat, pennate muscle lies anterior to the gastrocnemius muscle, arising from the posterior surface of the upper tibia and inserting onto the calcaneus. The gastrocnemius and soleus muscles form the three-headed triceps

surae muscle, which acts to plantarflex the ankle joint via AT (Seebacher et al., 1982; Watanabe et al., 1993). The whole AT consists of two structurally distinct parts: (1) the proximal AT, which originates at the muscle-tendon junction (MTJ) with the gastrocnemius muscle and runs contiguous with the soleus muscle; and (2) the free AT, which continues from the distal end of the soleus muscle to its insertion on the calcaneus (Farris et al., 2013a; Lichtwark et al., 2013a; Obst et al., 2015a) (Figure 2).

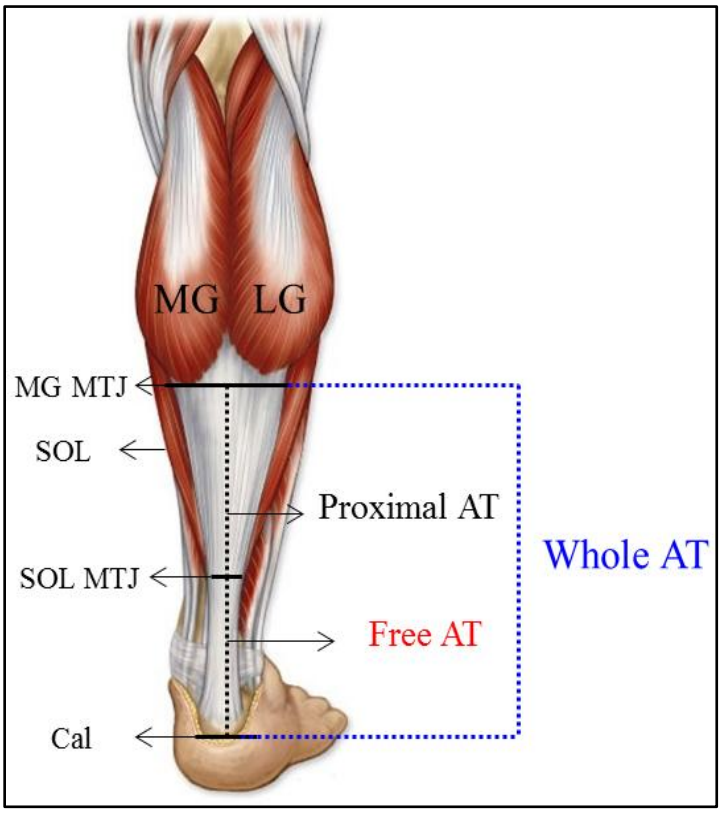

Figure 2: *Human right triceps surae muscle and Achilles tendon anatomy. MG, medial gastrocnemius; LG, lateral gastrocnemius; MG MTJ, medial gastrocnemius muscle-tendon junction, SOL, soleus; SOL MTJ, soleus muscle-tendon junction; AT, Achilles tendon; Cal, calcaneus.*

The fibers and fascicles from particular parts of the triceps surae muscle within AT are not aligned strictly vertically between the muscle and the bone and display a variable degree of twist at approximately 3-5 cm proximal to the calcaneal insertion, producing an area of concentrated stress (Edama et al., 2015a; Obst et al., 2014b; Szaro et al., 2009; van Gils et al., 1996; White, 1943). Tendon twist causes the medial and lateral group of fibers from the medial head of the gastrocnemius to become oriented on the posterior and lateral portion of the tendon, respectively while fibers from the lateral head of the gastrocnemius muscle and soleus become located on the anterior and antero-medial portion of the tendon, respectively (Edama et al., 2015a; Szaro et al., 2009) (Figure 3). The direction of AT twist from proximal to distal is counterclockwise in the right AT and clockwise in the left AT (Edama et al., 2015a). It has been suggested that tendon twist may enhance the elastic and recoil properties of AT during locomotion (Bojsen-Møller and Magnusson, 2015; Thorpe et al., 2014).

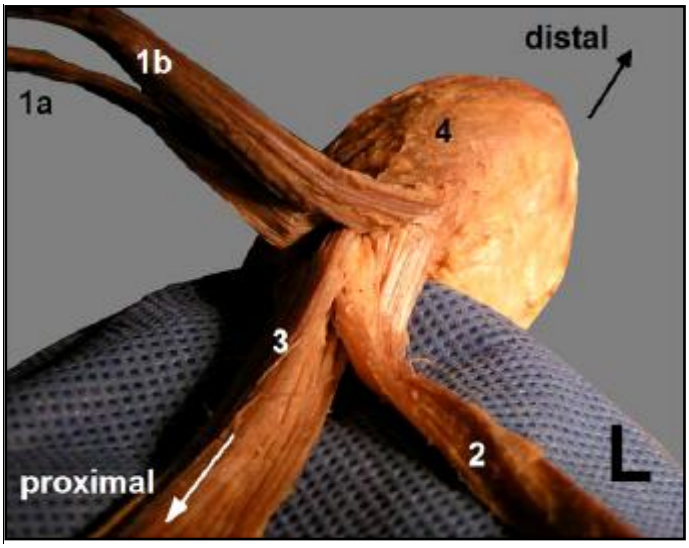

Figure 3: *The left Achilles tendon, superior view. (1a) the fibers from the medial part of the medial gastrocnemius; (1b) the fibers from the lateral part of the medial*

gastrocnemius; (2) the fibers from the lateral gastrocnemius; (3) the fibers from the soleus; (4) insertion of the Achilles tendon to the calcaneal notch. L, left. Adapted from Szaro et al (2009).

In comparison to other tendons in human body, AT exhibits similar material properties despite experiencing greater mechanical loads during physical activities (Wren et al., 2001). AT force exposure ranges from 1.9 kN in the counter movement jump (Fukashiro et al., 1995), 2.6 kN during walking (Giddings et al., 2000), 3 kN during maximal voluntary isometric contraction (Maganaris et al., 2008), 5 kN during unilateral hopping (Lichtwark and Wilson, 2007), and 9 kN during running, exceeding up to 12 times the body weight (Komi et al., 1992). The high magnitude of loads on the Achilles tendon and the continual stresses placed on it during locomotion make it one of the most common tendons to sustain overuse injuries (e.g., tendinopathy) and rupture (Kvist et al., 1991).

2.4 Tendon mechanical and material properties

Tendon strain (%) is the ratio of tendon deformation to resting length. Tendon stress (Pa) is the ratio of tendon force to tendon cross-sectional area (CSA) (Fang and Lake, 2016). The unique structure and composition of tendons afford them the characteristic mechanical behavior, which is reflected by a typical stress-strain curve consisting of three regions (Wang, 2006). The first region is the non-linear toe region in which the "stretching out" or "un-crimping" of crimped collagen fibers occurs from the mechanically loading the tendon up to 2% strain. Due to stretching of the crimp pattern of tendon collagen fibers, the tendon tangent modulus of elasticity (i.e., slope of the stress-strain curve) for this region increases with strain at low strain rates (Wang, 2006; Wilmink et al., 1992). Following the toe

region, tendon exhibits a linear region where tendon is strained up to approximately 4% and the collagen fibrils orient themselves in the direction of the tensile mechanical load. This region of the curve is elastic and reversible and the slope of the curve is referred to as Young's modulus, which represents tendon stiffness (i.e., force/deformation) (Morales-Orcajo et al., 2016; Reyes et al., 2014; Zajac, 1989). If the tendon strains more than its linear region, microscopic tearing of the tendon occurs. If the strain further increases beyond 8-10%, macroscopic tearing of tendon fibers ensues, eventually leading to tendon rupture (Figure 4) (Wang and Ker, 1995; Wren et al., 2001).

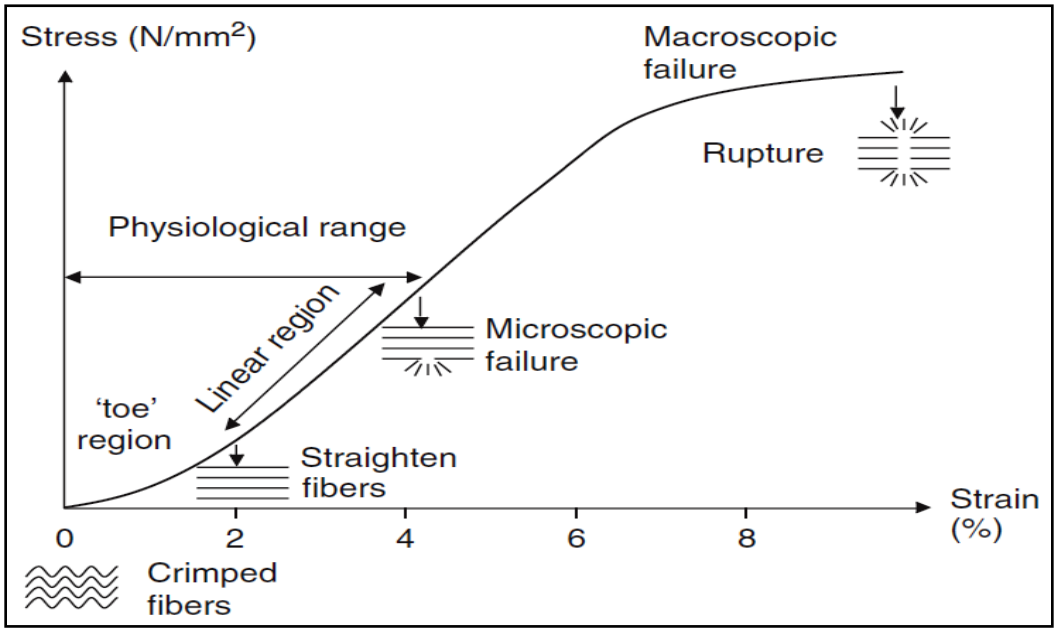

Figure 4: *The stress-strain tendon curve. Adapted from Wang et al. (2006).*

Like other soft tissues in the body, tendons exhibit viscoelastic, or time- and-history dependent behavior during mechanical testing, which is the result of the complex interactions between the collagen fibers, the surrounding proteins, ground substance, and fluid flow. The important time- and-history dependent viscoelastic characteristics of

tendons are stress-relaxation, creep, hysteresis, and conditioning (Carlstedt and Nordin, 1989; Fung, 2013; Woo et al., 1981). Stress relaxation means that the stress required to cause a constant tendon deformation declines over time in a predictable curvilinear pattern (Figure 5A). Conversely, creep is an increase in tendon deformation over time under a constant load (Figure 5B). Hysteresis refers to the energy loss between the loading and unloading cycle of the tendon determined from the area between these two curves (Pollock and Shadwick, 1994) (Figure 5C). The average mechanical hysteresis of the tendon is approximately 10% of the total work done on the tendon during stretching (Pollock and Shadwick, 1994).

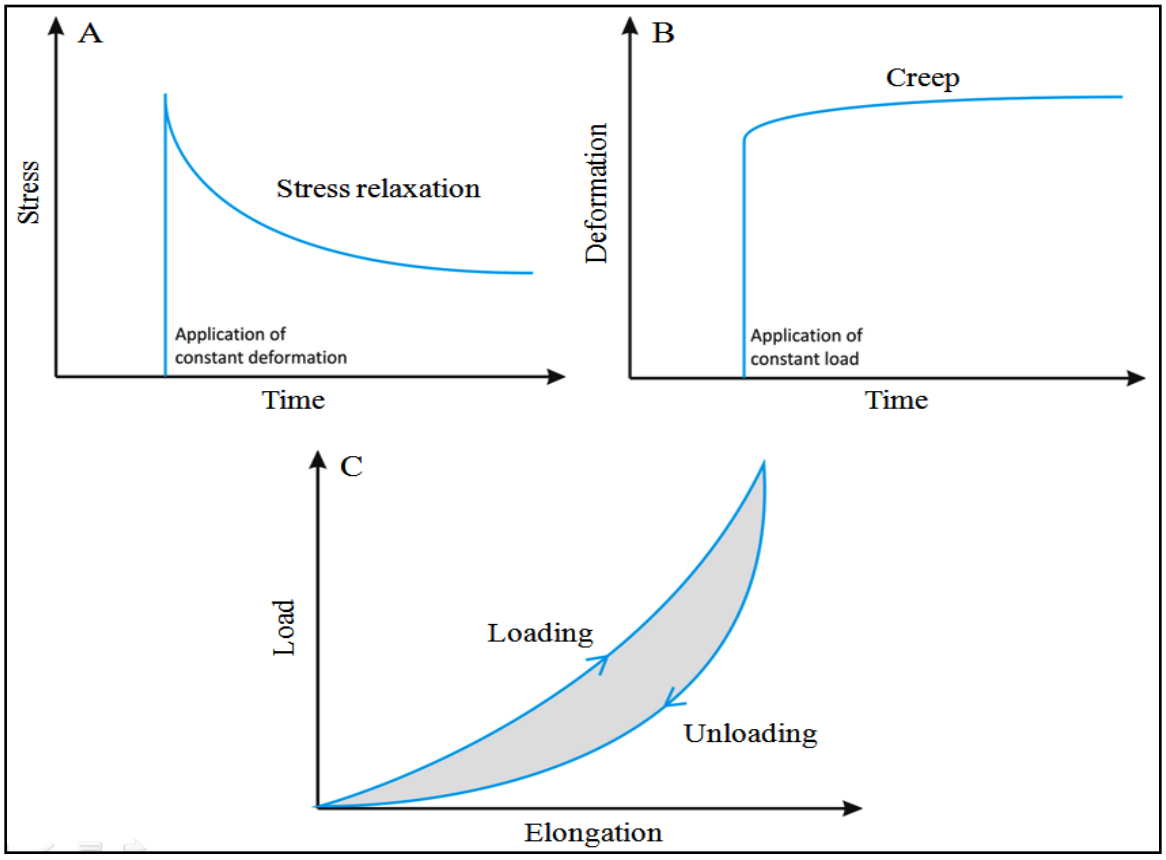

Figure 5: *Tendon viscoelastic properties. (A) stress relaxation; (B) creep; (C) hysteresis. Adapted from Fung et al. (2013).*

Another widely recognized viscoelastic property of tendon, although still not thoroughly understood, is conditioning. Conditioning is a gradual adaption of tendon mechanical behavior to the cyclic sub-failure loading (Elliott et al., 2003; Fung, 2013). Conditioning is usually performed in two types of experiments; load controlled and deformation controlled. In the load controlled experiment, the maximum load of each successive cycle is fixed as a constant while in the deformation controlled experiment, the maximum deformation of each successive cycle is kept constant. During cyclic loading, in the deformation controlled experiment, the peak load decreases with an increasing number of cycles and the difference between cycles and also the size of the hysteresis loop become smaller (Figure 6A). In the load controlled experiment, however, tendon experiences a gradual increase in deformation, with the difference in tendon deformation between cycles becoming smaller over the course of several cycles until tendon reaches a steady-state mechanical behavior, with no progressive changes in the response to additional loading cycles (Carew et al., 2000; Graf et al., 1994; Hawkins et al., 2009; Hosseini et al., 2014; Maganaris, 2003; Sopakayang, 2013) (Figure 6B). Therefore, a standardized tendon conditioning protocol is commonly performed prior to mechanical tests to minimize the tendon loading/stretching history for establishing consistent and repeatable mechanical results.

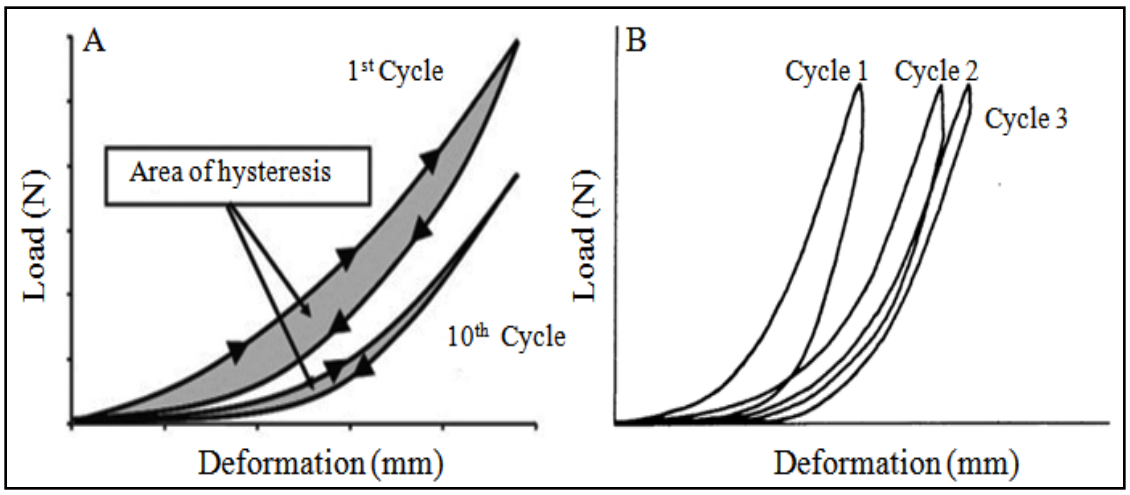

Figure 6: *Conditioning. (A) deformation controlled experiment; (B) load controlled experiment. During cyclic loading of the tendon, the load-deformation curve gradually shifts to the right. Usually, after a few cycles, the curves become quite repeatable and steady. Adapted from Fung et al. (2013).*

2.5 Mechanisms of conditioning

Micro-structural alterations, such as collagen fiber re-alignment, un-crimping, fascicle/fiber sliding, and interstitial fluid distribution have been suggested as potential underlying mechanisms responsible for conditioning (Hosseini et al., 2014; Houssen et al., 2011; Miller et al., 2012a; Miller et al., 2012b; Quinn and Winkelstein, 2011; Schatzmann et al., 1998; Sopakayang, 2013; Thorpe et al., 2014). For example, Houssen et al. (2011) monitored the collagen morphology of a rat tail tendon during a conditioning protocol (10 N of constant tensile loading for 5 min) using second harmonic generation microscopy. Their results indicated that the tendon conditioning was mostly due to the sliding between collagen fibrils inside the fascicles, which only changed the resting length of the tendon fascicles. Similarly, Thorp et al. (2014) studied the effect of a conditioning protocol (30

cycles from 0.2-10 N at 1 Hz) on equine superficial digital flexor tendon micro-structural strain response. Following conditioning, tendon samples exhibited some negligible alterations in micro-structural strain response such as reductions in fiber extension, transverse strain, and rotation relative to the non-conditioned control tendon samples, suggesting that the conditioning protocol loaded the fascicles only within their elastic limits. Furthermore, a strong correlation between cyclic conditioning (30 cycles of 0.1-0.5 N at 0.22 Hz) and early re-alignment and un-crimping of collagen fibers has been identified using polarized light microscopy in a rat supraspinatus tendon model (Figure 7) (Miller et al., 2012a; Miller et al., 2012b). The decreases in peak force and tangent stiffness between the 1st and 30th cycles of conditioning (30 cycles of tensile loading between 0 and 1 mm at 0.4 mm/s) were also significantly correlated with the change in fiber alignment and rotation in a human cadaveric facet capsular ligament, suggesting that both viscoelasticity and micro-structural reorganization contribute to the time-history dependence of the mechanical properties of soft tissues (Quinn and Winkelstein, 2011). Sopakayang et al. (2013) presented a new modeling framework for describing the viscoelastic behavior exhibited during conditioning process. According to their model, the energy dissipation during tendon conditioning is due to the effect of the structural changes in the coupling between collagen fibers and the matrix, which associate to the friction loss or the disconnection of some contact surfaces between the collagen fibers and the matrix. Hosseini et al. (2014) further investigated the time-dependent effects of fluid flow and of solid matrix viscoelasticity on the stress-relaxation of cartilage during conditioning by means of a computational modeling. According to their results, collagen viscoelasticity and fluid flow have opposite effects on the tissue reaction force and cancel each other out in a

stress-strain curve during the first conditioning cycles in a mechanical test, resulting in an equilibrium stress-stain relationship. When only fluid-dependent poroelasticity or only collagen viscoelasticity was accounted for conditioning, the steady state was reached faster than when both effects interacted, indicating that both time-dependent phenomena together change the whole mechanical response of the soft tissue during conditioning.

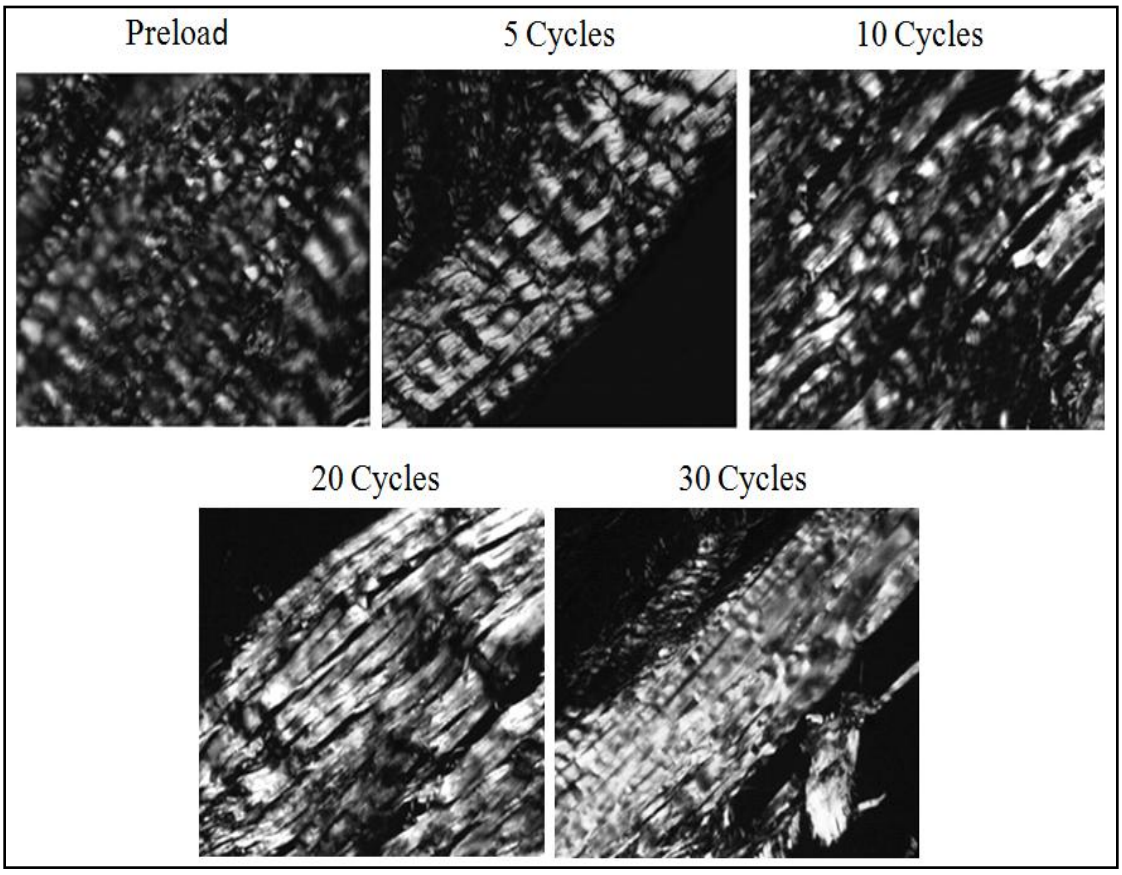

Figure 7: *Collagen fiber un-crimping during conditioning cycles in rat supraspinatus tendon. Adapted from Miller et al. (2012a).*

2.6 Conditioning effects on tendon

2.6.1 Changes in tendon viscoelastic properties during conditioning

Sverdlik and Lanir (2002) investigated the conditioning of sheep digital extensor tendons using a test protocol consisting of sets of stress relaxation loadings, each with first increasing maximal strain levels (4, 6, 8% sequence) and then decreasing strains (7-6%) at consecutive sets. They showed that conditioning manifested in sheep digital tendons as stress decay in the cyclic phase and as elongation of the tendon's reference length. These effects intensified with increased strain level and subdued as the strain decreased. They suggested that the tendon conditioning effects are an integral component of the tendon viscoelastic response. Schatzman et al. (1998) used 200 uniaxial conditioning cycles from 75 to 800 N at 0.5 Hz in human cadaveric quadriceps and patellar tendons. The hysteresis and creep effects were highest during the first few loading cycles and reached a steady state after 160 cycles. Furthermore, the conditioning protocol augmented the mechanical properties and the ultimate failure load of both tendons, suggesting the progressive collagen fiber recruitment and alterations of tendon interstitial fluid milieu. Piedade et al. (2006) also applied 10 successive cycles of three established levels of constant deformation (2.5, 3, and 4%) to the human cadaveric gracilis and semitendinosus tendons. The stress value in both tendons at each deformation level decreased by ~ 23% from the first to the tenth cycle.

2.6.2 Conditioning effects on tendon tension, stiffness, and mechanical strength

Graf et al. (1994) compared the effect of a cyclic conditioning (10 min of 0 to 2.5% sinusoidal strain at 0.1 Hz) with a static conditioning protocol (10 min of 2.5% strain at a strain rate of 10% per second) in the primate patellar tendon grafts. Both conditioning protocols significantly reduced the tension lost in tendon grafts due to viscoelastic relaxation. No differences were found in the relaxation behavior of tendon grafts that were cyclically or isometrically conditioned, suggesting that a simple static isometric conditioning is as effective as cyclic conditioning protocol. Likewise, Elias et al. (2009) reported that increasing the tension applied to human cadaveric hamstring tendon grafts from 80 N to 160 N during conditioning decreased the post-operative loss of tension and stiffness due to reduction in the influence of tendon viscoelasticity. Jeffery et al. (2014) compared the effect of six conditioning protocols including three cyclic (10 cycles at 0.5 Hz between 10-80, 100-300, and 399-600 N) and three static loading protocols (20 s at 80, 300, and 600 N) on bovine extensor tendon graft elongation. The high-load conditioning protocols (i.e., cyclic 300-600 N and static 600 N loading protocols) removed the most graft elongation during conditioning and led to less residual laxity in tendon grafts resulting from post-operative graft elongation and the intrinsic viscoelastic properties of the tendon graft tissue. Similarly, Pilia et al. (2015) compared the effects of four different conditioning protocols (1: single initial pull at 80 N, 2: 20 min of static loading at 88 N, 3: 20 min of 0 to 80 N cyclic loading at 1 mm/s, 4: 20 min of static loading at 88 N+20 min of 0 to 80 N cyclic loading at 1 mm/s) on human cadaveric semi-tendinosus and tibialis anterior tendon grafts. All conditioning protocols increased the tension and stiffness of tendon grafts, with protocol 4 resulting in significantly greater effects in tendon grafts

compared with protocols 1-3. Teramoto and Luo (2008) also investigated the time-dependent effect of a conditioning protocol (30, 100, 300, 600, and 1000 s stretching at 2% strain) on the mechanical strength of rat's Achilles tendon and the optimal duration of conditioning for tendon strengthening. They found that conditioning from 30 s to 600 s significantly enhanced the tendon mechanical strength, indicating the progressive recruitment of collagen fibers. However, 1000 s conditioning had no effect on tendon mechanical strength, indicating tendon microstructural fatigue.

2.6.3 Conditioning effects on tendon length

Howard et al. (1996) showed a significant patellar tendon graft length increase in both the *in vivo* (~14%) and *in vitro* (~10%) cases following the application of a 4 min sustained load of 89 N and a 15 min sustained tensile load of 89 N at a rate of 20% per second, respectively. Figueroa et al. (2010) reported that tendon conditioning with static tensile loading at 80 N for 10 min produced a 3% average elongation in porcine extensor tendon. Fujii et al. (2016) similarly showed that a conditioning of human hamstring tendon graft using a continuous load of 150 N twice for 30 seconds resulted in 2 mm elongation of the tendon grafts. The results of these studies supported the previous findings that without conditioning of tendon grafts, significant post-implantation graft creep will occur.

2.7 Human Achilles tendon conditioning

Human Achilles tendon conditioning has been reported in two previous *in vivo* studies and is confined only to the measures of longitudinal elongation and strain of the whole AT (Hawkins et al., 2009; Maganaris, 2003). The issue of conditioning in the mechanical

behavior of human AT *in vivo* was first addressed by Maganaris (2003) who investigated whole AT longitudinal elongation in response to 10 × 4-s successive plantarflexion contractions at 80% maximum voluntary isometric contraction (MVIC) using two-dimensional ultrasound (2DUS). AT longitudinal elongation gradually increased from the first contraction to the tenth contraction by 5 mm and reached steady-state behavior after 5 contractions (Figure 8A). Later, Hawkins et al. (2009) examined the effect of 7-min of cyclic isometric ankle plantarflexion (315 cycles) at 25-35% of MVIC on whole AT longitudinal strain using 2DUS. Tendon longitudinal strain increased from 0.3% at the start of activity to 3.3% after seven minutes, giving a total dynamic creep of 3% with no significant changes observed after 270 loading cycles. They reported that 270 loading cycles or a 6-min warm-up is required to achieve a steady-state strain response in the whole AT (Figure 8B).

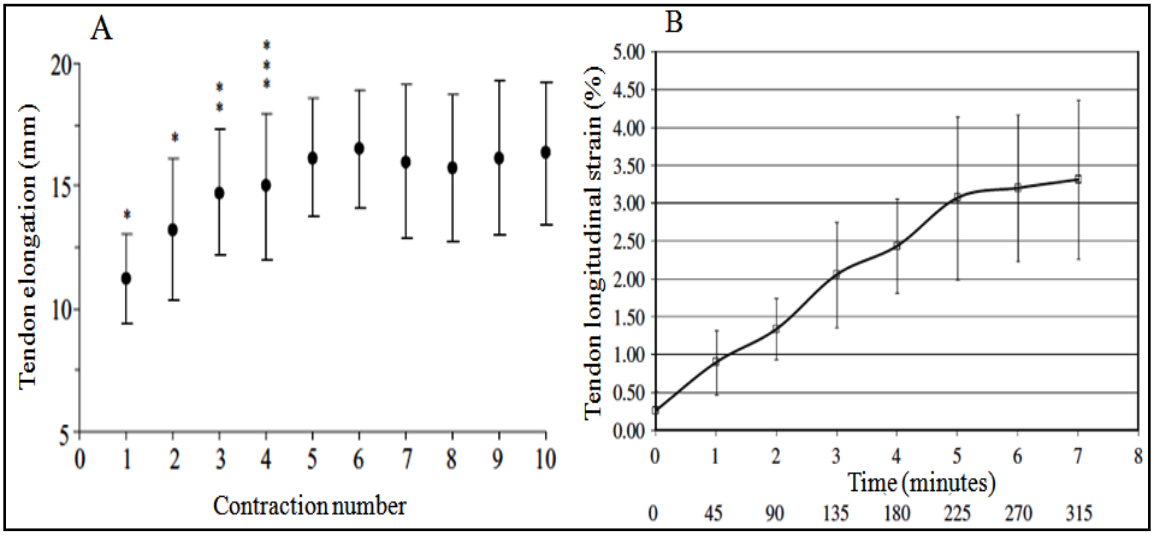

Figure 8: *Human Achilles tendon conditioning. (A) tendon longitudinal elongation in response to 10× 4-s successive isometric plantarflexion contractions at 80% MVIC*

(Maganaris, 2003). (B) tendon longitudinal strain in response to 315 isometric plantarflexion contractions at 25-35% MVIC (Hawkins et al., 2009).

2.8 Free Achilles tendon versus proximal Achilles tendon

Recent biomechanical studies have reported the non-uniform nature of the whole human AT with respect to the compliance, with the free AT exhibiting greater strain than proximal AT during mechanical testing both before (Farris et al., 2013a; Finni et al., 2003; Magnusson et al., 2003) and after fatigue loading (Lichtwark et al., 2013a; Obst et al., 2015a). Magnusson et al. (2003) investigated the longitudinal elongation of the free AT (9 cm proximal to calcaneal bone) and distal (deep) proximal AT of the medial gastrocnemius muscle during a 10-s slow ramp voluntary isometric plantarflexion contraction at a common tendon force of 2641 N using 2DUS. Under the same tensile load, the free AT demonstrated greater longitudinal strain (~8%) compared with that of the proximal AT (~1.4%). Similarly, Finni et al. (2003) evaluated the longitudinal strain of free AT and soleus mid-aponeurosis simultaneously during cyclic isometric plantarflexion contractions at 40% MVIC using magnetic resonance imaging (MRI) and demonstrated that the free AT strained (4.7%) more than soleus mid-aponeurosis (2.2.%). Farris et al. (2013a) supported previous findings by demonstrating a greater longitudinal strain in the free AT (5.2%) than in the proximal AT (2.6%) during an isometric plantarflexion contraction at 50% MVIC using freehand three-dimensional ultrasound (3DUS). Lichtwark et al. (2013a) quantified the longitudinal strain of both the free and whole AT during isometric contractions at three ankle torque levels (14, 42 and 70 N.m) to determine whether this relationship changes in response to a running task (5 km at a comfortable self-selected pace) using 3DUS. There

was a small, significant increase only in the free AT strain across the prescribed torque levels immediately following running. As no significant changes in tendon stiffness or tendon CSA were detected after running, the increase in free tendon length was indicative of tendon creep in response to the net tensile load during the running task. Obst et al. (2015a) extended the findings of Lichtwark et al. (2013a) by simultaneously examining changes in the free AT, proximal AT, and whole AT strain during a 30% and 70% isometric plantarflexion contractions immediately before and after a single bout of eccentric exercise (3 × 15 eccentric heel drops). The immediate changes in AT length and strain following exercise were only confined to the free AT, without changes evident at the level of proximal AT or whole AT. Overall, these findings suggest that the free AT and proximal AT may have differing mechanical demands and functional roles during *in vivo* force transmission and highlight the vulnerable nature of the free AT to the exercise-induced tendon creep or early stage mechanical fatigue effects.

2.9 Recovery from conditioning effects

Conditioning effects are transient, non-damaging, and recoverable (Fung, 2013; Graf et al., 1994; Lanir and Fung, 1974; McPherson et al., 1992; Nurmi et al., 2004; O'Brien et al., 1989; Pilia et al., 2015; Thorpe et al., 2014). The small alterations in equine superficial digital flexor tendon micro-structural strain response (i.e., reduction in fiber extension, transverse strain, and rotation) relative to the non-conditioned control tendon samples following the conditioning protocol (30 cycles from 0.2-10 N at 1 Hz) observed by Thorp et al. (2014) were fully recovered only 15 min after conditioning. The increased rabbit skin length following a conditioning protocol (20 cycles at 0.02-2 N at 1 Hz) reported by Lanir

et al. (1974) was shown to considerably recover (~70%) after 30 min of recovery. Obrien et al. (1989) reported a 42% recovery in human cadaveric patellar tendon graft tension 15 minutes after conditioning (static loading at 22 N for 20 min). Likewise, a 69% recovery in primate patellar tendon graft tension and stiffness was reported by Graf et al. (1994) 30 minutes after conditioning. McPherson et al. (1992), also found a significant recovery (~70%) in rabbit medial collateral ligament length, tension, and stiffness 60 minutes after conditioning. A steady recovery in human anterior tibialis tendon graft tension and stiffness (60% within 60 min) was also observed after cyclic (25 cycles 0-80 N for 100 s) and static (80 N for 100 s) conditioning protocols (Nurmi et al., 2004). Pilia et al. (2015) supported previous findings and reported 30%, 15%, 23%, and 15% recovery in human cadaveric semi-tendinosus and tibialis anterior tendon grafts tension and stiffness 30 min after conditioning protocols consisting of a single initial pull at 80 N, 20 min of static loading at 88 N, 20 min of 0 to 80 N cyclic loading at 1 mm/s, 20 min of static loading at 88 N+20 min of 0 to 80 N cyclic loading at 1 mm/s, respectively.

2.10 Recovery of human Achilles tendon from conditioning effects

The time course of recovery of human AT *in vivo* has been reported in several studies only following the application of an acute bout of fatiguing exercise (Grigg et al., 2009; Grigg et al., 2012; Grosse et al., 2015; Rosengarten et al., 2014; Wearing et al., 2013) and no study, to date, has investigated the recovery of the AT following a conditioning protocol. For example, Grigg et al. (2009) investigated the acute effects of isolated fatiguing eccentric (2 × 3 sets of 15 repetitions of eccentric heel drops) and concentric (2 × 3 sets of 15 repetitions of concentric ankle loading exercise) calf muscle exercise on AT thickness

at 2-4 cm proximal to the calcaneal notch. Both loading conditions resulted in an immediate decrease in AT thickness. The time constant for tendon thickness recovery following exercise was 2.5 h, which was representative of a 63% recovery in tendon thickness and the full recovery of tendon pre-exercise thickness values was achieved 24 h after exercise completion (Grigg et al., 2012). Wearing et al. (2013) similarly reported that 24 h is required for the full recovery of the AT thickness measured at 2 cm proximal to the calcaneal notch following an acute bout of fatiguing resistance exercise (90 repetitions of calf-raise exercise against an effective resistance of 250% body weight), with the primary recovery (63% of the pre-exercise value) occurring 7 h post-exercise. Gross et al. (2015) evaluated the temporal alterations of AT volume and hydration state after cross-country-running with a fixed distance of 3.9 km. After a transient decrease of AT volume immediately following running (~4%), a tendency toward full recovery (~%88) relative to the baseline measurement after 72 h was observed. Furthermore, the transient changes in AT ultrasound tissue characterization echo-pattern (i.e., reduction in echo type I and increase in echo-type II) as a result of an Australian football game reported by Rosengarten et al. (2014) was shown to return to the baseline values 4 days following the game.

2.11 Application of freehand three-dimensional ultrasound for investigation of human Achilles tendon mechanical and morphological properties

2DUS has been increasingly employed in investigation of the human AT morphological and mechanical properties and has advanced our understanding of triceps surae muscle-tendon interaction during dynamic and static tasks (Cronin et al., 2011), AT properties

(Magnusson et al., 2003), and its plasticity to reduced (Reeves et al., 2005) or increased loading (Arampatzis et al., 2007), aging (Slane et al., 2015; Stenroth et al., 2012), and various pathological conditions (Arya and Kulig, 2010; Child et al., 2010; Chimenti et al., 2016). Although 2DUS is less expensive and more available than MRI for the assessment of AT properties, there are a number of inherent limitations associated with the use of 2DUS. The 2D scanning methods to capture the deformation of tendinous structures are confined to single longitudinal or transverse plane images at the predefined locations along the tendon length. The image plane is also highly sensitive to probe position and orientation, which can be difficult to control. Furthermore, the shape and elongation of tendinous structures is encompassed in a 3D space and the line of action of certain tendons does not follow a linear path (Obst et al., 2014a; Obst et al., 2014b). The narrow field of view in 2DUS does not provide the 3D representation of whole tendon morphology and volume. Disregarding the 3D morphology of tendon introduces a systematic underestimation of tendon length and thus an overestimation of length changes (Cronin and Lichtwark, 2013; Seynnes et al., 2015). The anatomical structures, landmark of interest, and tendon line of action may also shift away from their original positions and move out of the image plane during muscular contraction. Such changes are unaccounted for during 2DUS imaging (Cronin et al., 2011; Cronin and Lichtwark, 2013; Obst et al., 2014b; Seynnes et al., 2015).

These limitations can be overcome by 3DUS, which involves combining 2DUS imaging and 3D motion analysis to generate 3D reconstruction of tissue morphology in a fixed coordinate system. A stack of 2D B-mode images is created by recording consecutive ultrasound scans while simultaneously tracking the position and orientation of the

ultrasound transducer using 3D motion analysis. The orientation and position of each sequential 2D image is then transformed into a global coordinate system using a rigid body calibration method and a 3D reconstruction of the tissue of interest can be reconstructed for morphological measurement purposes (Prager et al., 1998; Treece et al., 2003; Treece et al., 1999; Treece et al., 2000). However, the 3DUS requires long scanning time and the measurement of tissue morphology is only limited to the resting state or during static isometric contraction (Lichtwark et al., 2013a; Seynnes et al., 2015).

Freehand 3DUS has been shown to provide accurate measures of human free AT volume and length compared with phantoms similar in size (0.05 mL and 0.2 mm, respectively), and repeatable measures of free AT volume, length, and average CSA *in vivo* at rest and during three ankle conditions: 15° passive dorsiflexion, 15° passive plantarflexion and 15° plantarflexion at 70% MVIC (ICC > 0.98) (Obst et al., 2014a). The 3DUS system has been used in recent biomechanical studies for measurement of the 3D morphology [i.e., tendon CSA, length, antero-posterior (AP) diameter, and medio-lateral (ML) diameter] and volume of the free AT at rest and during a single isometric contraction before (Farris et al., 2013a; Obst et al., 2014b) and after an acute bout of exercise (Lichtwark et al., 2013a; Obst et al., 2015a).

2.12 3D morphology of healthy free AT at rest and under load

The 3D morphology of the healthy free AT at rest and under tensile load has been well documented in the literature. At resting state, there is a non-uniform tendon morphological profile along the length of the healthy free AT, with gradually decreasing tendon CSA (Magnusson and Kjaer, 2003; Muraoka et al., 2005; Obst et al., 2015b; Obst et al., 2014b)

and ML diameter (Gatt et al., 2015; Iwanuma et al., 2011; Obst et al., 2015b; Obst et al., 2014b) and increasing tendon AP diameter (Fredberg et al., 2008; Leung and Griffith, 2008; O'Reilly and Massouh, 1993; Obst et al., 2015b; Obst et al., 2014b) from the calcaneal notch to the SOL MTJ (Figure 9A). The minimum free AT CSA has been reported to be at around 70% of the tendon length (Obst et al., 2014b). Such variation in tendon morphology along the free AT length has been related to the differences in tendon structure-function relationship between different regions of the AT (Magnusson and Kjaer, 2003; Muraoka et al., 2005). During a sub-maximal isometric plantarflexion contraction, the healthy free AT experiences a longitudinal strain (Farris et al., 2013a; Finni et al., 2003; Iwanuma et al., 2011; Lichtwark et al., 2013a; Magnusson et al., 2003; Obst et al., 2015a; Obst et al., 2014b), which is coupled to the corresponding reduction in tendon CSA (Obst et al., 2015b; Obst et al., 2014b; Reeves and Cooper, 2014) across all the tendon regions. The load-induced changes in tendon length and CSA are accompanied by a reduction in tendon ML diameter (Iwanuma et al., 2011; Obst et al., 2015b; Obst et al., 2014b) and an increase in tendon AP diameter (Obst et al., 2015b; Obst et al., 2014b) along the entire tendon length, with no significant changes in tendon volume observed (Figure 9B). The alterations in free tendon transverse morphology (i.e., CSA, AP diameter, and ML diameter) deformation and strain during load is region-specific within the tendon, with the mid portion undergoing greater transverse deformation and strain compared to the proximal and distal portions (Iwanuma et al., 2011; Obst et al., 2015b; Obst et al., 2014b; Reeves and Cooper, 2014). The relationship between the longitudinal and transverse morphologies of the healthy free AT during isometric contraction has been suggested to be the result of the interfascicle reorganization (Obst et al., 2014b). Overall these findings

suggest that during tensile loading, the alterations in free tendon longitudinal deformation and strain are associated with the region-specific changes in tendon transverse morphology and strain, highlighting the importance of characterizing the regional 3D morphology of the free AT during load.

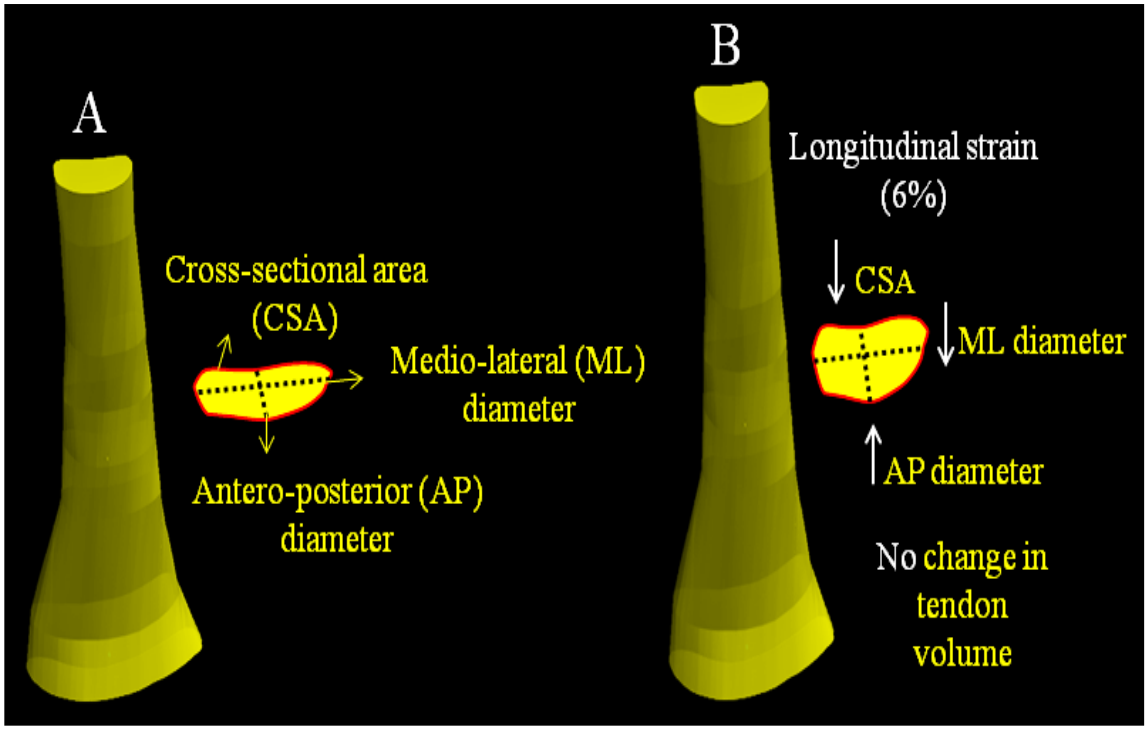

Figure 9: *An example of changes in morphology of 3D surface-rendered healthy free tendon and tendon CSA at 60% of the tendon length from resting (A) to the loading states (isometric plantarflexion contraction at 50% MVIC) (B).*

2.13 Achilles tendinopathy

2.13.1 Definition, prevalence, etiology, and impact of Achilles tendinopathy

AT disorders include chronic overuse injuries involving inflammatory and degenerative changes within the tendon and surrounding tissues as well as acute and chronic tendon

ruptures (Asplund and Best, 2013; Järvinen et al., 2005). The degenerative disorders of the AT are referred to as "tendinopathy" in the literature (Maffulli, 1998). Mid-portion Achilles tendinopathy accounts for 55-65% of all AT disorders (Kvist, 1990) and is characterised by impaired performance, morning stiffness, and pain and swelling in the mid-portion of the tendon, typically located 2-7 cm proximal to the calcaneal insertion (Maffulli, 1998; Van Dijk et al., 2011). Achilles tendinopathy occurs frequently in competitive and recreational athletes involved in track and field (Lopes et al., 2012), racquet sports (Fahlström et al., 2002), volleyball and soccer (Jhingan et al., 2011; Maffulli et al., 2004), and it is also common in the general population (de Jonge et al., 2011). The etiology of the Achilles tendinopathy in known to be multi-factorial and can be caused by an interaction between intrinsic and extrinsic factors (Maffulli et al., 2004). The intrinsic factors such as genetics (El Khoury et al., 2016), gender (Andrew and Jonathan, 2014), age (Aiyegbusi et al., 2016), lower limb biomechanical abnormalities (e.g., limited ankle dorsiflexion and hyperpronation and altered knee kinematic) (Azevedo et al., 2009; Nigg, 2001), muscle weakness and imbalance (Debenham et al., 2016; Wyndow et al., 2013), and extrinsic factors such as excessive and repetitive loading (Åström, 1997; Maganaris et al., 2004), training errors (Oestergaard Nielsen et al., 2012), inappropriate footwear (Lorimer and Hume, 2014), and poor environmental conditions, such as cold weather and hard ground surface (Järvinen et al., 2005) have been proposed as possible predisposing factors for Achilles tendinopathy. It has been reported that Achilles tendinopathy has a substantial negative socioeconomic impact and frequently causes considerable morbidity and functional impairment such as limited ability to walk, climb stairs, or participate in

recreational activities and may lead to sport cessation for long periods (Hopkins et al., 2016).

2.13.2 Histopathological findings in tendinopathy

Studies of the histopathology of the tendinopathic tendon have demonstrated: (1) degeneration, fragmentation, thinning and disorganized arrangement of collagen fibers (Pingel et al., 2014), (2) hypervascularity (i.e., proliferation of capillaries and arterioles in the tendon core and peri-tendinous tissue) (Åström and Rausing, 1995), (3) hypercellularity (e.g., increase in the number of tenocytes without their normal, fine spindle shape and with more rounded nuclei (Figure 10A,B) (Andersson et al., 2011a; Andersson et al., 2011b; Åström and Rausing, 1995), (4) increase in inter-fibrillar ground substance and grayish discoloration of ground substance (Kleiner, 1998), (5) increase in concentration of proteoglycan/glycosaminoglycan in tendon matrix (Corps et al., 2006), (6) neovascularization (i.e., appearance of abnormal vessels) and the ingrowth of the neonerves (De Jonge et al., 2014; Yang et al., 2012), (7) increase in expression of the messenger RNA of collagen type III and degradation of collagen type I (Maffulli et al., 2000; Pingel et al., 2014), (8) accumulation of free and bound water molecules in tendon matrix (de Mos et al., 2007), (9) and presence of apoptotic cells (Pearce et al., 2009).

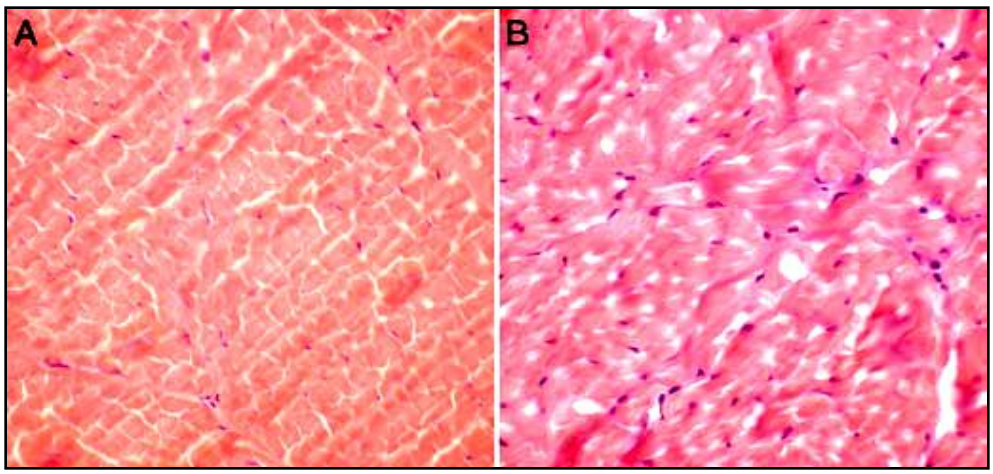

Figure 10: *Transverse sections of healthy (A) and tendinopathic (B) rabbit Achilles tendon tissue stained with haematoxylineosin. In (A) the tenocytes are moderate in number and are seen in parallel rows between uniform and well organized collagen fibers. In (B) the tenocytes are numerous and look abnormal and the collagen fibers are irregular, thin, wavy, angulated, and fragmented. Adapted from Cetti et al. (2003).*

2.13.3 Clinical examination and presentation of Achilles tendinopathy

The diagnosis of Achilles tendinopathy is mainly based on the patient's history and detailed clinical examination (Maffulli et al., 2003). The subjective assessment of patients with Achilles tendinopathy includes a thorough history of the injury mechanism, previous AT problems and treatments, onset of symptoms, duration, aggravating factors, the relation of symptoms to various activities, intensity of training, and exercise technique. The clinical examination includes a thorough observation and inspection of the foot and heel for any deformity, malalignment, previous scars, asymmetry in the AT size, and localized AT swelling and thickening (Figure 11A). The palpation of AT is also performed by gently palpating and squeezing the AT between thumb and index finger from the calcaneal

insertion to the soleus muscle-tendon junction to detect any pain, tenderness, thickening, and creptation in tendon (Figure 11B) (Cook et al., 2002; Kader et al., 2002; Maffulli et al., 2003). The patients are also requested to fill in the Victorian Institute of Sports Assessment-Achilles (VISA-A) questionnaire. The VISA-A questionnaire consists of 8 questions based on visual analogue score and assesses pain, function, and activity. Questions 1 to 7 are scored out of 10, and question 8 is scored out of 30. The scores range from 0 to 100, where 100 represents no symptoms and normal function. The VISA-A questionnaire provides a valid, reliable, and user friendly index of the severity of Achilles tendinopathy (Robinson et al., 2001). It has been suggested that tendon symptoms present for less than 2 weeks be described as “acute”, for 2–6 weeks as “sub-acute”, and for more than 6 weeks as “chronic” (El Hawary et al., 1997). Generally, in the acute and sub-acute phase of the Achilles tendinopathy, the tendon is swollen and edematous, and on the palpation, pain, tenderness, and crepitation are evident at 2-7 cm proximal to calcaneal insertion. In chronic Achilles tendinopathy, the pain is still the main symptom, but the tendon edema, effusion, and crepitation are reduced and a tender localized nodular swelling is more evident in tendon (Khan et al., 1999; Longo et al., 2009).

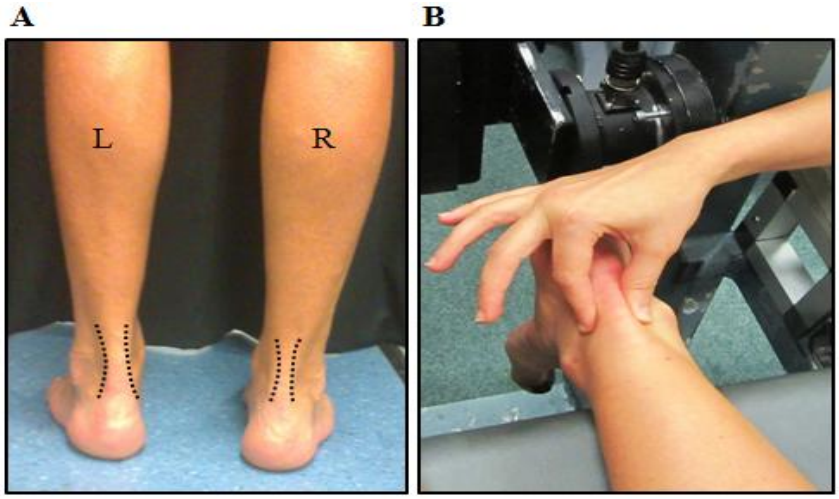

Figure 11: *An example of clinical examination of a patient with Achilles tendinopathy. (A) Observation: the picture shows swelling and thickening over the involved Achilles tendon (AT) (left side) of a patient with mid-portion Achilles tendinopathy in standing position. Black dotted lines outline the AT. (B) Palpation: the patient is positioned prone with his feet off the end of the plinth. Palpation of the AT is performed by gently palpating and squeezing the AT between thumb and index finger from the calcaneal insertion to the soleus muscle-tendon junction. The patient is asked to report any pain and tenderness during tendon palpation. L; left, R; right.*

2.13.4 Imaging of Achilles tendinopathy

2DUS and MRI are the current imaging modalities of choice for verifying the existence and location of the lesions in patients with Achilles tendinopathy. Extensive pathological alterations such as increase in tendon CSA (Arya and Kulig, 2010; Child et al., 2010; Docking and Cook, 2015; Leung and Griffith, 2008), increase in tendon AP diameter (Figure 12A,B) (Alfredson et al., 2014; Cassel et al., 2015; Chang and Kulig, 2015; Docking et al., 2015; Grigg et al., 2012; Lind et al., 2006; Van Schie et al., 2010), increase

in tendon volume (Gärdin et al., 2006; Gärdin et al., 2010; Shalabi et al., 2004a; Shalabi et al., 2004b; Shalabi et al., 2005), focal hypoechoic intratendinous areas and calcification (Blankstein et al., 2001; Fornage, 1986; Leung and Griffith, 2008; Ryan et al., 2010), discontinuity of the collagen fibers (Blankstein et al., 2001), loss of fascicle organization and interrupted appearance of tendon tissue (Fredberg and Stengaard-Pedersen, 2008), neovascularization (Van Snellenberg et al., 2007; Yang et al., 2012), thickening of the paratenon with poorly defined borders (van Sterkenburg and van Dijk, 2011), adhesion between the epitenon and paratenon (Benazzo et al., 2000), and partial rupture (Åström, 1998; Fornage, 1986) have been identified with US and MRI in previous *in vivo* studies in patients with chronic Achilles tendinopathy. These US and MRI findings in tendinopathy correlate well with the histopathological findings of tendinopathy. For example, the AT degeneration areas evident as an increased signal on MRI and as hypoechoic region on US correspond with areas of disorganized collagen fibers, increased interfibrillar ground substance and increased concentration of proteoglycan/glycosaminoglycan (Gärdin et al., 2006; Movin et al., 1998a; Movin et al., 1998b).

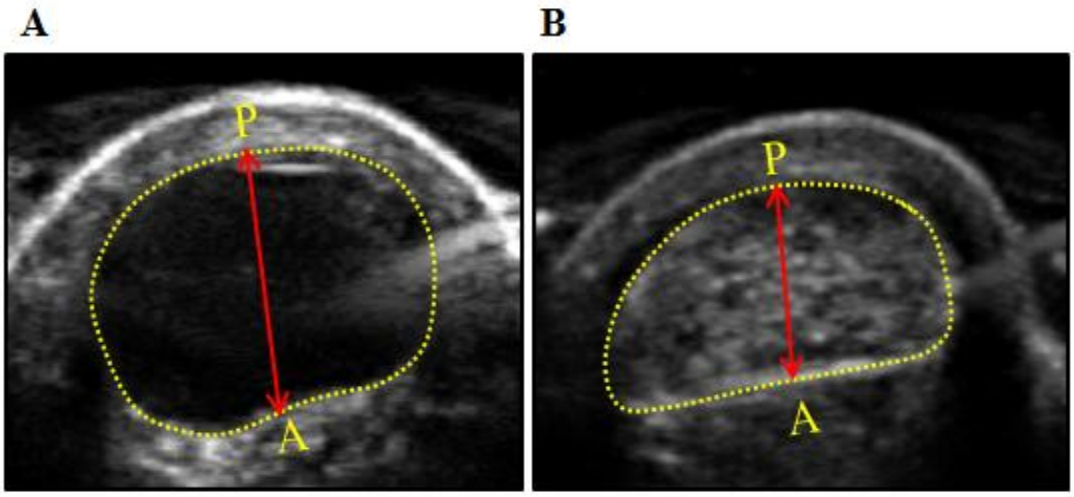

Figure 12: *The transverse two-dimensional ultrasound images of a tendinopathic (A) and the corresponding control healthy matched Achilles tendon (B) at 60% of the tendon length in a patient with mid-portion Achilles tendinopathy. Yellow dotted line outlines the Achilles tendon cross-sectional area. Red solid double-headed arrow indicates tendon antero-posterior diameter. A; anterior, P; posterior.*

2.13.5 Altered plantarflexor and dorsiflexor muscle activities in chronic Achilles tendinopathy

Achilles tendinopathy is associated with altered plantarflexor and dorsiflexor muscle activations (Azevedo et al., 2009; Baur et al., 2011; Debenham et al., 2016; Wyndow et al., 2013). Debenham et al. (2016) demonstrated a delay in soleus onset, tibialis anterior peak, and tibialis anterior offset timing during a sub-maximal hopping task in individuals with chronic Achilles tendinopathy compared to healthy control group. Wyndow et al. (2013) similarly reported a delay of ~18 ms in relative offset timing between soleus and lateral gastrocnemius muscle during a over-ground running task in regular runners with Achilles tendinopathy compared to healthy controls. A reduction in muscle activity of the tibialis

anterior and gastrocnemius muscle during the critical pre-and post-heel strike and weight bearing periods of the running cycle during a running task in runners with Achilles tendinopathy in comparison with the matched control runners has been also reported by Azevedo et al. (2009) and Baur et al. (2011). Overall, the finding that the plantarflexor and dorsiflexor muscle activities are altered in people with Achilles tendinopathy suggests that the intra-tendinous loading pattern in tendinopathic AT may be altered, which may lead to further pathological changes within tendon.

2.13.6 Altered Achilles tendon mechanical and material properties in chronic Achilles tendinopathy

The pathological alterations in AT structure and composition associated with tendinopathy, as discussed above, have been shown to adversely affect whole AT mechanical and material properties in previous *in vivo* studies (Arya and Kulig, 2010; Chang and Kulig, 2015; Child et al., 2010; Kulig et al., 2016; Wang et al., 2012). For example, it was shown that the tendinopathic ATs had a lower stiffness and Young's modulus (Arya and Kulig, 2010; Chang and Kulig, 2015) and exhibited higher longitudinal strain (Child et al., 2010) relative to the contralateral healthy, and the age- and gender-matched healthy controls during a maximum voluntary isometric plantarflexion contraction. Likewise, Kulig et al. (2016) who investigated the relationship between tendon micro-morphology and tendon mechanical properties in individuals with Achilles tendinopathy reported a lower stiffness and elastic modulus in tendinopathic tendon compared with the contralateral and healthy control tendons, which were highly correlated with the lower peak spatial frequency (i.e., disorganized tendon architecture) within the region of interest in tendinopathic tendon.

Furthermore, Wang et al. (2012) demonstrated a greater mechanical hysteresis and lower stored and released elastic energy in tendinopathic tendon relative to the contralateral healthy tendon in athletes with Achilles tendinopathy during a maximum voluntary isometric plantarflexion contraction and relaxation that were correlated to the decreased explosive neuromuscular performance of the athletes. Taken together, these previous findings indicate that the tendinopathic tendon is more compliant, which could affect the capacity of the triceps surae muscles to store and utilize elastic energy during functional activities and could lead to high strain injuries (e.g., rupture) and prolonged recovery time.

2.14 Load-induced changes in tendon morphology in the presence of tendinopathy

Our understanding of load-induced changes in tendon morphology in the presence of tendinopathy *in vivo* is limited to post-exercise alterations in tendon AP diameter, volume, and water content (Fahlström and Alfredson, 2010; Grigg et al., 2012; Ho and Kulig, 2016b; Shalabi et al., 2004b; Wearing et al., 2015). Grigg et al. (2012) investigated the effect of an acute bout of eccentric exercise (2 × 3 sets of 15 repetitions of eccentric heel drops) on tendon AP diameter at a single site (4 cm proximal to the calcaneal insertion) in the tendinopathic, contralateral, and healthy control matched tendons in people with Achilles tendinopathy. They observed a reduction in tendon AP diameter immediately following exercise in all three tendons, with the tendinopathic tendon undergoing less negative AP diameter strain than contralateral and healthy control tendons. Similarly, Wearing et al. (2015) reported a reduction in patellar tendon AP diameter at 0.5 and 2.5 cm distal to the patellar pole following the application of an acute bout of resistance

quadriceps exercise (45 repetitions of decline squat against an effective resistance of 145% body weight) in the tendinopathic, contralateral healthy and healthy control sides in individuals with patellar tendinopathy. The tendon negative AP diameter strain in response to exercise in the tendinopathic side was significantly lower than those of the contralateral and healthy sides. A reduction in tendon AP diameter at three sites (3 and 4.5 cm proximal to the calcaneal insertion and the thickest part of the tendon) along the AT length in both normal tendons and tendons with structural changes after a 1-h floor-ball match has been also reported in recreational floorball players (Fahlström and Alfredson, 2010). The reduction in tendon AP diameter reported in above-mentioned studies is in agreement with a recent case study by Ho and Kulig et al. (2016b) who demonstrated an immediate decrease in patellar tendon water content using MRI following an acute bout of eccentric loading (45 repetitions of decline squat against an effective resistance of 25% body weight) in both tendinopathic and contralateral healthy sides in a female recreational basketball player with a history of patellar tendinopathy. A similar amount of decrease in patellar tendon water content was observed in both sides following the exercise. Shalabi et al. (2004b) similarly observed a reduction in AT volume measured via MRI in the tendinopathic and contralateral healthy sides in people with Achilles tendinopathy after 3 months of daily eccentric calf muscle strength training (2 × 3 sets of 15 repetitions of eccentric heel drops). The reduction in AT volume after exercise was significantly higher in the tendinopathic side relative to the contralateral side. These short-term reductions in tendon AP diameter, water content, and volume following exercise have been postulated to reflect the load-induced fluid exudation from tendon core to the peri-tendinous space and the reduction in the interfibrillar space associated with the straightening and extension of

collagen fibers (Ahmadzadeh et al., 2015; Grigg et al., 2012; Han et al., 2000; Hannafin and Arnoczky, 1994; Helmer et al., 2004; Wellen et al., 2004; Wellen et al., 2005). However, no study to date has investigated the tendinopathic tendon morphology and volume under load. Given that cyclically loading the tendon is the most common conservative treatment option in people with tendinopathy in rehabilitation settings (O'Neill et al., 2015), there is a need to understand the morphology and volume of the tendinopathic tendon during tensile loading. This could provide valuable information regarding the possible mechanisms by which the cyclic loading can alleviate tendon pain and restore its function (O'Neill et al., 2015; Rio et al., 2015).

2.15 Evidence of load-induced fluid exudation from tendon core to the peri-tendinous space

Tensile loading of the tendon causes extrusion of fluid from the core to the periphery of the tendon (Ahmadzadeh et al., 2015; Han et al., 2000; Hannafin and Arnoczky, 1994; Helmer et al., 2004; Wellen et al., 2004; Wellen et al., 2005). To directly measure the fluid dynamics in tendon during tensile loading, the apparent diffusion coefficient (ADC) of the tendon fluid has been measured along two directions (i.e., parallel and perpendicular to the long axis of the tendon) in New Zealand white rabbit AT under different mechanical loading conditions (500 g mass and 5 N) using a nuclear magnetic resonance spectroscopy. The ADC of the entire tendon along both directions was found to increase when the tendon was loaded and the increase in the direction perpendicular to the tendon long axis was approximately 2.5 times greater than that in the parallel direction. The increase in absolute ADC in both directions during mechanical loading was attributed to the fluid transport

model, whereby fluid was transported from the core of the tendon, where there are significant barriers to diffusion to a bulk phase outside of the tendon with no restrictions to diffusion (Han et al., 2000; Wellen et al., 2004). In order to test this model, the ADC and the rate of proton density of the rabbit AT core and its periphery space were measured simultaneously during tensile loading (5 and 10 N) using three-dimensional MRI. As expected, loading caused the fluid ADC to drop in the central core region, where the extruded fluid originates, and rise in the periphery space, where the extruded fluid accumulates (Figure 13) (Helmer et al., 2004; Wellen et al., 2005). Similarly, the application of 100 g static and cyclic tensile loading to canine flexor tendons was shown to result in a significant loss of water from tendon core (Hannafin and Arnoczky, 1994).

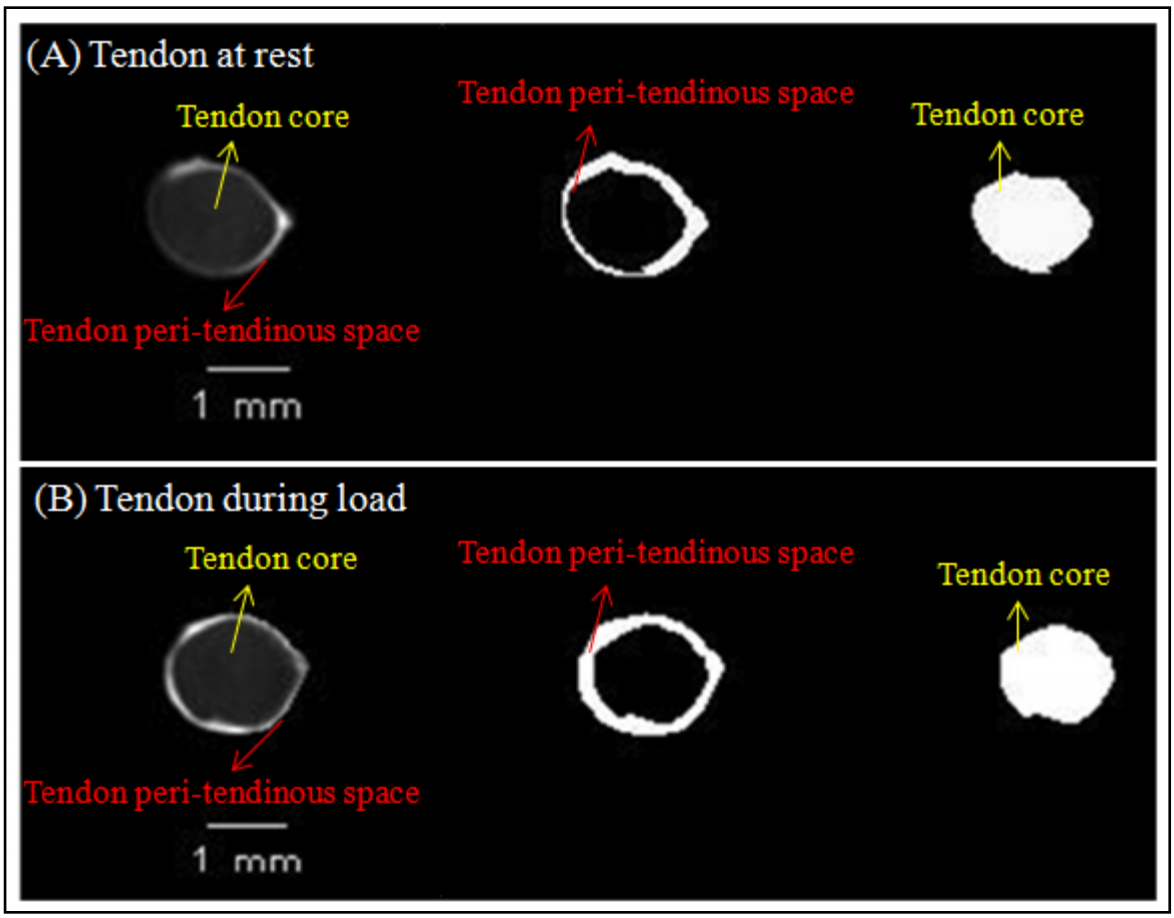

Figure 13: *Changes in rabbit Achilles tendon fluid apparent diffusion coefficient and proton density in tendon core and the peri-tendinous space from the resting (A) to the loading states (B). Adapted from Wellen et al. (2005).*

Additionally, Ahmadzadeh et al. (2015) recently presented a novel computational model to attribute the macroscopic tendon poroelastic behavior to the microscopic mechanism of the load transfer between tendon fibrils during tensile loading. Their model could predict the following key findings: (1) during tensile loading, the interfibrillar-linkers pull the tendon fibrils toward each other and generate a compressive force exerted on tendon matrix, leading to the radial fluid exudation from core to the surrounding medium and volume reduction; (2) during tensile loading, lateral fibril contraction generates a positive fluid

pressure along the length of the tendon fibril; and (3) the lateral fibril contraction, the compressive force, positive fluid pressure, and the resultant fluid exudation from core during tensile loading are most pronounced at the ends of the tendon fibrils and are lowest in the interior regions (Figure 14).

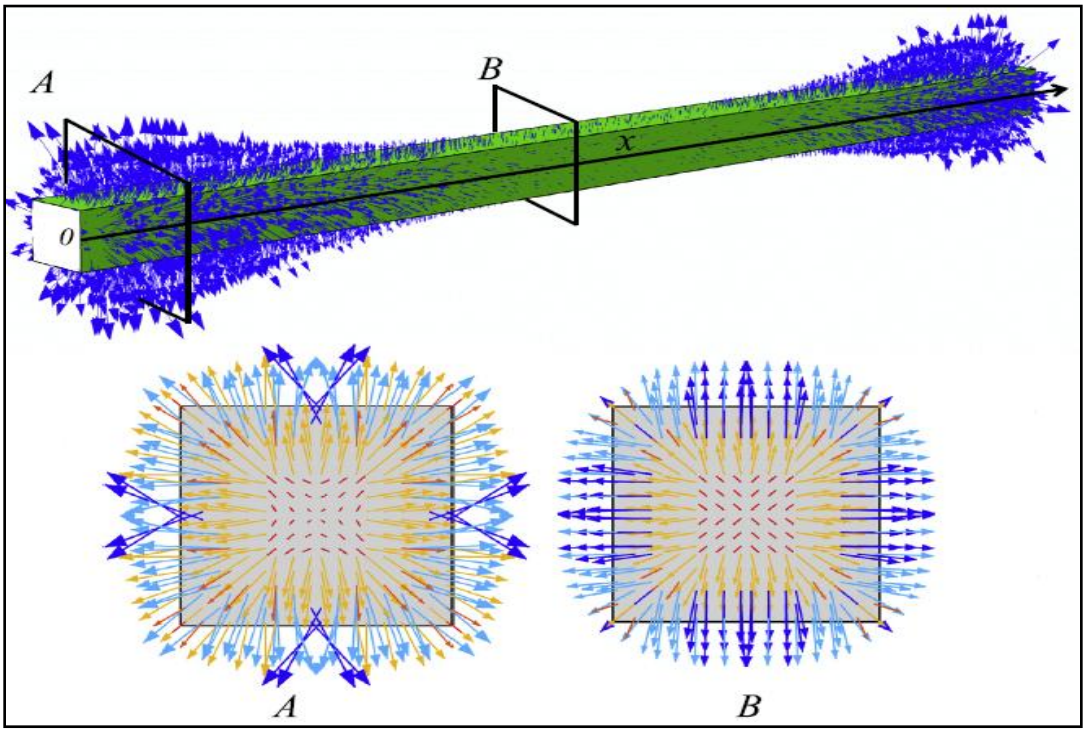

Figure 14: *Fluid exudation pattern during a tensile strain of 3% along the tendon fibril. Two cross-sections (A) and (B) illustrate the fibril region-specific fluid exudation velocity magnitude. The magnitude of fluid exudation velocity at cross section (A) (near the fibril ends) is larger. Adapted from Ahmadzadeh et al. (2015)*

2.16 Widespread development of tendon injury from injury location

The pathological alterations associated with tendon injury affect the entire tendon length and are not localised to the focal injury site (Cetti et al., 2003; Choi et al., 2016; Jacobsen et al., 2015; Smith et al., 2008). For example, Smith et al. (2008) demonstrated

degenerative histologic, immunohistochemical, molecular, and gene expression changes throughout the whole length of the infraspinatus tendon in an ovine model four weeks after 50% of the fibers were surgically transected at the mid-portion of the tendon. Jacobsen et al. (2015) found similar pathological changes in histology and gene expression of the equine forelimb superficial digital flexor tendon at least 10 cm proximal and distal to the injury site six weeks after a lateral hemi-transaction of the tendon in the mid-metacarpus, suggesting rapid and active development of tendinopathy throughout the entire tendon length. Choi et al. (2016) extended the findings of Jacobsen et al. (2015) using the same tendon samples by investigating the tendon biomechanical properties (i.e., elastic modulus and ultimate tensile strength) at different tendon regions and its association with tendon glycosaminoglycan content. They found that the induced localised tendon injury resulted in widespread increase in tendon glycosaminoglycan content with concomitant reduction in tendon elastic modulus and ultimate tensile strength throughout the entire tendon length (Figure 15). Furthermore, in a study of 60 cases of human AT rupture, Cetti et al. (2003) observed collagen degeneration, tenocyte necrosis, and acute inflammation not only constantly at the site of AT rupture, but also in most cases in the proximal part of the tendon and at the site of insertion (~90%), indicating that the entire tendon is involved in the pathological process.

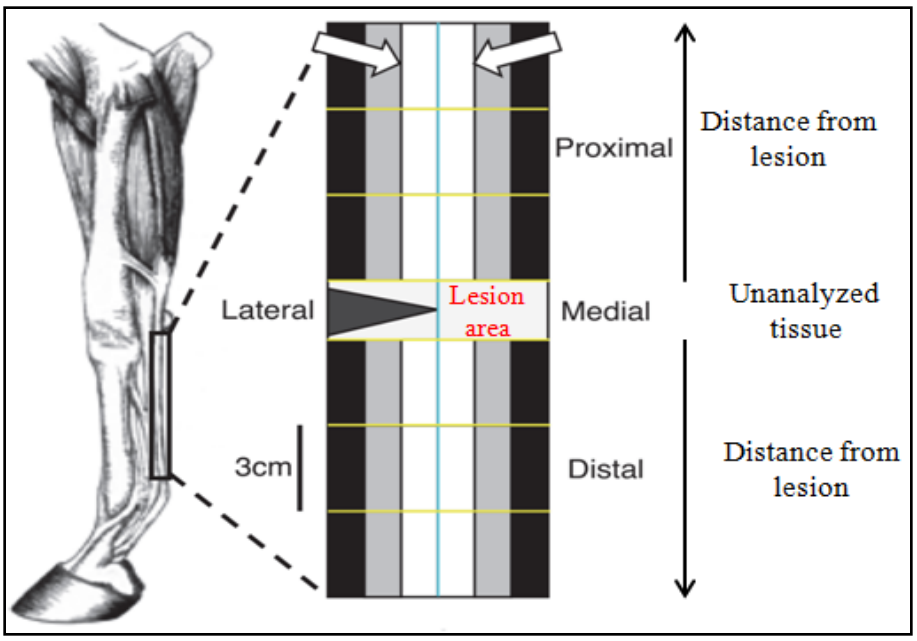

Figure 15: *Equine forelimb superficial digital flexor tendon injury model. The whole tendon was divided into 12 regions; longitudinally into lateral and medial and transversely into three regions proximal to the lesion and 3 regions distal to the lesion area in each of the medial and lateral halves. Gray, white, and black regions were allocated to biomechanical, histology, and gene expression analysis, respectively. Adapted from Jacobsen et al. (2015) and Choi et al. (2016).*

2.17 Pathological alterations in contralateral healthy tendon in the presence of unilateral tendinopathy

Pathological changes in tendon histology, structure, and morphology evident in the tendinopathic side are also present within the contralateral healthy tendon (Andersson et al., 2011b; Cetti et al., 2003; Docking and Cook, 2015; Docking et al., 2013; Docking et al., 2015; Grigg et al., 2012; Paavola et al., 2000; Williams et al., 1984). Andersson et al. (2011b) showed increase in New Zealand white rabbit AT tenocyte number and vascularity

in both legs after 3 and 6 weeks of mechanically inducing tendinopathy via repetitive passive ankle dorsiflexion and plantarflexion exercise in one AT. William et al. (1984) observed a similar histopathological changes in both equine digital flexor tendons after unilateral injection of collagenase and inflammatory substance. Cetti et al. (2003) also observed a histopathological appearance of human AT rupture specimens (e.g., collagen degeneration, tenocyte necrosis, and acute inflammation) in unaffected contralateral tendons in 47 out of 50 patients with unilateral AT rupture. Additionally, it has been shown that the contralateral healthy tendon has less aligned fibrillar structure (i.e., echo-type I + II) and more disorganized tissue (i.e., echo-type III+IV) (Docking and Cook, 2015; Docking et al., 2013; Docking et al., 2015), greater CSA (Docking and Cook, 2015; Docking et al., 2015), and greater AP diameter (Docking and Cook, 2015; Grigg et al., 2012) compared to healthy matched control tendons in people with unilateral Achilles tendinopathy, suggesting that the contralateral tendon structure and morphology are compromised in the presence of unilateral Achilles tendinopathy. The possible mechanisms proposed for the development of the tendinopathic characteristics in the conralateral tendon in the literature are: (1) altered biomechanical and neuromuscular characteristics associated with tendinopathy (Azevedo et al., 2009; Munteanu and Barton, 2011), (2) the systemic and central neuronal mechanisms (Andersson et al., 2011b; Cetti et al., 2003; Williams et al., 1984), (3) and genetic and demographic factors (Franceschi et al., 2014; Gaida et al., 2009; Nell et al., 2012; September et al., 2016). However, previous *in vivo* studies investigating the mechanical properties of AT in people with unilateral Achilles tendinopathy reported no significant differences in tendon AP diameter strain following exercise (Grigg et al., 2012) and tendon stiffness and Young's modules during a

maximum voluntary isometric plantarflexion contraction (Chang and Kulig, 2015; Kulig et al., 2016) between the contralateral and healthy matched control tendons. This supports the recently proposed iceberg theory, which describes the continuum model of tendon pathology ranging from pathological findings in tendon structure and composition to symptomatic clinical presentation (Abate et al., 2009), suggesting that the pathological alterations in contralateral tendon may need to progress along the continuum model to a point associated with critical threshold of tendinopathic symptoms before the mechanical properties of the tendon are affected. Indeed, it has been shown that 41% of people initially presenting with unilateral Achilles tendinopathy developed clinical tendinopathic symptoms in the contralateral tendon during an 8-year longitudinal study (Paavola et al., 2000).

2.18 Summary

- Conditioning of tendon is an important tendon viscoelastic property. Our knowledge regarding human AT conditioning effects is only confined to the whole AT longitudinal deformation and strain. As the longitudinal tensile deformation and strain behavior of the whole human AT varies between the proximal AT and free AT and free AT longitudinal deformation and strain are associated with the region-specific transverse morphology deformation and strain within the tendon, the conditioning effects measured at the level of the whole AT may not reflect the 3D deformation of AT at the regional level during conditioning. Therefore, there is a need to investigate the regional 3D deformation of human AT during conditioning.

- Conditioning effects are transient and recoverable. Failure to account for the time course of recovery from conditioning during mechanical testing has the potential to lead to errors in estimates of tendon mechanical properties, particularly if the recovery time between conditioning and the actual mechanical testing is long. Although, several studies have reported the recovery of human AT from fatigue loading, no study, to date, has investigated the recovery of the AT following a conditioning protocol. The fatiguing exercise interventions are usually performed after a conditioning or warm-up protocol, and therefore are unable to distinguish between recovery from conditioning compared to recovery from conditioning plus fatigue loading. Therefore, there is a need to investigate the recovery of AT following a standardized conditioning protocol only.

- MAT is a debilitating musculoskeletal condition, causing disability and functional impairment in competitive and recreational athletes as well as general population. Extensive pathological changes in free tendon structure, morphology, and composition accompanying MAT have been demonstrated in previous studies. The pathological alterations associated with tendinopathy in animal models have been shown to affect the entire tendon length and are not localised to the injury site. However, the alterations in free tendon transverse morphology (i.e., increase in tendon CSA and AP diameter) in individuals with MAT have only been reported at the single site of the injury location and no study, to date, has investigated the tendon transverse morphology along the whole tendon length. Furthermore, the pathological alterations in free tendon structure and composition have been shown to adversely affect AT mechanical and material properties. However, no study, to date, has examined the tendinopathic free tendon 3D morphology and volume during load *in vivo* and our understanding of load-induced changes in tendinopathic free tendon morphology is only confined to the post-exercise alterations in tendon AP diameter, volume, and water content. Investigation of 3D morphology and volume of the tendinopathic free tendon during load could advance our understanding of the tendinopathic tendon physiology, mehanobiology, and the possible mechanisms (e.g., fluid redistribution from tendon core to the peri-tendinous space) by which the cyclic loading can reduce tendon pain and restore its function. Additionally, the pathological alterations in tendon composition, structure, and morphology evident in the tendinopathic side have been shown to be present in the contralateral tendon. Characterizing the contralateral tendon

transverse morphology and volume at rest and under load could broaden our understanding of the extent that contralateral tendon morphology and structure are compromised in the presence of unilateral MAT.

- To our knowledge, no study has investigated the 3D morphological deformation and volume of the AT in the presence of MAT during repeated loading. Given the importance of AT repeated loading in mechanical tests, physical activities, and treatment protocols in individuals with MAT and the regional 3D deformation of AT during load, there is a need to investigate the effect of MAT on AT 3D deformation during repeated loading at the whole and regional level. Such information would give insight into interaction between the solid and fluid components of tendinopathic tendon matrix during repeated loading.

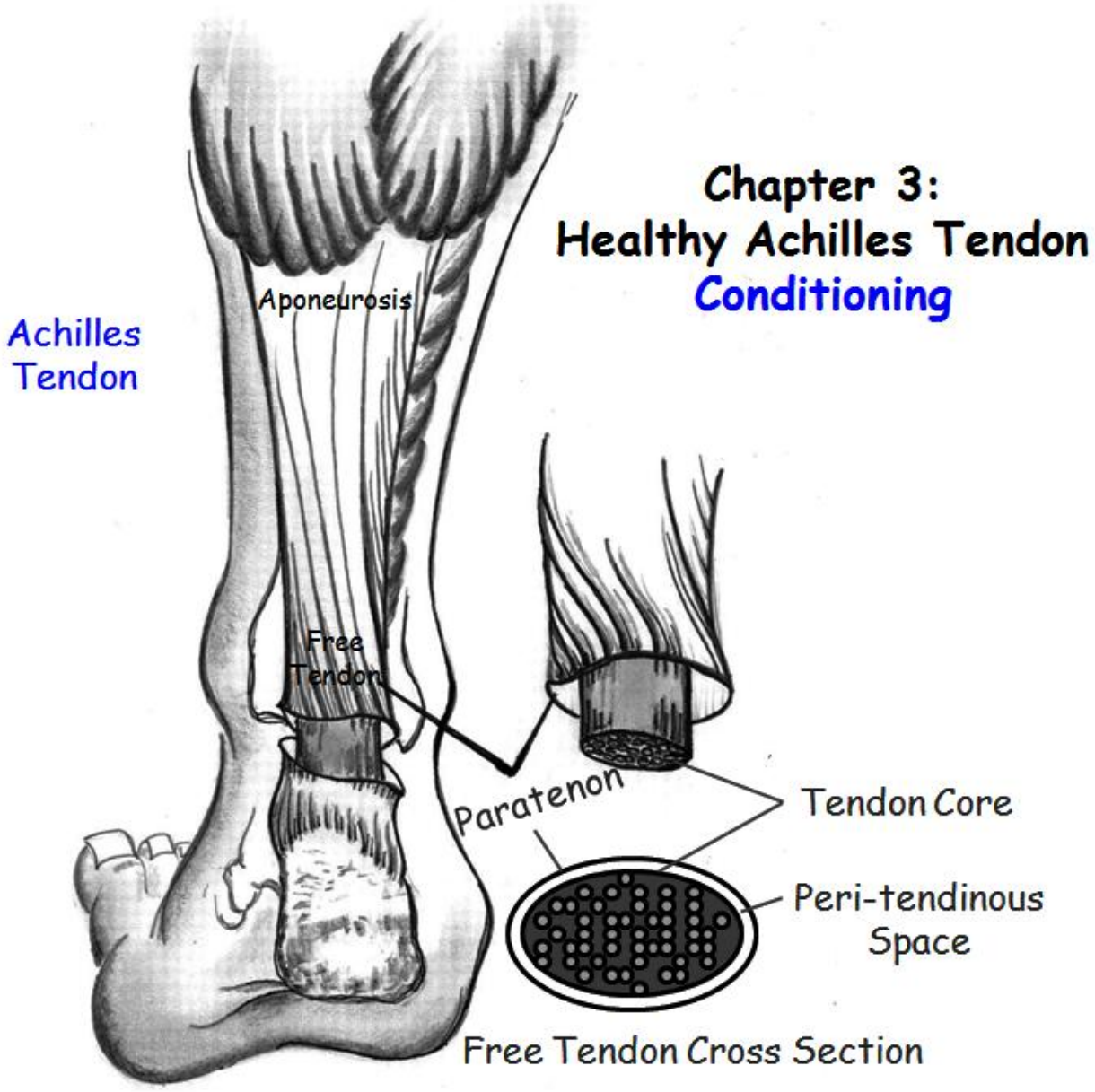
Chapter 3:
Healthy Achilles Tendon
Conditioning
Achilles
Tendon
Aponeurosis
Free
Tendon
Paratenon
Tendon Core
Peri-tendinous
Space
Free Tendon Cross Section

Chapter 3. Regional three-dimensional deformation of human Achilles tendon during conditioning

Acknowledgement of co-authorship:

This chapter includes a co-authored paper that has been re-formatted for this thesis. The bibliographic details/status of the co-authored paper, including all authors, are:

L. Nuri, S. J. Obst, R. Newsham-West, R. S. Barrett (2016). "Regional three dimensional deformation of human Achilles tendon during conditioning." Scandinavian Journal of Medicine & Science in Sports (SJMSS). **DOI: 0.1111/sms.12742.**

I have made a substantial contribution in the conception and design of this study, analysis and interpretation of the research data, and the drafting and critical revising of the final manuscript.

(Signed) Leila Nuri (Date) 10th March 2017

Student/corresponding author: Leila Nuri

(Countersigned) _____ (Date) _____

Principal Supervisor: Rod Barrett

(Countersigned) _____ (Date) _____

Principal Supervisor: Richard New-sham West

3.1 Abstract

Our understanding of *in vivo* Achilles tendon (AT) conditioning is limited to two-dimensional ultrasound measures of longitudinal deformation of the whole tendon. This study investigated the regional three-dimensional (3D) deformation of the AT during conditioning. Eighteen ATs were scanned using 3D freehand ultrasound during 10 successive 25-s submaximal (50%) voluntary isometric plantarflexion contractions. Longitudinal strain was assessed for the whole AT, proximal AT, and free AT and transverse strain was assessed for the proximal-, mid-, and distal portions of the free AT. Longitudinal conditioning of the whole AT was primarily driven by creep response of the free AT and transverse conditioning was greatest for the mid-portion of the free AT. Whole and free AT longitudinal strain increased up to the third contraction and were accompanied by a corresponding reduction in free AT cross-sectional area (CSA) strain in proximal-, mid-, and distal portions. No significant changes in proximal AT strain or tendon volume were detected between contractions. These findings suggest that conditioning alters free AT shape, with increased tendon length attained at the expense of reduction in free AT CSA. Although AT experiences different amounts of strain in different regions, the number of contractions required to reach steady-state strain during conditioning is uniform throughout the tendon.

3.2 Introduction

Tendon conditioning involves the repeated application of a tensile load to the tendon in an effort to minimize the influence of tissue creep when measuring mechanical properties during mechanical testing. Micro-structural alterations, such as collagen fiber un-crimping, recruitment, re-alignment, fascicle/fiber sliding, and interstitial fluid flow have been proposed as possible mechanisms of conditioning (Grigg et al., 2010; Houssen et al., 2011; Miller et al., 2012b; Schatzmann et al., 1998). The conditioning effects are non-damaging and transient, but must be considered when assessing tendon mechanical properties (Seynnes et al., 2015). It is therefore customary when assessing the mechanical properties of tendons to condition the tendon via repeated application of a tensile load prior to performing mechanical tests.

Mechanical properties of the *in vivo* Achilles tendon (AT) are frequently reported in the literature and most studies include some form of conditioning protocols prior to mechanical testing (Lichtwark et al., 2013b; Magnusson et al., 2003; Obst et al., 2015a; Peltonen et al., 2012). Despite the importance of tendon conditioning in mechanical testing, few *in vivo* studies have investigated the AT conditioning process itself. In *vivo* conditioning of the human AT was first addressed by Maganaris (2003), who used two-dimensional (2D) ultrasound to examine the effect of 10 successive 4-s isometric plantarflexion contractions to 80% of maximum voluntary isometric contraction (MVIC) on longitudinal deformation of the whole AT (i.e. gastrocnemius muscle-tendon junction (MTJ) to calcaneus). The loading protocol caused tendon elongation to increase by 5 mm from the first contraction to the tenth contraction, with no significant changes in length

obtained after the fifth contraction. More recently Hawkins et al. (2009) used a similar method to investigate the effect of 7-min of 0.75 Hz cyclic plantarflexion contractions at 25–35% MVIC on dynamic creep response of whole AT. It was suggested that a minimum of 270 loading cycles or a 6-min warm-up is required for the whole AT to reach a relatively steady state behavior. Since both Maganaris (2003) and Hawkins et al. (2009) reported conditioning of the whole AT, it is not possible to determine the relative contributions of the free tendon (i.e. soleus MTJ to calcaneus) and proximal AT (i.e. gastrocnemius MTJ to soleus MTJ) to the conditioning effect. Studies have consistently highlighted the non-uniform nature of AT mechanical properties between the free AT and proximal AT, with the free AT demonstrating greater compliance compared to the proximal AT during mechanical testing both before (Farris et al., 2013b; Finni et al., 2003; Magnusson et al., 2003) and following exercise-induced fatigue loading (Lichtwark et al., 2013b; Obst et al., 2015a). The free AT also experiences torsion of tendon fascicles (Edama et al., 2015b; Szaro et al., 2009), and has a high fiber crimp angle (Magnusson et al., 2002), and substantial fluid content (Grosse et al., 2015; Syha et al., 2014). It is therefore possible that the number of conditioning contractions required to reach steady state longitudinal strain may differ between the free AT and whole AT. Furthermore, the free AT has variable cross-sectional area (CSA) along its length (Magnusson and Kjaer, 2003; Obst et al., 2014b), reaching a minimum at around 70% of the length from the calcaneus to soleus MTJ (Obst et al., 2014b), and is known to undergo region-specific changes in CSA under tensile loading (Iwanuma et al., 2011; Obst et al., 2014b; Reeves and Cooper, 2014) that are most pronounced in the mid region (Obst et al., 2014b; Reeves and Cooper, 2014). The amount of transverse deformation and number of contractions

required for transverse conditioning could therefore also differ along the length of the free tendon.

The purpose of the present study was therefore to determine the effect of a conditioning protocol consisting of successive submaximal isometric plantarflexion contractions on the longitudinal deformation of the whole AT, proximal AT, and free AT and the transverse deformation of the free AT. We hypothesised that the longitudinal conditioning effect would be most pronounced in the free AT and be accompanied by transverse deformation that would be most pronounced in the region of the free AT where the CSA is minimal and corresponding stress concentration is the highest.

3.3 Materials and Methods

3.3.1 Participants

Eighteen healthy adults (age: 29.3 ± 3.9 years, height: 178 ± 8.5 cm, and body mass: 76.1 ± 8.2 kg) from the local university community voluntarily participated in the study following provision of written informed consent. To eliminate any potential effects of gender on tendon properties, only male participants were recruited for this study (Kubo et al., 2003). Participants were excluded if they reported any recent or current Achilles tendon pain, injury or surgery. Ethical approval was granted by the institutional human research ethics committee and the study was conducted in accordance with the Declaration of Helsinki.

3.3.2 Experimental protocol

All participants attended the laboratory on two occasions one week apart. During the first session, participants performed 3 × 5 s MVICs of the plantarflexors and dorsiflexors of the test leg, with 60-s rest periods between trials. Participants were instructed to lie in the prone position on a test bench, with their left knee and hip fully extended, and the left ankle joint in 0° dorsiflexion. The left foot was securely fastened against a fixed torque transducer (Futek TFF600, Irvine, California, USA) using a custom-built ratchet system to restrict ankle movement (Obst et al., 2014a; Obst et al., 2014b). The axis of rotation of the torque transducer was carefully aligned with the axis of rotation of the ankle joint. Real-time visual feedback of ankle joint torque was provided to the participants via a computer monitor to maintain target ankle torque during contractions. All torque data was recorded using LabVIEW data acquisition software (LabView 9.9, National Instruments, Austin, Texas, USA) sampling at 1000 Hz. Verbal encouragement during each MVIC was provided. Peak torque was recorded for each plantarflexion MVIC, and the highest MVIC value was used to determine the target torque (50% MVIC) for the subsequent testing session. Participants also performed a series of contractions to the target torque for familiarisation purposes.

Prior to the second session, participants were requested to refrain from any vigorous physical activities (e.g. running) for at least 48 hours and to use motorized transport instead of cycling or walking to reach the laboratory on the morning of the test day. Upon arrival, participants sat quietly with both feet flat on the floor for 45 min to minimize the effect of pre-loading on AT mechanical properties. All participants completed 10 × 25-s

isometric plantarflexion contractions at the target torque (50% MVIC) during which ultrasound scans of their AT and EMG data from their leg muscles were acquired using the same procedure as outlined above for the familiarization session. Resting scans were also acquired immediately before and after the 10 conditioning contractions.

3.3.3 Freehand 3D ultrasound set-up and scanning

Our freehand three-dimensional ultrasound (3DUS) set-up has been described in detail previously for morphological measurement of muscle (Barber et al., 2009) and more recently the measurement of AT mechanical and morphological properties (Obst et al., 2014a; Obst et al., 2015b). Briefly, the 3DUS system consisted of a conventional 2D ultrasound machine (SonixTouch, Ultrasonix, Richmond, BC, Canada) and a five-camera optical tracking system (OptiTrack V100:R2, Tracking Tools v 2.5.2, NaturalPoint, Corvallis, Oregon, USA). Position and orientation of the transducer in space during scanning were recorded by tracking four reflective markers rigidly attached to the transducer using the optical tracking system. A coordinate transformation was used to map the individual 2D B-mode images into global coordinate system and a 3D rendering of AT was constructed using Stradwin software (Stradwin 5.0, Cambridge University, UK; http://mi.eng.cam.ac.uk/~rwp/stradwin/). The system was calibrated prior to data collection using single wall phantom calibration protocol (Prager et al., 1998). The 3D point accuracy of spatial calibrations using an optical tracking system, and according to the single wall phantom calibrations procedure, has been reported to be less than 1 mm (0.4 mm) (Prager et al., 1998). All ultrasound scans were performed by a single investigator (L.N) using a 58-mm linear transducer (L14-5 W/60 linear, Ultrasonix, Richmond, BC, Canada) with

sampling frequency of 60 Hz and standardized image generation parameters (depth 40 mm, gain 50%, dynamic range 65 dB, map 4, power 0). To provide adequate visualization and proper contact between transducer and skin, a flexible stand-off gel pad (Ultra/Phonic Focus, Pharmaceutical Innovations Inc., Newark, New Jersey, USA) was attached to the end of the transducer using a custom-made plastic brace. Ultrasound coupling gel was applied to the skin to improve the acoustic interface and reduce friction during scanning. Prior to scanning, the anatomical locations of the calcaneal notch, soleus (SOL) MTJ, and medial gastrocnemius (MG) MTJ were visualized on real-time ultrasound using a single longitudinal 2D ultrasound scan and a line was drawn on the skin surface with a permanent marker to guide the scan direction. A series of 2D B-mode ultrasound images was then acquired by sweeping the transducer manually from the base of the heel to MG MTJ in a transverse orientation at a steady speed (~9 mm s^{-1}) (Figure 16A). The finalized reconstructed 3D images of AT consisted of approximately 1300 2D images with an average distance between frames of 0.1 mm (Figure 16B). The 3D US approach is limited to evaluating tendon morphology under static loading condition and the accuracy of measurement, particularly for tendon length, depends on the scanning time and the number of 2D B-mode images acquired during scanning (Lichtwark et al., 2013; Obst et al., 2014a). Therefore, the tendon loading condition under which the AT ultrasound scanning was performed in the present study (i.e. ~25-s isometric plantarflexion contraction at 50% MVIC) was a compromise between allowing sufficient scan time to capture a sufficiently dense ultrasound image stack, and ensuring that participants were able to maintain the target contraction intensity over the scan period (Nuri et al., 2016).

3.3.4 3D ultrasound image reconstruction and analysis

Analysis of all 3DUS scans were performed using Stradwin software as follows. Three anatomical point landmarks (calcaneal notch, SOL MTJ, and MG MTJ) were digitized manually in reconstructed 3D images using the 3D landmark tool. The approximate 3D position of each landmark was first estimated using the sagittal and coronal image re-slices and then accurately identified using the corresponding 3D transverse image slices. The most distal points where the first cross sections of MG and SOL muscle tissue were visible in the transverse images during the sweep were selected (Figure 16C). Whole AT length was defined as the point-to-point distance between the calcaneal notch and MG MTJ. Proximal AT length was defined as the point-to-point distance between MG MTJ and SOL MTJ. It is however acknowledged that this definition of proximal AT refers to only part of a larger aponeurotic structure, which surrounds the muscle bellies of the triceps surae and experiences strain due to changes in muscle shape during contraction. Free AT length was defined as the point-to-point distance between the calcaneal notch and SOL MTJ. For each tendon region, tendon elongation was obtained by subtracting tendon length in the 50% MVIC condition from the resting length. Tendon strain for each region was calculated as the ratio (%) of tendon elongation relative to the resting length. Free AT boundaries during each contraction and resting state were outlined manually from the original B-mode transverse images at each 10% interval of tendon length from the calcaneal notch to the SOL MTJ to determine free AT CSA. The free tendon was subsequently divided into distal, mid and proximal portions defined as 10%-30%, 40%-70%, and 80%-100% of the free AT length (0: calcaneal notch; 100%: SOL MTJ) (Figure 17A,B). Free tendon volume reconstruction was then performed on the segmented cross sections using the 3D rendering

algorithms in Stradwin (Treece et al., 1999) (Figure 17C,D). The accuracy of our 3DUS for measurement of volume compared with phantoms similar in size to that of the human free AT was estimated to be ± 0.05 ml (Obst et al., 2014a). Similarly, the minimal detectable change for *in vivo* free AT volume at rest using our 3DUS system was estimated to be ± 0.2 ml (Obst et al., 2014a). For each contraction, free AT CSA deformation was computed by subtracting the mean CSA of each portion in the 50% MVIC condition from the corresponding resting CSA. Tendon CSA strain for each portion of free AT was then calculated as the ratio (%) of CSA deformation relative to the corresponding resting CSA. Poisson's ratio (v) was calculated as a function of the mean CSA during each contraction at 50% MVIC ($CSA_{50\%MVIC}$) and mean CSA at rest (CSA_{Rest}) and the longitudinal free AT strain (ε_L) using the equation proposed by Vergari et al. (2011):

$$v = -0.5\left[\ln\left(\frac{\mathrm{CSA}_{50\%\mathrm{MVIC}}}{\mathrm{CSA}_{\mathrm{Rest}}}\right)/\ln(1+\varepsilon_{\mathrm{L}})\right]$$

The measurement of free AT transverse strain during tensile loading could have important implications for our understanding of the AT elastic energy storage and release action (Lichtwark and Wilson, 2006), triceps surae muscle bulging characteristics (Aziz et al., 2008), and AT in vivo mechanobiology (Wang et al., 2012).

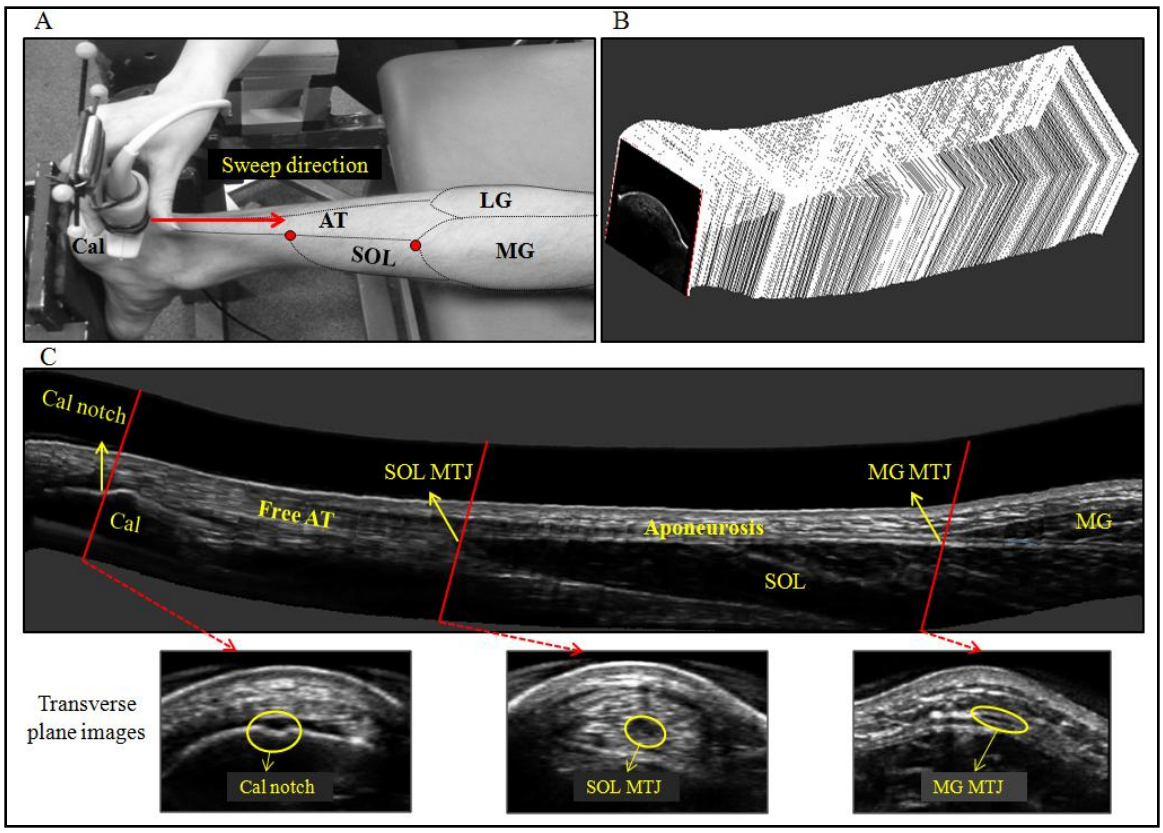

Figure 16: *Experimental setup and three-dimensional (3D) reconstruction of the Achilles tendon (AT). (A) Participants positioned prone with the left ankle in neutral position. The ultrasound transducer with four motion analysis markers was swept manually along the AT from the base of the heel to the muscle-tendon junction (MTJ) of the medial gastrocnemius muscle (MG). The arrow shows the sweep direction. (B) A typical series of two-dimensional (2D) ultrasound images based on their relative orientation to form the 3D reconstructed AT image. (C) The resultant sagittal plane re-slice of the reconstructed 3D ultrasound image of AT. The calcaneal notch (Cal notch) and MTJ of MG and soleus (SOL) were identified within the corresponding transverse images indicated by the three transverse lines.*

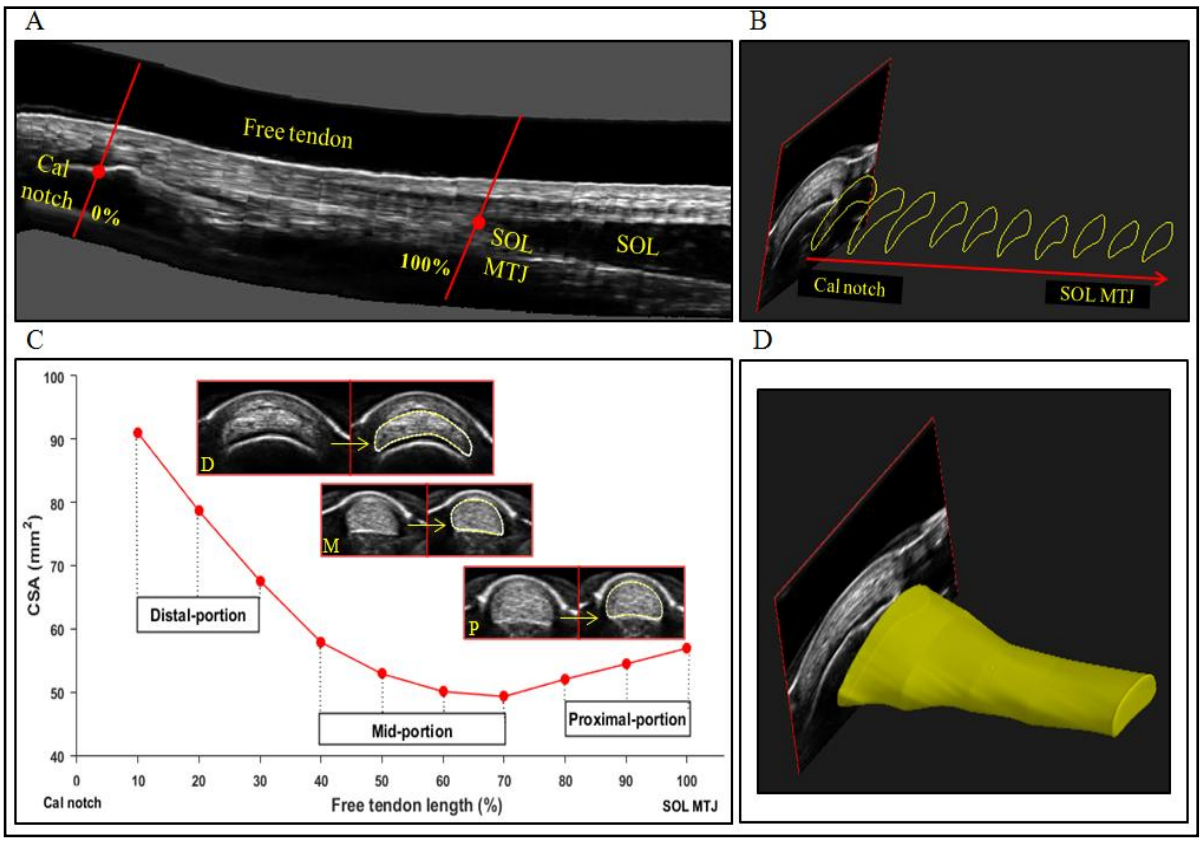

Figure 17: *An example of cross-sectional area (CSA) segmentation and three-dimensional (3D) volume rendering process of free Achilles tendon (AT). (A) The sagittal plane re-slice of the reconstructed 3D ultrasound image of free AT served to define the borders of free AT (two solid red lines) for CSA segmentation. (B) The boundaries of the free AT were outlined manually in 10% intervals of the tendon length on corresponding 3D transversal images. The graph shows tendon CSA form calcaneal notch (Cal notch) to soleus muscle-tendon junction (SOL MTJ) from a single representative participant. (C) Ten segmented CSAs along the length of the free AT. (D) 3D volume rendering of the free AT from the segmented CSAs. D, distal portion; M, mid portion; P, proximal portion.*

3.3.5 Electromyography

Surface electromyography (EMG) was recorded using a four channel double differential EMG system (Bagnoli-8™, Delsys Inc., Boston, Massachusetts, USA). To minimize skin impedance, the recording site was shaved and cleansed by mild scrubbing with 70% isopropyl alcohol (Briemarpak, Briemar Nominees Pty Ltd, Australia) and an abrasive skin prepping gel (NuPrep, DO Weaver & Co., Aurora, Colorado, USA). Surface electrodes (24 mm, model H124SG, Covidien Kendall, Neustadt, Germany) were then positioned (inter-electrode distance = 20 mm) over the central portion of the muscle bellies of MG, lateral gastrocnemius (LG), SOL, and tibialis anterior (TA) muscles in accordance with the recommendations of Hermens et al. (2000). A single, pre-gelled, disposable reference electrode (Dermatrode, American Imex, Irvine, California, USA) was placed over the fibular head. All electrodes were secured to the skin with self-adhesive compression bandage (Cohesive Bandage Latex Free, 7.5M x 4.5 M-Blue, MediChill, Wuxi, China). EMG raw signals were collected at 1000 Hz, pre-amplified (× 300) and sent to a personal computer and filtered (20-400 Hz band-pass filter, Butterworth fourth-order zero-lag filters) using custom-written program in Matlab software (version R2015a, The MathWorks, Natick, Massachusetts, USA). The filtered signals were then converted to a root mean square value (RMS) using a 20-ms non-overlapping window and normalized as a percentage of the RMS EMG activity recorded during the MVIC dorsiflexion (TA) and plantarflexion (MG, LG, SOL) trials.

3.3.6 Reliability of tendon length and CSA measurements from ultrasound

Intra-rater reliability for tendon lengths (whole AT, proximal AT, and free AT) and mean CSA measurements was evaluated from 3DUS scans of contraction 9 and 10 using the intra-class correlation coefficient (ICC), coefficient of variation (CV), and standard error of measurement (SEM). The ICCs for tendon lengths and CSA measurements were greater than 0.98 and 0.97, respectively. The mean CVs and SEMs for whole AT length were 0.05% and 0.05 mm, for proximal AT length were 0.04% and 0.07 mm, for free AT length were 0.08% and 0.08 mm, and for tendon CSA were 1.17% and 0.28 mm^2, respectively.

3.3.7 Statistical analysis

Two-way full factorial repeated measures General Linear Models were used to examine the effect of AT region (whole AT, proximal AT, and free AT) and contraction number (ten contractions) on tendon longitudinal strain and the effect of free AT region (proximal, mid, and distal portions) and contraction number (ten contractions) on tendon CSA strain. Planned contrasts (SPSS CONTRAST syntax) were used to compare tendon strain between regions for each contraction and between consecutive contractions. Furthermore, a one-way repeated measure General Linear Model was used to determine the effect of contraction number (ten contractions) on tendon volume, Poisson's ratio, ankle joint torque, and EMG activity of the MG, LG, SOL, and TA. Significance for all statistical tests was accepted at the 0.05 level of probability. All analyses were conducted using the Statistical Package for the Social Sciences version 22 (SPSS Inc, Chicago, Illinois, USA). Data are expressed as mean ± standard deviation (SD) in the text and mean ± standard error of mean (SEM) in all the figures.

3.4 Results

3.4.1 Effect of AT region and contraction number on tendon longitudinal strain

The resting lengths of the whole AT, free AT, and proximal AT prior to conditioning were 210 ± 26, 68 ± 19, and 142 ± 26 mm, respectively. The whole AT underwent the greatest elongation during conditioning (Figure 18A), whereas the free AT experienced the greatest strain (Figure 18B). There was a significant region-by-contraction interaction for tendon longitudinal strain ($F_{18,\ 306}$ = 82.98, P < 0.001). Planned contrasts revealed the free AT strained significantly more compared with the whole AT and proximal AT during contractions 2-10 (P < 0.001), with no significant differences found between whole AT and proximal AT strain (P > 0.05). Significant increases in whole AT and free AT strain were observed between contractions 1-3 (P < 0.05), with no further increases after the third contraction (P > 0.05). No significant differences in proximal AT strain were found between contractions during conditioning (P > 0.05) (Figure 18A,B).

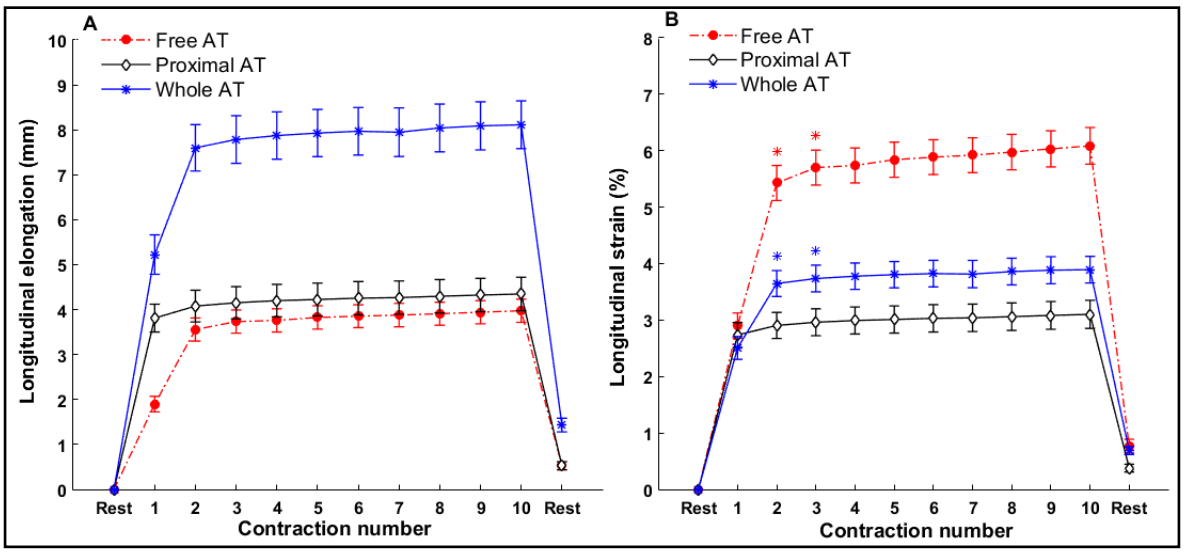

Figure 18: *Change in Achilles tendon (AT) longitudinal elongation and strain during the conditioning process. (A) The mean group elongation for the free AT, proximal AT, and whole AT during 10 successive isometric plantarflexion contractions at 50% MVIC. (B) The corresponding mean group strain for each region by contraction number. Error bars represent standard error of the mean (N = 18). Asterisk (*) indicates significant differences between contractions for each region (P < 0.05). The whole and free AT experienced a significant increase in strain from contraction 1 to 2 and 2 to 3.*

3.4.2 Effect of free AT region and contraction number on tendon CSA strain

The resting CSAs of the proximal-, mid-, and distal portions of the free tendon prior to conditioning were 54 ± 7, 52 ± 6, and 66 ± 12 mm^2, respectively. The largest CSA deformations and strains were experienced by the mid-portion of the free AT (Figure 19A,B). There was a significant region-by-contraction interaction for free AT CSA strain ($F_{18, 306}$ = 11.35, P < 0.001). Planned contrasts revealed that the reduction in mid-portion free AT CSA strain was significantly greater than for the proximal and distal portions

during each contraction ($P < 0.001$), with no significant differences in free AT CSA strain found between proximal and distal portions ($P > 0.05$). Significant decreases in free AT CSA strain were detected between contractions for the proximal-, mid- and distal portions up to and including the third contraction ($P < 0.05$) (Figure 19A,B).

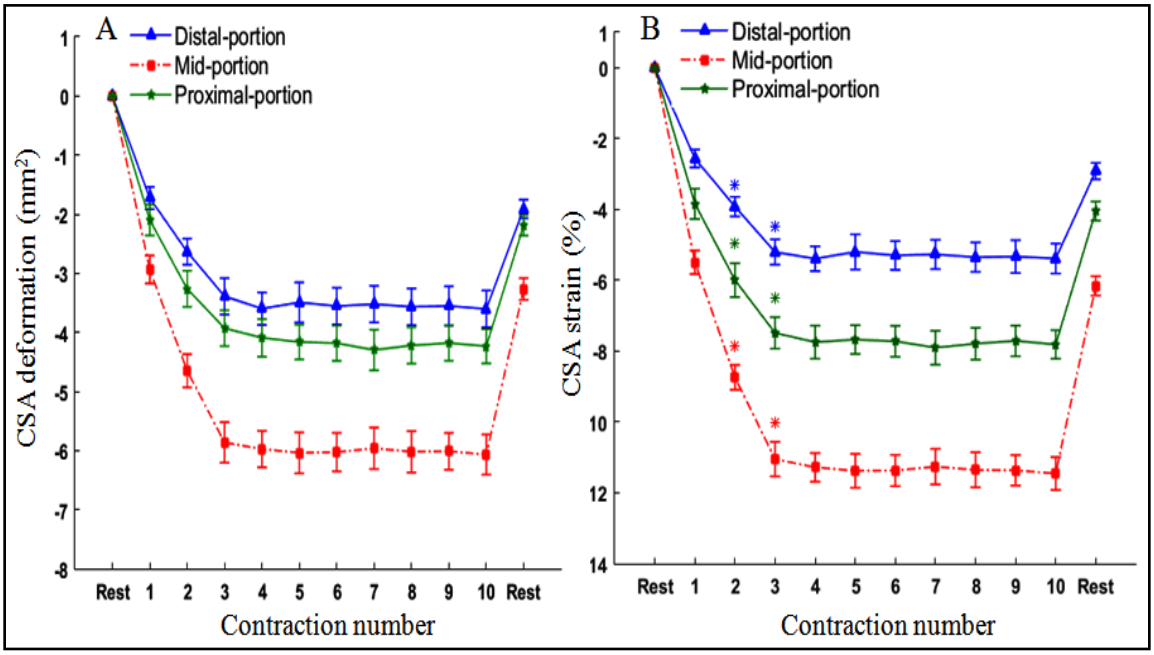

Figure 19: *Change in free Achilles tendon cross-sectional area (CSA) deformation and strain during the conditioning process. (A) The mean group CSA deformation for the distal portion, mid portion, and proximal portion during 10 successive isometric plantarflexion contractions at 50% MVIC. (B) The corresponding mean group strain for each region by contraction number. Error bars represent standard error of the mean (N = 18). Asterisk (*) indicates significant differences between contractions for each region (P < 0.05). The distal-, mid- and proximal portions of the free AT experienced a significant decrease in transverse strain from contraction 1 to 2 and 2 to 3.*

3.4.3 Effect of contraction number on ankle joint torque, EMG, tendon volume and Poisson's ratio

Group mean ankle plantarflexor torque for MVIC and submaximal contractions were 81.0 ± 25.0 N.m and 40.53 ± 12.15 N.m, respectively. The mean ankle joint torque for the resting trials was 1.1 ± 0.3%. No significant differences were found in ankle joint torque between contractions ($F_{9, 153} = 0.49$, $P = 0.87$). Group mean normalized EMG activities for MG, LG, SOL, and TA during contractions were 25.0 ± 4.2%, 22.99 ± 3.11%, 33.56 ± 9.22%, and 5.3 ± 1.71%, respectively. There were no significant differences in MG, LG, SOL, and TA EMG activities between contractions ($F_{9, 153} = 1.39$, $P = 0.19$; $F_{9, 153} = 1.45$, $P = 0.16$; $F_{9, 153} = 1.48$, $P = 0.26$; $F_{9, 153} = 0.8$, $P = 0.61$, respectively).

The resting volume of the free tendon was 3.91 ± 1.27 ml. No significant differences in free AT volume were found between contractions during conditioning (Grand mean: 3.91 ± 1.67 ml; $F_{9, 153} = 0.60$, $P = 0.79$). Similarly, no significant changes in tendon Poisson's ratio were detected between contractions (Grand mean: $v = 0.56 \pm 0.05$; $F_{9, 153} = 0.81$, $P = 0.19$).

3.5 Discussion

Prior *in vivo* studies have reported the effects of AT conditioning on longitudinal deformation for the whole AT, measured from the gastrocnemius muscle-tendon junction to the calcaneus (Hawkins et al., 2009; Maganaris, 2003). In the present study 3D deformation of the AT was evaluated during a conditioning protocol that consisted of ten consecutive 25-s plantarflexion contractions at 50% MVIC. In support of our hypothesis,

longitudinal conditioning of the whole AT was primarily driven by free AT elongation (from the soleus muscle-tendon junction to the calcaneus) and was accompanied by a corresponding reduction in CSA that was most pronounced within the mid-portion of the free AT. As no significant changes in tendon volume were detected between contractions, these findings suggest that tendon conditioning is mostly driven by a change in tendon shape, with increased tendon length attained at the expense of reduction in free tendon CSA. We also found that although tendon strain differed according to tendon region, the longitudinal conditioning of the whole and free AT, as well as the transverse conditioning of the free AT, was complete following three submaximal isometric plantarflexion contractions.

3.5.1 Three-dimensional deformation during conditioning

Longitudinal conditioning of the whole AT was found to be primarily driven by creep within the free AT. The free AT contributed ~80% of the total increase in whole AT strain during the conditioning contractions, with remainder from the proximal AT. Regional conditioning of the AT as observed in the present study is consistent with studies that demonstrated localized creep of the free tendon, over and above conditioning effects, immediately following dynamic exercise (Lichtwark et al., 2013a; Obst et al., 2015a). Isolated conditioning of the free tendon, as observed in the current study is likely due to some combination of differences in tendon structure, composition, and loading between free AT and proximal AT. Factors such as complex fascicle/fiber orientation (Edama et al., 2015a; Szaro et al., 2009), fascicle/fiber sliding as a result of elastic behavior of interfascicular matrix (Slane and Thelen, 2014; Thorpe et al., 2015b), high collagen fiber

crimp angle (Magnusson et al., 2002) as well as fluid redistribution under load (Grosse et al., 2015; Syha et al., 2014) have been reported to contribute to the unique mechanical behavior of the free AT. The free tendon is also longitudinally tensioned by forces from all three triceps surae muscles, whereas the proximal AT experiences transverse strain due to soleus muscle bulging (Bojsen-Møller and Magnusson, 2015; Farris et al., 2013a; Iwanuma et al., 2011). Given the greater relative physiological CSA of the soleus compared to gastrocnemius muscles (Fukunaga et al., 1992), differences in the magnitude and direction of the force between the free AT and proximal AT could be quite large, with the free AT experiencing more longitudinal force under a given load. These factors likely underpin the micro-structural alterations within the free AT during the conditioning process (Houssen et al., 2011; Miller et al., 2012a; Miller et al., 2012b; Schatzmann et al., 1998). Findings from the present study also indicate that failure to condition the AT before mechanical testing would lead to an underestimation of whole AT and free AT longitudinal elongation by 2.88 mm and 2.19 mm and strain by 1.37% and 3.36%, respectively, and hence lead to overestimation of tendon stiffness and modulus at the same ankle joint torque.

Free AT CSA strain measured at the proximal-, mid- and distal portions progressively increased between contractions one and three, consistent with the corresponding change in tendon longitudinal strain. These findings provide the first evidence of both longitudinal and transverse conditioning of the free AT in response to cyclic tensile loading. Our finding that the free AT volume remained unaltered by conditioning is consistent with prior studies that report isovolumetric behavior of the *in vivo* free AT under load following conditioning (Iwanuma et al., 2011; Obst et al., 2014b), and therefore suggest alterations in

longitudinal and transverse strain during conditioning are indicative of a change only in tendon shape. Our results also indicate that the transverse conditioning effects were not consistent across the length of free tendon, with the mid-portion experiencing the most pronounced changes in tendon CSA prior to reaching steady state. These findings are consistent with recent studies whereby exercise-induced changes in transverse morphology and strain of the free AT under load were localized to the mid-proximal region (Obst et al., 2015b; Obst et al., 2014b). There are several potential factors contributing to the greater amount of strain in the mid compared to the proximal and distal portions of the free AT. The smaller CSA in the mid-portion of the AT may result in greater mechanical stress and hence fluid exudation from the tendon core (Helmer et al., 2006). More highly aligned collagen could also lead to enhanced collagen compaction following un-crimping (Miller et al., 2012a; Miller et al., 2012b). In addition, tendon twist appears to occur primarily in the mid-portion of the tendon (Edama et al., 2015a; Obst et al., 2014b) and could therefore exacerbate the aforementioned effects. Failure to account for conditioning effects on transverse free AT deformation would underestimate the negative transverse strain of proximal-, mid-, and distal portions of free AT by ~4%, 6%, and 3%, respectively, which in turn could lead to underestimation of AT true regional stress and Young's modulus (true stress: the ratio of instantaneous load to instantaneous CSA) (Vergari et al., 2011).

3.5.2 Number of contractions required for conditioning

Three voluntary isometric contractions at 50% of peak intensity and 25-s duration were sufficient to induce steady state strain behavior along the longitudinal dimension for the whole and free AT and the transverse dimension of the free AT when assessed at a

constant external plantarflexion ankle torque. The lack of a difference in the number of contractions required to induce longitudinal and transverse conditioning of the AT suggests that measuring the effect of conditioning along any tendon dimension is likely to closely reflect the effect of conditioning along other dimensions. In particular the practice of assessing tendon conditioning using whole tendon length measured from the gastrocnemius muscle-tendon junction to the calcaneus, appears likely to closely reflect longitudinal and transverse conditioning of the free AT. Although the magnitude of whole AT longitudinal conditioning in the present study (~3 mm and 3.86% strain) was consistent with Hawkins et al. (2009) (~3.2% strain) and Maganaris (2003) (~5 mm) this was not the case for the number of isometric contractions required to reach steady state behavior. AT conditioning was completed following 5 × 4-s isometric plantarflexion contractions at 80% MVIC (Maganaris, 2003) and following 270 × 1.33-s duration isometric ankle plantarflexion contractions at 25-35% MVIC (Hawkins et al., 2009). The smaller number of contractions required to induce conditioning in the present study compared to Maganaris (2003) and Hawkins et al. (2009) likely reflect differences between studies in contraction intensity and duration as these factors are known to be important determinants of short-term changes in tendon mechanical behavior, with longer load duration in particular leading to more pronounced effects (Kubo et al., 2001; Obst et al., 2013). Finally, the findings that the whole AT, proximal AT, and free AT lengths immediately following conditioning had recovered to within 1% of their corresponding resting lengths and within 6% of resting CSA for the proximal-, mid-, and distal portions of free AT, are broadly indicative of the transient and non-damaging effects of tendon conditioning.

3.5.3 Limitations

The findings from this study need to be interpreted with the following limitations in mind. Firstly, all participants underwent a 45 min period of tendon unloading prior to tendon conditioning. As the duration of the conditioning effect due to incidental activity such as walking is unknown, we cannot completely rule out the possibility that some residual effect of tendon loading history prior to the rest period persisted following the rest period. If such effects did persist, then the magnitude of the conditioning effect detected in our experiment is likely to have been underestimated. Secondly, we were not able to visualize the whole tendon CSA along the proximal AT during a single transverse ultrasound sweep in the present study. Such information could be obtained in future using other imaging approaches such as MRI (Iwanuma et al., 2011; Reeves and Cooper, 2017). While 3DUS has the advantage of being able to assess tendon structure under load, the approach is limited to measures made under isometric conditions. Small spatial errors are also associated with the single wall phantom 3DUS calibration process (Prager et al., 1998), but were minimized in the current study by following recommended procedures (Mercier et al., 2005). Further, although all measurements were made at the same relative ankle joint plantarflexion torque (50% MVIC), the force experienced by tendon was not directly measured and was therefore unknown. If it can be assumed that the force applied to the tendon was constant throughout conditioning, it might be expected that the EMG activity of the triceps surae would increase to account for the effect of shorter muscle fiber lengths on muscle force. Our inability to detect increased EMG activity of the plantarflexors during conditioning likely indicates that these effects were small (millimetres) and therefore difficult to detect using surface EMG. Finally, as our study was conducted in healthy

young males, caution is warranted in generalizing these findings to other population groups including older adults, females and individuals with Achilles tendinopathy.

3.6 Conclusion

This study demonstrated that *in vivo* longitudinal deformation of human AT during conditioning is primarily driven from free AT and was coupled to a corresponding transverse deformation within the free AT. The free AT transverse conditioning was most pronounced within the mid-portion, reflecting structural and/or mechanical factors that are unique to this region. The longitudinal and transverse conditioning of AT occur simultaneously throughout the tendon following 3 × 25-s plantarflexion contractions at 50% MVIC. There are several potential practical implications of these findings. Firstly, consistent with reports that the free AT is the most common site of AT tendinopathy and rupture (Järvinen et al., 2005), the isolated conditioning of the free AT may explain why the free AT is more susceptible to strain-related injury. Secondly, conditioning of whole AT appears likely to closely reflect longitudinal and transverse conditioning of the free AT and there is no differential effect of tendon region and dimension on the number of contractions required for conditioning.

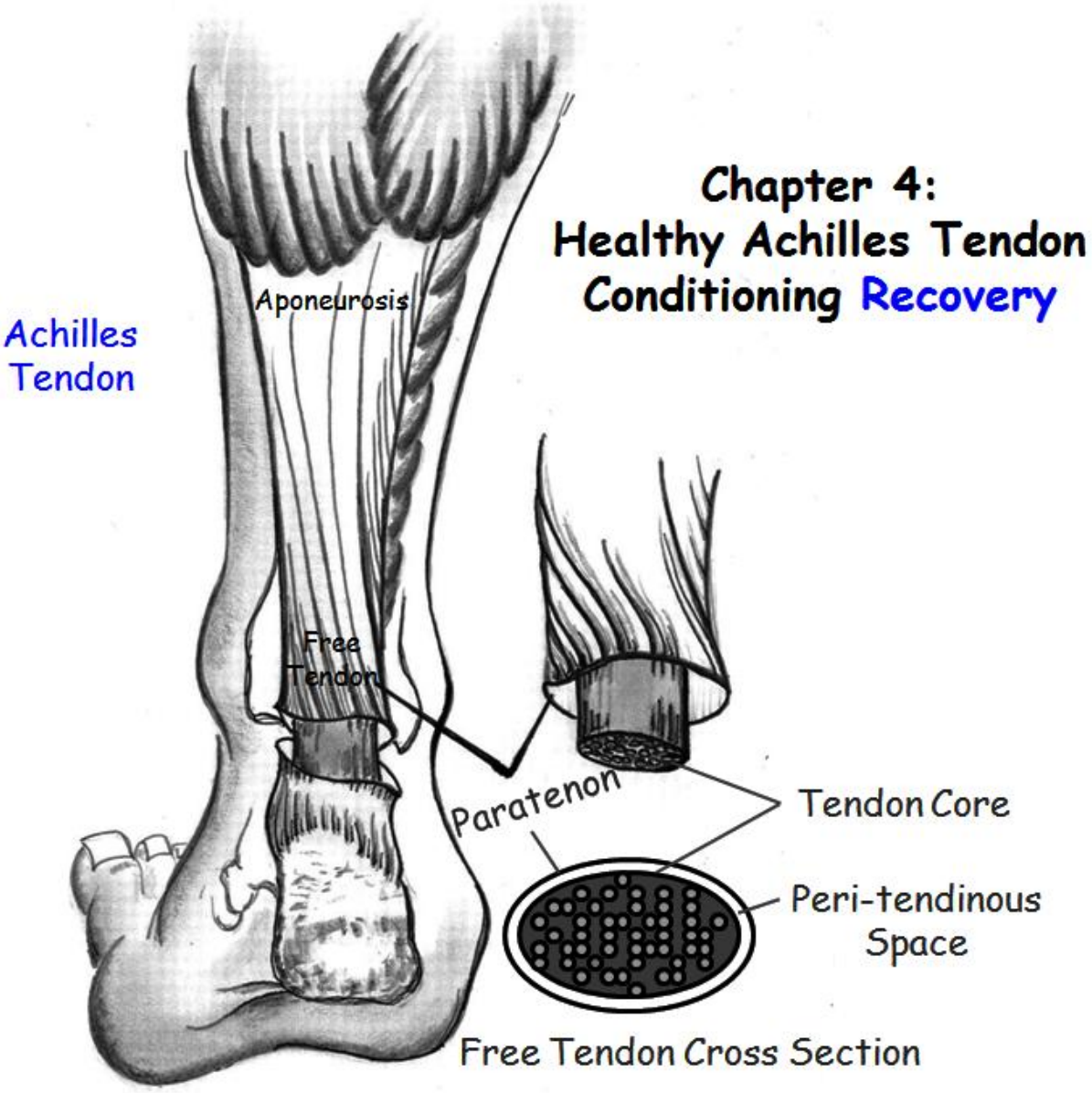
Chapter 4:
Healthy Achilles Tendon
Conditioning Recovery
Achilles
Tendon
Aponeurosis
Free
Tendon
Paratenon
Tendon Core
Peri-tendinous
Space
Free Tendon Cross Section

Chapter 4. Recovery of human Achilles tendon three-dimensional deformation following conditioning

Acknowledgement of co-authorship:

This chapter includes a co-authored paper that has been re-formatted for this thesis. The bibliographic details/status of the co-authored paper, including all authors, are:

L. Nuri, S. J. Obst, R. Newsham-West, R. S. Barrett (2017). "Recovery of human Achilles tendon three-dimensional deformation following conditioning". **Under Review.**

I have made a substantial contribution in the conception and design of this study, analysis and interpretation of the research data, and the drafting and critical revising of the final manuscript.

(Signed) Leila Nuri (Date) 10th March 2017

Student/corresponding author: Leila Nuri

(Countersigned) _____ (Date) _____

Principal Supervisor: Rod Barrett

(Countersigned) _____ (Date) _____

Principal Supervisor: Richard New-sham West

4.1 Abstract

This study examined the time-course recovery of three-dimensional (3D) Achilles tendon (AT) deformation immediately following a standardized AT conditioning protocol, which could have implications for designing the experiments that measure AT mechanical properties. Ten healthy male adults (age: 24 ± 5 y; height: 175.8 ± 4.1 cm; body mass: 78.4 ± 6.3 kg) attended the laboratory on 6 occasions. ATs were scanned using freehand 3D ultrasound during a 50% maximal voluntary isometric contraction (MVIC) of the plantarflexors immediately prior to and following the conditioning protocol (10 × 25-s plantarflexion contractions at 50% MVIC), and then at either 15, 30, 60, 90 or 120 mins post-conditioning, randomized by session. Free AT longitudinal strain was significantly increased from 3.13±0.19% pre-conditioning to 7.49±0.20% immediately post-conditioning and was accompanied by a corresponding reduction in free AT transverse strain from -5.35±0.48% to -10.16±0.49% ($P < 0.001$). There were no significant differences in free AT longitudinal or transverse strains at 60 min relative to 0 min post-conditioning, or between pre-conditioning strains and strains measured at 2 hours ($P > 0.05$). The free AT undergoes a creep response during conditioning, which is recoverable within 2 hours following conditioning. Recovery from conditioning has the potential to be a source of error during *in vivo* measurement of AT mechanical properties. The time window in which the free AT longitudinal and transverse strains could be achieved without a large confounding effect of creep recovery is 0-60 min post-conditioning.

4.2 Introduction

Following initiation of tensile loading, tendons such as the Achilles tendon (AT) experience an increase in longitudinal deformation/strain and the corresponding reduction in transverse deformation/strain with successive loading cycles until steady state mechanical behavior is reached (Hawkins et al., 2009; Maganaris, 2003; Nuri et al., 2016). At this point the tendon is said to be "conditioned" (Fung et al., 2013; Graf et al., 1994). For studies of AT mechanical behavior, it is recommended that a standardized tendon conditioning protocol be used prior to testing to ensure repeatable results (Seynnes et al., 2015), as either inadequate or inconsistent tendon conditioning can alter measured tendon mechanical properties. The conditioning effect for the whole AT (i.e. gastrocnemius muscle-tendon junction (MTJ) to calcaneus) is primarily driven by a creep response from the free AT (i.e. soleus (SOL) MTJ to calcaneus) and is accompanied by a corresponding reduction in free tendon cross-sectional area (CSA) that is most pronounced within tendon mid-portion (Nuri et al., 2016). The mechanisms responsible for tendon conditioning likely reflect some combination of load-dependent changes in tendon microstructure and interstitial fluid distribution (Houssen et al., 2011; Miller et al., 2012). Tendon conditioning is believed to occur at a force intensity that is below the threshold for tendon damage (i.e. within the toe and/or elastic region of the tendon stress-strain curve), and is transient, with tendons returning to their preloaded state following a period of unloading (Fung et al., 2013). Identifying the nature and time course of tendon recovery following tendon conditioning could have implications for the design of experiments that measure tendon mechanical properties and could provide information about the tendon viscoelastic properties that underpin the tendon function and adaptation.

Several *in vivo* studies have investigated AT recovery following training and sport activities, but the mechanical loads used in those studies were well in excess of those required for tendon conditioning. For example, recovery of AT thickness has been shown to be complete compared to pre-exercise values after 24 hours following eccentric loading (2 × 3 sets of 15 repetitions of eccentric heel drops), concentric loading (2 × 3 sets of 15 repetitions of concentric ankle loading exercise), and resistance exercise (90 repetitions of calf-raise exercise against an effective resistance of 250% body weight) (Grigg et al., 2009; Grigg et al., 2012; Wearing et al., 2014). Furthermore, a duration of 4 days has been reported for full recovery of AT structural integrity following an Australian Rules Football game (Rosengarten et al., 2014) and 3 days for recovery of AT volume and hydration after cross-country running (Gross et al., 2015). However, a steady-state strain response in the AT can be achieved with as little as 5 × 4-s plantarflexion contractions at 80% maximum voluntary isometric contraction (MVIC) (Maganaris, 2003), 3 × 25-s plantarflexion contractions at 50% MVIC (Nuri et al., 2016), or 6 min of 0.75 Hz cyclic plantarflexion contractions at 25–35% MVIC (Hawkins et al., 2009). No known studies to date have examined AT recovery from conditioning only, which would be expected to occur on a shorter time-scale (i.e. hours) compared to the recovery durations reported for the abovementioned studies of training and sport activities (i.e. 1-4 days). A further feature of the studies conducted to date on AT recovery following mechanical loading is that structural measurements were typically made at a single site using two-dimensional (2D) ultrasound (Grigg et al., 2009; Grigg et al., 2012; Wearing et al., 2014; Rosengarten et al., 2014; Gross et al., 2015). Three-dimensional (3D) ultrasound methods are now available that can overcome some of the limitations of 2D ultrasound including the ability to: image

the whole AT during a single scan, identify landmarks such at the muscle-tendon junction and calcaneal insertion in 3D space, and eliminate errors associated with controlling the 2D image plane (Obst et al., 2016; Lichtwark et al., 2013).

The purpose of this study was to examine the time course of the recovery of 3D AT deformation under load following tendon conditioning. The time required for recovery from conditioning effects was assessed by comparing the 3D tendon deformation during recovery with the deformation immediately prior to and immediately following conditioning. It was hypothesised that the recovery would be primarily driven by changes in the free AT and would occur on a shorter time scale (i.e. hours rather than days).

4.3 Materials and Methods

4.3.1 Participants

Ten healthy active male adults (age: 24 ± 5 y, height: 175.8 ± 4.1 cm, and mass: 78.4 ± 6.3 kg) provided voluntary informed consent to participate in the study. None of the participants reported any current or ongoing lower limb musculoskeletal and neuromuscular conditions. The study was approved by the local institutional Human Research Ethics Committee and was performed in accordance with the principles of the Declaration of Helsinki.

4.3.2 Experimental design and conditioning protocol

A randomized repeated measures crossover design was used to determine the time course of recovery of AT longitudinal and transverse deformation following conditioning. Participants attended the laboratory at approximately the same time of the day (± 40 min)

on 6 separate occasions within an 18 day period. Individual sessions were separated by 2-5 days. At the first session, the peak ankle joint torque associated with MVIC of the plantarflexor and dorsiflexor muscles was established. Participants performed 3 × 5-s maximal plantarflexor and dorsiflexor contractions with their left leg with a rest interval of 60 seconds between each contraction. The highest ankle torque recorded over the 3 trials was selected as the peak torque. Participants were then asked to practice holding contractions at 50% intensity until they became familiarized with the testing procedure. Participants were required to refrain from any strenuous activity for at least 48 hours prior to all 5 subsequent test sessions. Upon arrival at the laboratory, participants were instructed to sit for 45 minutes and then performed the AT conditioning protocol described by Nuri et al. (2016). In brief, this involved performing 10 successive 25-s isometric plantarflexion contractions at 50% of the peak torque. Measures of AT strain were assessed during a 50% plantarflexor MVIC using ultrasound immediately prior to conditioning, immediately following conditioning, and then at one further time point at either 15, 30, 60, 90 or 120 minutes during recovery, which was randomized by session. Participants otherwise sat comfortably on the chair with both feet flat throughout recovery. This testing design eliminates any possible confounding effects of the tendon testing trial on tendon recovery response (Figure 20). Ankle joint torque and muscle activation for the medial gastrocnemius (MG), lateral gastrocnemius (LG), soleus (SOL) and tibialis anterior (TA) were recorded during all test contractions. Statistical analysis revealed that there were no significant differences in ankle joint torque during conditioning between the 5 conditioning sessions. Furthermore, no differences in measures of AT deformation and strain, ankle torque, and muscle activity measured immediately prior to and following conditioning

were detected between sessions. Pre- and immediate post-conditioning values were therefore averaged across the 5 test sessions for each participant in all subsequent analyses.

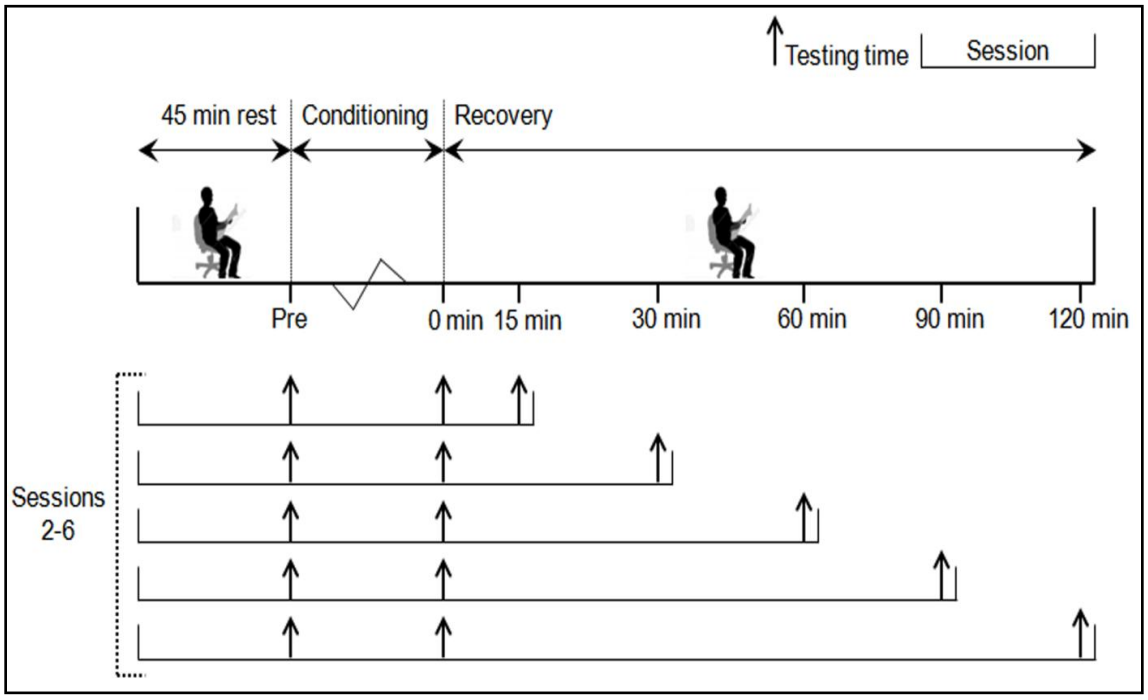

Figure 20: *Schematic representation of the whole experimental protocol. The participants (N =10) reported to the laboratory for 6 different sessions. The first session was a familiarization session and the subsequent 5 sessions (sessions 2-6) were testing sessions. In each testing session, upon arrival, participants sat quietly with both feet flat on the floor for 45 minutes to minimize the effect of pre-loading on Achilles tendon (AT) mechanical properties and then performed the AT conditioning protocol (10 × 25-s plantarflexion contractions at 50% maximum voluntary isometric contraction (MVIC)). The AT strain measurement (testing time) was performed during a plantarflexion contraction at 50% MVIC immediately prior to conditioning (pre), immediately following conditioning (0 minute), and then at either 15, 30, 60, 90 or 120 minutes during recovery, which was*

randomized by session. To prevent loading the AT during recovery period, participants were requested to sit comfortably on the chair.

4.3.3 Data collection procedures

During each test contraction and during conditioning, participants lay prone on a plinth with the hip and knee fully extended and the ankle in neutral position (i.e., 90° angle between the sole of the foot and the shank). The participants' left foot was then attached securely to the footplate of a fixed torque transducer (Futek TFF600, Irvine, California, USA) using a custom-built ratchet system (Obst et al., 2014a; Obst et al., 2014b) and the axis of rotation of the ankle joint was carefully aligned with the axis of rotation of the torque transducer. The real-time visual feedback of ankle joint torque was displayed on a computer monitor for participants to match their exerted torque to a target torque (50% MVIC) and maintain target ankle torque for the entire duration of the contraction. The ankle joint torque data was recorded at a sampling frequency of 1000 Hz using a custom LabVIEW program (LabVIEW 9.9, National Instruments, Austin, Texas, USA). 3DUS system (a conventional 2DUS machine (SonixTouch, Ultrasonix, Richmond, BC, Canada) and a five-camera optical tracking system (OptiTrack V100:R2, Tracking Tools Version 2.5.2, NaturalPoint, Corvallis, OR, USA) was used for imagining of AT during each testing trial (Obst et al., 2015a; Obst et al., 2015b). A single examiner (L.N) obtained all AT images at frequency of 60 Hz, using a 58-mm linear transducer (L14-5 W/60 linear, Ultrasonix, Richmond, BC, Canada) with following ultrasound image parameters: depth = 40 mm, gain = 50%, dynamic range = 65 dB, map = 4, and power = 0. To improve ultrasound image quality and proper contact between transducer and skin during scanning, a rectangular shaped commercially available stand-off pad (Ultra/Phonic Focus,

Pharmaceutical Innovations Inc., Newark, New Jersey, USA) was positioned over the end of the transducer using a custom-made ultrasound stand-off holder. Prior to scanning, a thin layer of ultrasound coupling gel was applied over the skin to reduce friction and assist in the transmission of the ultrasound waves. To construct 3D AT images from a sequence of conventional 2DUS images, the orientation and position of the four reflective markers rigidly mounted on the transducer was tracked using the optical tracking system. A coordinate transformation was then applied to map the 2D B-mode images into global coordinate system and a 3D rendering of AT was constructed using the Stradwin software package (Version 5.1, Mechanical Engineering, Cambridge University, UK). Prior to data collection, the system was calibrated according to the single wall phantom calibration protocol recommended by Stradwin software developers (Prager et al., 1998). Following calibration, pixel coordinates in any recorded 2DUS images were transformed into 3D space with an error of ± 0.4 mm. In each experimental session, initially, the anatomical locations of calcaneus, SOL MTJ, and MG MTJ were marked using a permanent maker with an assistance of a single longitudinal 2DUS scan and the ultrasound scanning path was outlined on the skin to ensure consistency within testing trials. The ultrasound transducer was then moved manually in a transverse orientation at a steady speed (~9 mm s^{-1}) from the base of the heel to MG MTJ and each scan took approximately 25-s to complete (Figure 21A). On average, a reconstructed AT image consisted of 1350 frames with an average distance between frames of 0.1 mm.

4.3.4 Ultrasound image analysis

All 3D ultrasound reconstructed images were processed in Stradwin software. The calcaneal notch, SOL MTJ, and MG MTJ were digitized manually in reconstructed images with the aid of a sagittal and transverse image re-slices. To obtain consistent MTJ points across testing trials and facilitate image processing, the most distal points where the first cross sections of MG and SOL appeared in the transverse images during the scan were selected (Figure 21B,C). The whole AT length was defined as the distance between the calcaneal notch and MG MTJ. Free AT length was defined as the distance between the calcaneal notch and SOL MTJ and proximal AT length was determined as the distance between MG MTJ and SOL MTJ. For each region, tendon elongation was calculated by subtracting tendon length in the 50% MVIC testing trial from the corresponding resting length. Free tendon CSAs in the resting state and each testing trial were also outlined manually from the original B-mode transverse images at ~1 mm intervals in tendon mid-portion (40%-70% of the free tendon length (Nuri et al., 2016)) (Figure 21B). The mean free AT mid-portion CSA was then computed by taking the average of all the digitized CSAs (mean number of digitized CSAs: 23 ± 8). Tendon transverse deformation was computed by subtracting the mean tendon CSA in the 50% MVIC testing trial from the corresponding resting CSA. Tendon longitudinal and transverse strain during recovery was expressed relative to their corresponding measures at rest. The measurement of free AT transverse strain during tensile loading could have important implications for our understanding of the AT elastic energy storage and release action (Lichtwark and Wilson, 2006), triceps surae muscle bulging characteristics (Aziz et al., 2008), and AT in vivo mechanobiology (Wang et al., 2012).

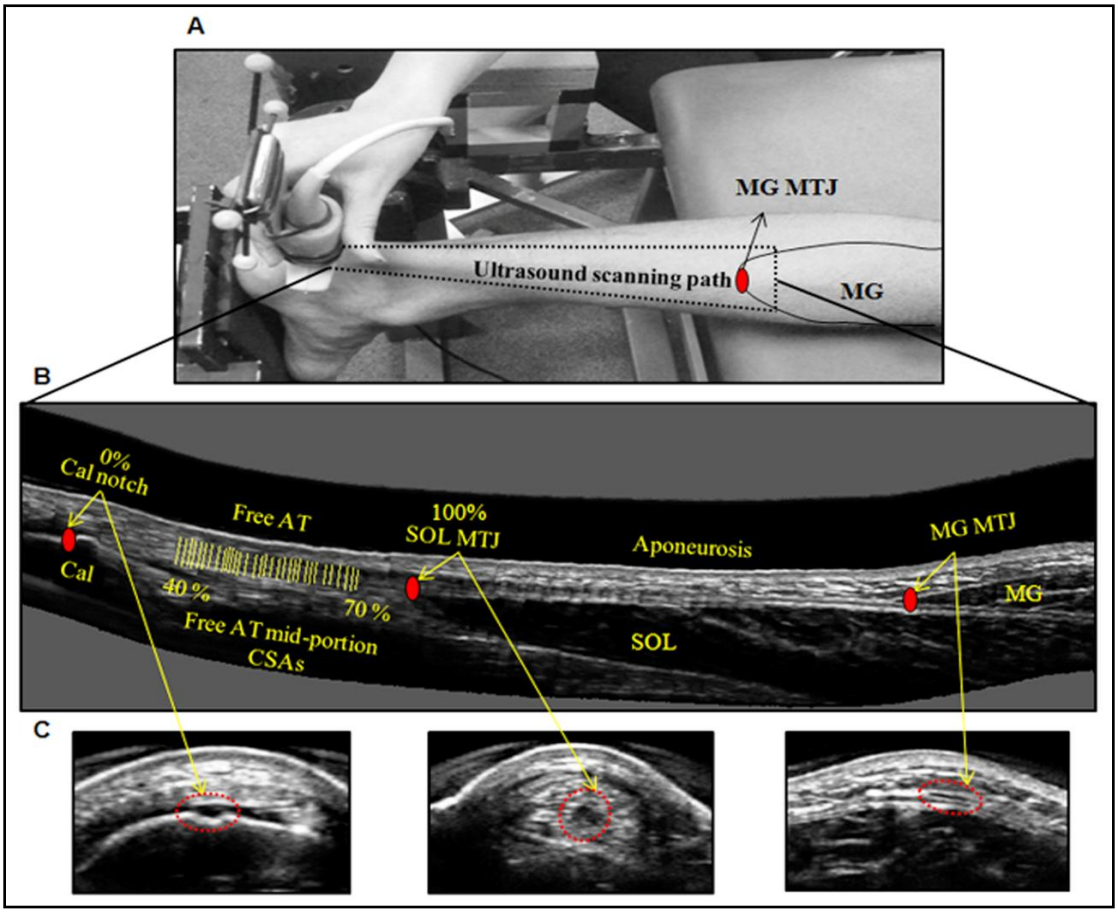

Figure 21: *An overview of the experimental setup and three dimensional (3D) Achilles tendon (AT) image analysis. (A) The 3D ultrasound scan involved synchronous B-mode ultrasound imaging and 3D motion capture of the four reflective markers rigidly attached to the transducer using 5 camera optical tracking system. A series of 2D B-mode ultrasound images was collected by moving the transducer from the base of the heel to the medial gastrocnemius (MG) muscle- tendon junction (MTJ) over the ultrasound scanning path in a transverse orientation at a steady speed. The sagittal plane image re-slices (B) and transversal images (C) of AT were served to detect the calcaneal notch (Cal notch), MG MTJ, and soleus (SOL) MTJ for calculation of tendon length and strain and*

digitization of free AT cross-sectional areas (CSAs) at ~1 mm intervals in tendon mid-portion (40%-70% of the free AT length).

4.3.5 Electromyography

EMG activity was recorded by a EMG system (Bagnoli-8 EMG, DELSYS, USA) from pre-gelled and self-adhesive electrodes (model H124SG, Covidien Kendall, 24 mm, Germany) with a fixed center-to-center interelectrode distance of 20 mm and a gain of 350 placed over the muscle bellies of the MG, LG, SOL, and TA according to SENIAM recommendations by Hermens et al. (2000). The ground electrode was placed over the fibular head. Prior to electrode placement, the skin was shaved, abraded, and then cleansed with skin prepping gel (NuPrep, DO Weaver & Co., Aurora, Colorado, USA) and 70% isopropyl alcohol (Briemarpak, Briemar Nominees Pty Ltd, Australia). The EMG raw signals were transmitted to a digital data recorder at a sampling rate of 1000 Hz and filtered with a band pass of 20–400 Hz using a fourth-order zero lag Butterworth filter in Matlab software (Version R2015a, The Mathworks, Natick, Massachusetts, USA) and subsequently converted to RMS activity. For each individual muscle, RMS was normalized as a percentage of the RMS EMG activity recorded during a MVIC.

4.3.6 Statistical analysis

A one-way repeated measures General Linear Model was used to determine the effect of testing time across the 7 time points assessed (pre-conditioning, 0, 15, 30, 60, 90 and 120 minutes) on tendon longitudinal and transverse strain, ankle plantarflexor torque, and EMG of MG, LG, SOL, and TA. Planned contrasts (SPSS CONTRAST syntax) were used to compare tendon strain values at each post-conditioning testing time relative to the strain

measured during pre-conditioning and 0 min post-conditioning testing times. Data are presented as group mean ± SD in the text and as group mean ± SEM in the figures. The level of significance was set at $P < 0.05$, and all statistical analyses were performed using Statistical Package for the Social Sciences version 22 (SPSS Inc, Chicago, Illinois, USA).

4.4 Results

4.4.1 Effect of testing time on tendon longitudinal and transverse strains

The mean resting lengths of the whole AT, proximal AT, and free AT prior to conditioning were 214 ± 26, 150 ± 20, and 64 ± 21 mm, respectively. Conditioning resulted in a 140% and 33% increase in longitudinal strain for the free and whole AT, respectively ($P < 0.001$). There was a significant main effect of testing time on free AT and whole AT longitudinal strain values (CI: 5.19-6.21, η^2: 0.83, $P< 0.001$ and CI: 3.19-3.47, η^2: 0.46, $P < 0.001$, respectively). Planned contrasts revealed that free and whole AT longitudinal strain values at 0, 15, 30, 60, and 90 minutes post-conditioning was significantly greater than that of the pre-conditioning ($P < 0.01$). The free and whole AT longitudinal strains at 90 and 120 minutes post-conditioning were significantly lower than that 0 min post-conditioning ($P < 0.01$) (Fig. 22a,b).

The mean resting free tendon mid-portion CSA prior to conditioning was 53 ± 6 mm^2. Conditioning resulted in a 90% reduction in free AT transverse strain ($P < 0.001$). There was a significant main effect of testing time on free AT transverse strain (CI: -8.84- -7.58, η^2: 0.84, $P < 0.001$). Planned contrasts revealed that the free AT transverse strain at 0, 15, 30, 60, and 90 minutes post-conditioning was significantly lower than at pre-conditioning

(P < 0.01). The free AT transverse strain at 90 and 120 minutes post-conditioning was significantly greater than at 0 min post-conditioning (P < 0.01) (Fig. 22c,d).

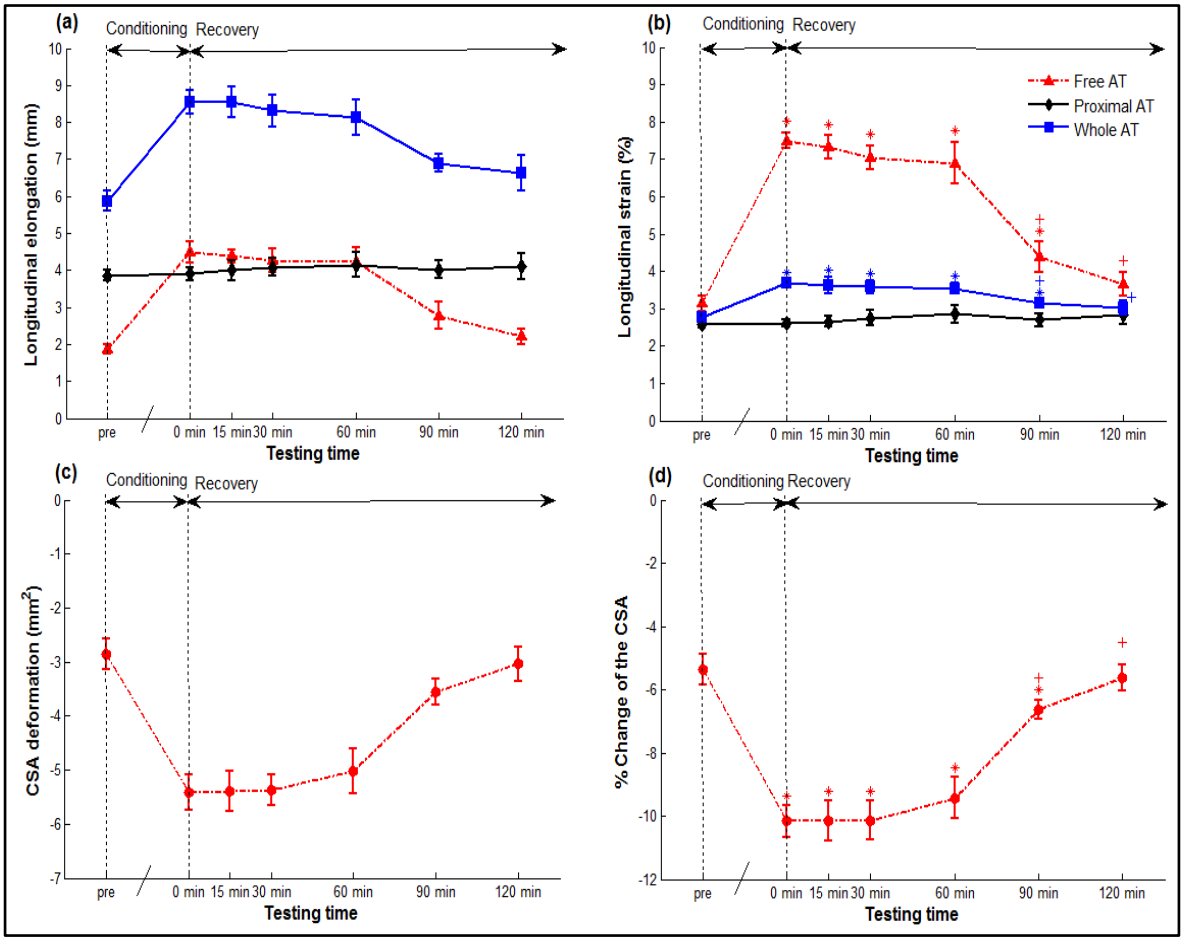

***Figure 22**: Time course of recovery of Achilles tendon (AT) longitudinal and transverse elongation and strain. (a) The mean longitudinal elongation for the free AT, proximal AT, and whole AT immediately prior to conditioning (pre) and during the recovery period (0, 15, 30, 60, 90, and 120 minutes). (b) The corresponding mean longitudinal strain for each region immediately prior to conditioning and during the recovery period. (c) The mean free AT mid-portion cross-sectional area (CSA) deformation immediately prior to conditioning and during the recovery period. (d) The corresponding % change of the free AT mid-portion CSA prior to conditioning and during the recovery period. *Significantly*

different from pre-conditioning strain value ($p < 0.05$). +Significantly different from 0 min post-conditioning strain value ($p < 0.05$). Data are expressed as mean ± SEM ($n = 10$).

4.4.2 Effect of testing time on ankle plantarflexion torque and EMG

The group mean ankle joint torque for MVIC, testing times, conditioning, and resting trials were 88.2 ± 13.8, 44.6 ± 7.3, 44.03 ± 6.32, and 1.25 ± 0.42 N.m, respectively. Group mean normalized EMG activities for MG, LG, SOL, and TA during testing times were 36.11 ± 3.2%, 42.19 ± 4.11%, 43.26 ± 5.22%, and 5.8 ± 1.01%, respectively. No significant main effect of testing time on ankle plantarflexion torque ($F_{6, 54}$ = 0.95, P = 0.19) or EMG amplitude (LG: $F_{6, 54}$ = 0.53, P = 0.82; MG: $F_{6, 54}$ = 0.32, P = 0.92; SOL: $F_{6, 54}$ = 0.32, P = 0.92; TA: $F_{6, 54}$ = 0.41, P = 0.86) were detected.

4.5 Discussion

The main findings of the present study were that the overall conditioning effect was most pronounced for the free AT and resulted in creep behavior of the whole AT consistent with other AT conditioning protocols (Maganaris, 2003; Hawkins et al., 2009; Nuri et al., 2016). The whole and free AT longitudinal strains and the free AT transverse strain had achieved ~71%, 88% and 94% recovery, respectively at 2 hours post-conditioning. Furthermore, the whole and free AT longitudinal strain and the free AT transverse strain values during the recovery period did not differ from values immediately following conditioning up to 60 min (~8% recovery), but were different at subsequent measurement time points. These findings have implications for the design of experiments to determine

AT mechanical properties where tendon recovery from conditioning could be a confounding factor.

The mean longitudinal strain in the whole AT during a 50% MVIC of the plantarflexors increased from 2.75% to 3.67% following conditioning that was primarily driven by an increase in free AT longitudinal strain from 3.13% to 7.49% and accompanied by a corresponding reduction in free AT mid-portion transverse strain from -5.35% to -10.16%. These findings are consistent with those of Nuri et al. (2016; 2017) who reported similar findings for whole and free AT longitudinal strains (~1% and 3.5%, respectively) and free AT transverse strain (~5%) following the same conditioning protocol. These results are also in line with those of other AT conditioning studies that reported similar amounts of whole AT longitudinal strain (~1-3%) following protocols consisting of 10 × 4-s repeated isometric contractions at 80% MVIC (Maganaris, 2003) and 7 min of 0.75 Hz cyclic isometric ankle plantarflexion at 25-35% of MVIC (Hawkins et al., 2009). The greater change in free AT longitudinal strain following conditioning observed here (~4.3%) compared to prior studies of whole AT longitudinal strain (Maganaris, 2003; Hawkins et al., 2009) is because measures of whole AT (i.e. proximal AT + free AT) strain underestimate the strain at the level of free AT (Farris et al., 2013; Nuri et al., 2016; Nuri et al., 2017).

The whole and free AT longitudinal strains and free AT transverse strain during recovery were significantly higher than the strains immediately prior to tendon conditioning at all measurement time points up to and including 90 minutes, and were no longer significantly different at 2 hours. Recovery of AT was therefore interpreted to be complete in both longitudinal and transverse directions at 2 hours post- conditioning. The time course of the

full recovery of AT longitudinal and transverse strains from conditioning effects reported here (2 hours) is considerably shorter than those reported in training and sports activities (1-4 days) (Grigg et al., 2009; Grigg et al., 2012; Wearing et al., 2014; Rosengarten et al., 2014; Gross et al., 2015). This discrepancy in time course of recovery for training and sport activities compared to the present study is likely due to a combination of differences between studies in outcome measures assessed (tendon strain, thickness, water content, and structural integrity), experimental design, including tendon test condition (loaded vs rest) and location (whole free AT vs mid-portion), and the total amount of loading experienced by the tendon prior to recovery.

It was also notable that creep recovery of the AT longitudinal and transverse strains were minimal up to 60 min (~8%), and increased markedly thereafter. This finding is in contrast to previous reports, which suggest the pattern of AT recovery is exponential (Grigg et al., 2009; Wearing et al., 2014). The most likely explanation for this discrepancy is that measurements were made in the present study under load, and so may have masked tendon recovery (i.e. overestimation of tendon deformation and strain) immediately following conditioning, whereas prior studies have assessed tendon recovery at rest. On the basis of the findings from the present study, it is recommended that in future studies of AT mechanical properties that measurements are made within 60 min of conditioning for longitudinal and transverse strains to minimize the confounding effects of creep recovery. Failure to account for the time course of AT creep recovery following conditioning would underestimate the AT longitudinal strain and overestimate the AT transverse strain, which in turn could lead to overestimation of tendon stiffness and underestimation of AT true stress (i.e. the ratio of instantaneous load to instantaneous CSA) (Vergari et al., 2011). This

study also showed that free AT longitudinal strain recovery was 71% complete at 90 min and 88% complete at 120 min post conditioning. Corresponding values for the whole AT recovery were 58% at 90 mins and 71% at 120 mins. The reason for the lower percentage recovery for the whole compared to the free AT at 90 and 120 mins is that although not statistically significant, there was an increase in mean proximal AT strain from 0 min to 120 min post recovery. Irrespective, both free and whole AT recovery were complete at 2 hours.

The following limitation is acknowledged. All participants underwent a 45 min period of tendon AT unloading prior to testing in each session. As the creep recovery from conditioning effects was complete for the whole and free AT at 2 hours post-conditioning, it is possible that some residual effects of tendon loading history prior to 45 min rest period persisted during testing and may have affected the magnitude of AT conditioning effect and its time course of recovery. It is recommended that participants in future tendon conditioning studies undergo at least 2 hours of tendon unloading prior to testing.

Conclusion

Achilles tendon creep recovery following conditioning was primarily driven by changes in the free AT and was complete after 2 hours. The magnitude of the conditioning and creep recovery response for the free AT is large and has the potential to be a confounding factor in studies where there is a delay between conditioning and mechanical testing of the AT. Restricting this time delay to 60 minutes could minimize these effects.

Practical implications

- Conditioning and recovery effects measured at the whole AT underestimate corresponding values for the free AT.

- Tendon conditioning and its time course of recovery alter the strain behavior of the AT and should be considered in the design of AT mechanical testing experiments.
- The effect of recovery on tendon strain can be minimized if repeated measurements are made within approximately 1 hour of conditioning.

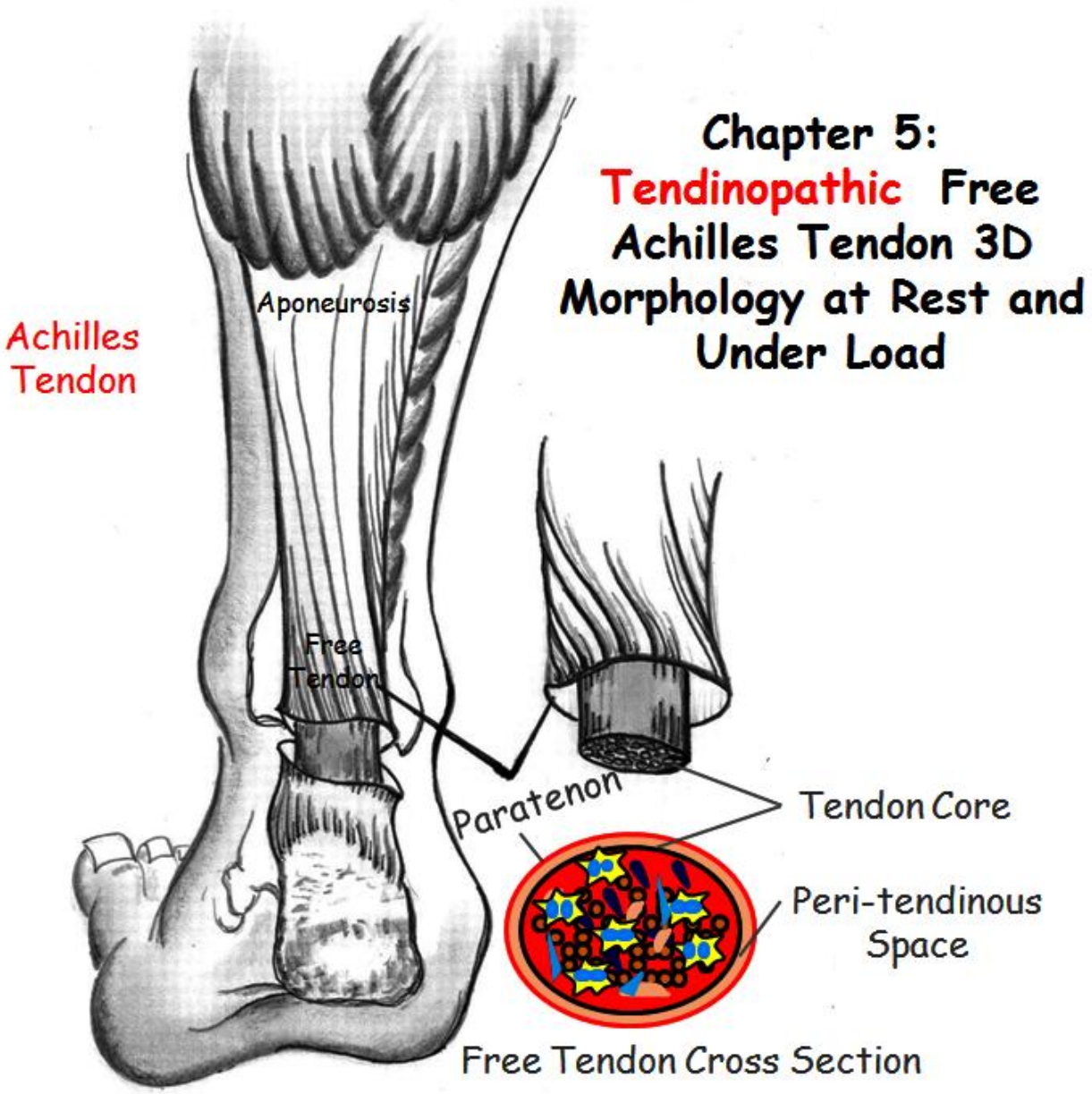
Chapter 5:
Tendinopathic Free Achilles Tendon 3D Morphology at Rest and Under Load
Achilles Tendon
Aponeurosis
Free Tendon
Paratenon
Tendon Core
Peri-tendinous Space
Free Tendon Cross Section

Chapter 5. Three-dimensional morphology and volume of the free Achilles tendon at rest and under load in people with unilateral mid-portion Achilles tendinopathy

Acknowledgement of co-authorship:

This chapter includes a co-authored paper that has been re-formatted for this thesis. The bibliographic details/status of the co-authored paper, including all authors, are:

L. Nuri, S. J. Obst, R. Newsham-West, R. S. Barrett (2017). "Three-dimensional morphology and volume of the free Achilles tendon at rest and under load in people with unilateral mid-portion Achilles tendinopathy". **Under Review.**

I have made a substantial contribution in the conception and design of this study, analysis and interpretation of the research data, and the drafting and critical revising of the final manuscript.

(Signed) Leila Nuri (Date) 10th March 2017

Student/corresponding author: Leila Nuri

(Countersigned) _____ (Date) _____

Principal Supervisor: Rod Barrett

(Countersigned) _____ (Date) _____

Principal Supervisor: Richard New-sham West

5.1 Abstract

Mid-portion Achilles tendinopathy (MAT) is a debilitating musculoskeletal condition, which adversely affects free Achilles tendon (AT) structure and composition. However, it is not known how these pathological alterations associated with MAT change the normal three-dimensional (3D) morphology of free AT at rest and under load throughout the entire free tendon length. Here, we used 3D ultrasound to examine the effect of unilateral MAT on free tendon 3D morphology [length, cross-sectional area (CSA), antero-posterior (AP) diameter, and medio-lateral (ML) diameter] and volume at rest and during a sub-maximal (50%) voluntary isometric plantarflexion contraction bilaterally in individuals with unilateral MAT (N = 10) compared to a matched healthy control group (N = 10). The tendinopathic free AT had a greater CSA relative to the contralateral and healthy control tendons along the entire tendon length, which was mainly driven by a greater tendon AP diameter. Under load, the tendinopathic tendon experienced greater longitudinal and transverse strains than the control tendons, which would be expected to increase the risk of strain-related injuries. In contrast to the contralateral and healthy tendons, which experienced a reduction in tendon CSA and ML diameter and bulged along the AP axis and behaved iso-volumetrically under load, the tendinopathic tendon experienced a reduction in tendon CSA, AP diameter, ML diameter, and a corresponding reduction in tendon volume. These findings are indicative of a fundamental reorganization of the tendon matrix and alterations in tendon fluid content and distribution under load in tendinopathic tendon.

5.2 Introduction

Mid-portion Achilles tendinopathy (MAT) is a degenerative disorder of the Achilles tendon (AT) characterized by swelling, morning stiffness, and pain in the mid-portion of the tendon, typically located 2-7 cm proximal to the calcaneal insertion (Maffulli, 1998; Van Dijk et al., 2011). MAT is a prevalent condition that causes disability and functional impairment in athletic and sedentary populations (de Jonge et al., 2011; Emerson et al., 2010; Kvist, 1994). Extensive pathologic alterations in the structure and composition of the AT associated with tendinopathy have been consistently reported in the literature. These alterations include: disruption and disorganization of the collagen bundles (Pingel et al., 2014), hypercellularity (Andersson et al., 2011a; Åström and Rausing, 1995), hypervascularity (Åström and Rausing, 1995), increase in proportion of type III collagen relative to type I collagen (Maffulli et al., 2000; Pingel et al., 2014), increase in ground substance (Józsa and Kannus, 1997) and the number of tenocytes without their normal fine spindle shape and more rounded nuclei (Andersson et al., 2011b), high concentration of glycosaminoglycan (GAG) content (Corps et al., 2006), accumulation of free and bound water molecules (de Mos et al., 2007), and presence of apoptotic cells (Pearce et al., 2009). Such micropathological changes in tendon structure and composition affect tendon macromorphology and function (Arya and Kulig, 2010; Child et al., 2010; Grigg et al., 2012; Leung and Griffith, 2008; Shalabi et al., 2004b). From a tendon injury prevention and rehabilitation perspective, it is important to understand how tendon macromorphology is altered in tendinopathy at rest and in the loaded state.

Free ATs [i.e., soleus muscle-tendon junction (MTJ) to calcaneus] with MAT have been reported to have a greater tendon cross-sectional area (CSA), antero-posterior (AP) diameter and volume in the tendinopathic and contralateral sides (Alfredson et al., 2014; Cassel et al., 2015; Docking et al., 2015; Gärdin et al., 2006; Gärdin et al., 2010; Grigg et al., 2012; Leung and Griffith, 2008; Lind et al., 2006; Shalabi et al., 2004a; Shalabi et al., 2004b; Shalabi et al., 2005; Van Schie et al., 2010) relative to age- and gender-matched healthy control tendons. However, reports of tendon transverse morphology (i.e., CSA and AP diameter) to date are limited to a single transverse or longitudinal plane images acquired at a single site of the tendon mid-portion using two-dimensional (2D) ultrasound and therefore do not provide a three-dimensional (3D) representation of the tendon morphology along the whole tendon length. While recent studies in animal models have demonstrated a widespread development of tendinopathy symptoms in tendon histology, gene expression, composition, and mechanical and morphological properties throughout the entire tendon length following an induced localized tendon injury (Choi et al., 2016; Jacobsen et al., 2015; Smith et al., 2008), it is not known whether pathological changes in tendon morphology in people with MAT are only confined to the injury location (i.e., tendon mid-portion) or affect the entire tendon length. It is also currently unclear whether tendon medio-lateral (ML) diameter is affected by the pathological changes associated with MAT similar to tendon AP diameter. A comprehensive characterization of the AT transverse morphology (i.e., CSA, AP diameter, and ML diameter) in an unloaded state in people with unilateral MAT along the entire tendon length in the tendinopathic and contralateral healthy sides could provide a novel diagnostic criteria for characterizing, and

monitoring pathologies of AT in clinical routine to minimize the risk of poor functional outcomes and potential recurrent AT injuries.

The 3D morphology of the healthy free AT under tensile load has been well characterized in previous *in vivo* studies. It has been shown that during sub-maximal isometric plantarflexion contractions [40-80% maximum voluntary isometric contraction (MVIC)] the free AT undergoes a mean longitudinal strain of 3.3-8% (Farris et al., 2013a; Finni et al., 2003; Iwanuma et al., 2011; Lichtwark et al., 2013a; Magnusson et al., 2003; Nuri et al., 2016; Obst et al., 2015b; Obst et al., 2014b), which is accompanied by a corresponding mean negative CSA strain of 5.5-8% (Nuri et al., 2016; Obst et al., 2015b; Obst et al., 2014b; Reeves and Cooper, 2014), negative ML diameter strain of 4.6-8.7% (Iwanuma et al., 2011; Obst et al., 2015b; Obst et al., 2014b), and positive AP diameter strain of 8-10.4% (Obst et al., 2015b; Obst et al., 2014b) throughout the entire tendon length, with the tendon volume remaining unaltered (Iwanuma et al., 2011; Nuri et al., 2016; Obst et al., 2015b; Obst et al., 2014b). As the healthy free AT behaves iso-volumetrically under load (Iwanuma et al., 2011; Nuri et al., 2016; Obst et al., 2015b; Obst et al., 2014b), the load-induced alterations in free tendon transverse and longitudinal morphologies are indicative of a change in tendon matrix shape, likely due to the reorganization of the collagenous and non-collagenous tendon matrix components resulting from the extension, sliding and rotation of the collagen fibrils (Puxkandl et al., 2002; Sasaki and Odajima, 1996), fibres (Cheng and Screen, 2007; Screen, 2008), and fascicles (Thorpe et al., 2013b; Thorpe et al., 2014) and the lateral compression of the collagen molecules (Wang et al., 2000) and glycoproteins (Thorpe et al., 2013a). Such reorganization in healthy free AT matrix components under load may provide a mechanism by which the free tendon balances the

heterogeneous force production of the triceps surae muscles (Arndt et al., 1998; Bojsen-Møller and Magnusson, 2015) and the resulting non-uniform deformation and stress concentration within the tendon (Franz et al., 2015; Slane and Thelen, 2014), and the intratendinous shear stress (Bojsen-Møller et al., 2004; Lersch et al., 2012). This may facilitate the transfer of high repetitive tensile loading within the free tendon, potentially reducing the likelihood of injury, a function, which is crucial in high-strain energy-storing tendons like human AT (Lichtwark and Wilson, 2005; Stephens et al., 1989). However it remains unclear how MAT changes the 3D morphology of the free tendon under load.

MAT has been shown to adversely affect AT mechanical and material properties, with the tendinopathic AT exhibiting greater longitudinal strain, lower stiffness, lower Young's modulus, and higher hysteresis in comparison to healthy tendon under the same tensile load (Arya and Kulig, 2010; Chang and Kulig, 2015; Child et al., 2010; Kulig et al., 2016; Wang et al., 2012). Our present knowledge regarding the load-induced changes in tendon morphology in MAT are limited to short-term alterations in tendon morphology following exercise. For example, studies of lower limb tendons (e.g. Achilles and patellar tendons) have demonstrated an immediate decrease in tendinopathic tendon AP diameter and water content after an acute bout of eccentric exercise (Grigg et al., 2012; Ho and Kulig, 2016b; Wearing et al., 2015) and 1-h floor-ball match (Fahlström et al., 2002) and tendon volume following long-term eccentric exercise (Shalabi et al., 2004b). Such post-exercise reduction in tendinopathic tendon AP diameter, water content, and volume has been speculated to be the result of the load-induced fluid exudation from tendon core to the peri-tendinous space and collagen fiber realignment (Grigg et al., 2012; Hannafin and Arnoczky, 1994; Helmer et al., 2006; Wellen et al., 2004; Wellen et al., 2005). These

studies have also reported conflicting results with respect to the magnitude of exercise-induced changes in tendon morphology between the tendinopathic and healthy tendons, with the tendinopathic tendon undergoing less, more, or equivalent reduction in tendon AP diameter, volume, and water content, respectively in comparison to healthy tendon (Grigg et al., 2012; Ho and Kulig, 2016b; Shalabi et al., 2004b; Wearing et al., 2015). Therefore, there is a need to investigate the tendinopathic tendon 3D transverse morphology and volume under load. Such information could advance our understanding of the tendinopathic AT physiology and mechanobiology, provide *in vivo* data for development of computation models of the tendinopathic AT during load, and provide a potential mechanism to explain the therapeutic effect of tendon loading via ankle exercise in reducing tendon pain and restoration of function in people with tendinopathy (O'Neill et al., 2015; Rio et al., 2015). Furthermore, AT longitudinal strain at the level of whole AT complex (i.e., gastrocnemius MTJ to calcaneus) in people with MAT has been characterised in previous *in vivo* studies and reported to be greater than that of the healthy AT under the same tensile loading (Arya and Kulig, 2010; Child et al., 2010). Given that free AT is mostly affected by Achilles tendinopathy, the whole AT longitudinal strain during tensile loading may not represent the strain at the location of tendinopathy and may underestimate the free AT strain.

The purpose of this study was to compare the 3D morphology and volume of the free AT at rest and during a sub-maximal isometric plantarflexion contraction in MAT, the contralateral AT and the AT of healthy controls. It was hypothesised that for MAT compared to the contralateral and healthy control tendons that: (1) resting CSA would be greater along the length of the tendon due to a greater AP diameter, (2) longitudinal and

transverse (i.e., CSA and AP diameter) strains would be greater under load and (3) tendon volume would decrease under load.

5.3 Materials and Methods

5.3.1 Participants

Participants were recruited through social networking sites, flyers, and mailings to physiotherapy clinics, sport medicine centres, and hospitals. The inclusion criteria were: male adults, 18-60 years of age with unilateral symptomatic MAT, minimal duration of symptoms of 3 months, and a Victorian Institute of Sports Assessment-Achilles tendon (VISA-A) of less than 80 points (Alfredson et al., 1998; Debenham et al., 2016). The definition of MAT was pain, discomfort, tenderness to palpation, and focal thickening of AT evident in both longitudinal and transverse scans of 2D ultrasound in tendon mid-portion (2 to 7 cm proximal to the AT calcaneal insertion) (Maffulli, 1998; Van Dijk et al., 2011) (Figure 23A,B,C). To avoid any possible effect of gender on tendon mechanical and morphological properties, only males were recruited for this study (Kubo et al., 2003). Potential participants were excluded if they had symptoms of bilateral tendinopathy, insertional tendinopathy, any lower limb musculoskeletal injuries, and/or history of AT rupture or lower limb surgery. All participants were examined by a physiotherapist (L.N) with 7 years of clinical experience in musculoskeletal injuries. A total of 14 patients took part in the study, of which 4 were excluded due to bilateral AT tendinopathy symptoms (n = 2), VISA score above 80 points (96, n = 1), and pain duration of less than 3 months (1 month, n = 1). Ten control male participants from the local university community were also included in the study and matched to patients with Achilles tendinopathy by age,

height, weight, physical activity level, and the length of free AT. The physical activity level was assessed using the International Physical Activity Questionnaire (IPAQ-long format) (Booth et al., 2003). The exclusion criteria for the control group were the same as those for patients with Achilles tendinopathy. Furthermore, they had no history of current or previous Achilles tendon pain and scored 100 on VISA-A. Participant characteristics are provided in Table 1. All participants were informed about the study protocol and signed the consent forms. The study was approved by the local university Ethical Committee and was performed in accordance with the Declaration of Helsinki.

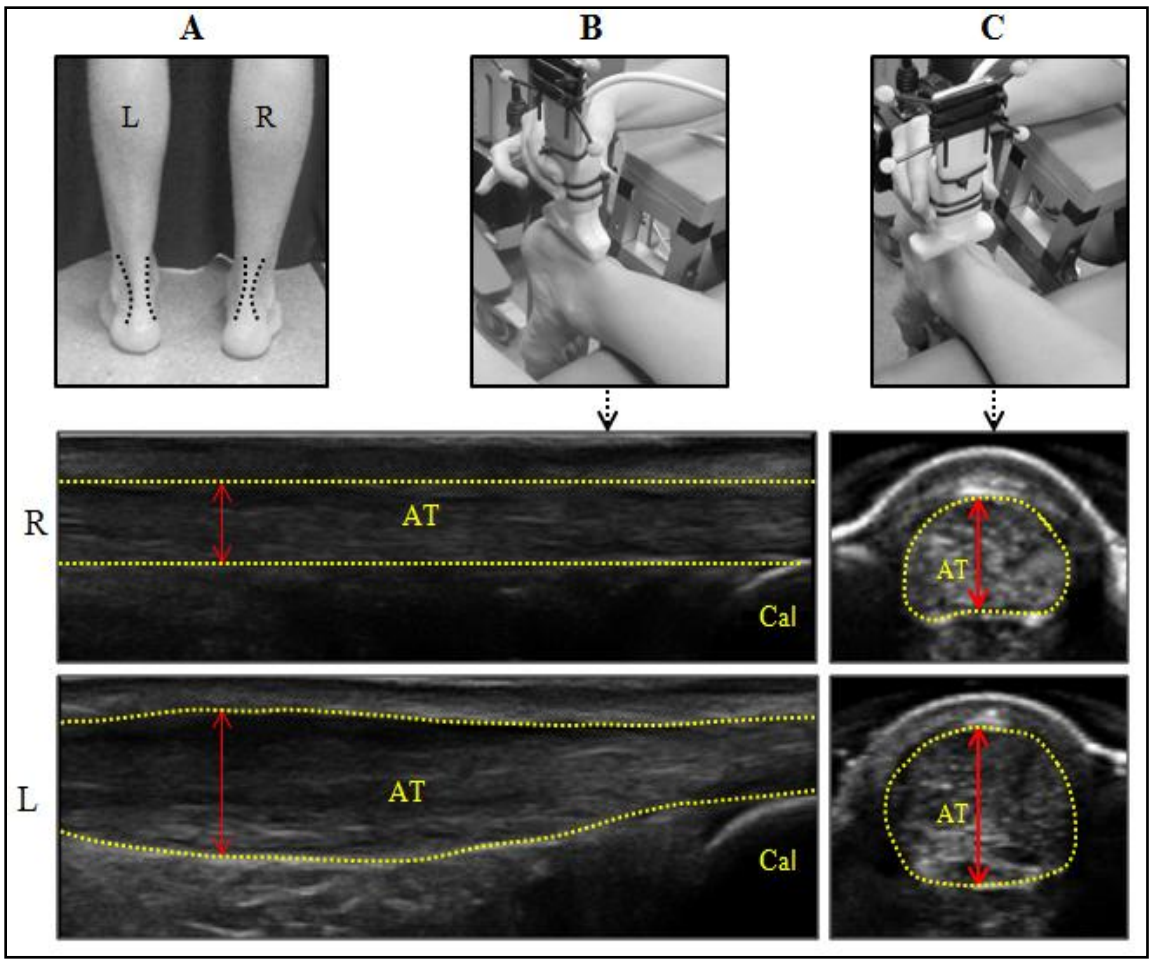

Figure 23: *(A) Posterior view of a participant with mid-portion Achilles tendinopathy showing swelling and thickening over the involved tendon (left side). Black dotted lines outline the tendon. The longitudinal (B) and transverse (C) two-dimensional ultrasound images of Achilles tendon (AT) of the participant show a thickened AT mid-portion with irregular structure on the left side (L) and a normal structure on the right side (R). Yellow dotted lines outline the tendon. The double-headed arrows indicate AT thickness. Cal, calcaneus.*

Table 1. Participant characteristics

	Achilles tendinopathy Group (*N* = 10)	Control Group (*N* = 10)	*P* Value
Age, y	42.2 ± 11.5	41.9 ± 12.2	0.95
Height, m	176.6 ± 7.5	176 ± 9.8	0.39
Body mass, kg	79.8 ± 7.8	82.2 ± 7.0	0.96
Physical activity level (MET-min/week)	5556 ± 3067	5969 ± 3789	0.63
VISA-A (0-100)	54.2 ± 16.5	100 ± 0.0	0.001*
Duration of symptoms, y	3.5 ± 2.9	NA	NA

*Data are expressed as means ± SD, N = 20. *Statistically significant difference between tendinopathy and control groups (P < 0.05). MET, metabolic equivalent of task; VISA-A, Victorian Institute of Sport Assessment-Achilles; NA, not applicable; y, year; m, meter; kg, kilogram; min, minutes.*

5.3.2 Experimental design and protocol

All participants completed two sessions (familiarization and testing), held 1 week apart. In each session, participants lay prone on a testing plinth with their knee and hip fully extended (0° flexion) and the ankle in 0° dorsiflexion (i.e., 90° angle between the sole of the foot and the shank). Their foot was tightly fixed to the foot plate of a fixed torque transducer (Futek TFF600, Irvine, California, USA) by using a custom-built ratchet system to minimize heel lift during plantarflexions (Obst et al., 2014a; Obst et al., 2014b). Care was taken to align the axis of rotation of the participant's ankle with that of the torque transducer. To ensure participants maintained the target ankle torque for the entire duration of the contraction, the real-time visual feedback of the torque generated at the ankle joint was displayed on a computer monitor. LabView data acquisition software (LabVIEW 9.9,

National Instruments, Austin, Texas, USA) was used to acquire the torque signals from the transducer at a sampling frequency of 1000 HZ. At the familiarization session, participants with tendinopathy completed 3 × 5-s MVIC of the ankle plantarflexion with their tendinopathy leg. Each contraction was separated by approximately 60 s of rest to minimize any possible effects of fatigue. The highest peak torque recorded across the three trials for the tendinopathy leg (90.5 ± 10.35 N.m) was used to determine the target torque (50% MVIC) for the tendinopathy and contralateral legs in tendinopathy group and healthy leg in control group in the subsequent testing session. For the control group, the healthy leg was randomly assigned via coin toss. Participants in both groups were then asked to perform a series of sub-maximal plantarflexion isometric contractions (50% MVIC of the tendinopathy leg) to ensure that they became familiarized with the testing procedure. They were also asked to refrain from any strenuous exercise for 48 hours before the testing session. In the testing session, participants initially performed 3 × 25-s isometric plantarflexion contractions at 50% MVIC to condition the relevant tendon (Nuri et al., 2016). Participants subsequently performed a single isometric plantarflexion contraction at 50% MVIC with their both legs separately in tendinopathy group and with the allocated healthy leg in control group, during which ultrasound scans of their posterior leg were acquired. The order of the testing the legs (tendinopathy, or contralateral healthy leg) in tendinopathy group was randomly determined for each patient. A resting scan of AT was also acquired immediately prior to isometric plantarflexion contraction for each leg separately. To avoid any potential confounding effects of conditioning recovery response of AT on tendon mechanical and morphological properties, the experiment was performed within the time course of AT recovery following conditioning (< 30 min). No differences

in target ankle plantarflexion torque were found between the three legs (MAT: 45.77 ± 4.22 N.m; contralateral: 44.52 ± 5.25 N.m; healthy control: 44.52 ± 5.25 N.m). The measured torque during resting trials was all below 1.3 N.m.

5.3.3 Freehand 3D ultrasound system

A freehand three dimensional ultrasound (3DUS) system [a conventional 2DUS machine (SonixTouch, Ultrasonix, Richmond, BC, Canada) that consisted of a 58-mm linear transducer (L14–5W/60 linear, Ultrasonix) and a five-camera optical tracking system (OptiTrack V100:R2, Tracking Tools Version 2.5.2, NaturalPoint, Corvallis, Oregon, USA)] was used to obtain 3D images of AT (Obst et al., 2015a; Obst et al., 2015b). The accuracy and reliability of our freehand 3DUS system for AT mechanical and morphological properties has been established in previous studies (Obst et al., 2014a; Obst et al., 2014b). To construct 3D AT images from a sequence of conventional 2DUS images, the 3D orientation and position of the four reflective markers rigidly attached to the transducer was recorded using the optical tracking system. Prior to data collection, our system was calibrated using a single wall phantom calibration procedure recommended by Stradwin software developers (Prager et al., 1998). Following calibration, pixel coordinates in any recorded 2DUS images were transformed into 3D coordinate system with a reported positional error of approximately of ± 0.4 mm (Prager et al., 1998).

One investigator (L.N) performed all the AT ultrasound scans with the following ultrasound image settings: frame rate = 60 Hz, depth = 40 mm, gain = 50%, dynamic range = 65 dB, map = 4, and power = 0. To guide the ultrasound scanning direction, the anatomical location of calcaneal notch (Cal notch) and soleus (SOL) MTJ were determined

in 2D real-time ultrasound and marked on the skin using a marking pen. The ultrasound scanning area was then drawn on the skin between these two landmarks and ultrasound gel was applied over the scanning area to minimize the pressure exerted by the transducer on the skin and assist in the transmission of the ultrasound signal. To maximize the tendon transverse image quality, a rectangular shaped stand-off pad was attached to the end of the transducer using a thermoplastic custom-made ultrasound stand-off holder. Images of the AT were acquired using a single transverse sweeping scan by moving the ultrasound transducer manually from the distal calcaneus to SOL MTJ at a steady speed. The total duration of scanning was ~10 s and the finalized stacks of 2D B-mode images consisted of ~600 frames with a distance between frames of ~0.1 mm.

5.3.4 Image segmentation, tendon longitudinal strain, surface rendering, and tendon transverse morphology measurement

All 3DUS images were segmented in Stradwin software. To determine tendon length, two main anatomical point landmarks (Cal notch and SOL MTJ) were manually digitized in reconstructed 3D images using the 3D landmark tool (Figure 24A). The 3D position of each landmark was visualised using a combination of frontal, sagittal, and transverse image re-slices (Figure 24B) and tendon length was defined as the point-point distance between Cal notch and SOL MTJ. Tendon elongation was calculated by subtracting tendon length in the 50% MVIC contraction from the corresponding resting length. Tendon longitudinal strain was then calculated by dividing tendon elongation by the corresponding resting length. Tendon cross-sections were digitized manually from the original B-mode transverse images from the calcaneal notch to the SOL MTJ at ~1-2 mm intervals. The 3D surface rendering of the free AT was then created from the digitized CSA contours using

the in-built surface interpolation algorithm in Stradwin software (Treece et al., 2000). The 3D reconstructed free AT surfaces were then exported into Matlab software (Version R2013b, The Mathworks, Natick, Massachusetts, USA) and analyzed using custom scripts (Obst et al., 2014b) to determine tendon transverse morphology (CSA, AP diameter, and ML diameter). The CSA, AP diameter and ML diameter transverse strains were then determined by dividing the tendon transverse deformation by the corresponding resting values. All tendon parameters measured were averaged over 10% intervals of normalized tendon length and expressed as a percentage of tendon length in 10% increments. The measurement of free AT transverse strain during tensile loading could have important implications for our understanding of the AT elastic energy storage and release action (Lichtwark and Wilson, 2006), triceps surae muscle bulging characteristics (Aziz et al., 2008), and AT in vivo mechanobiology (Wang et al., 2012).

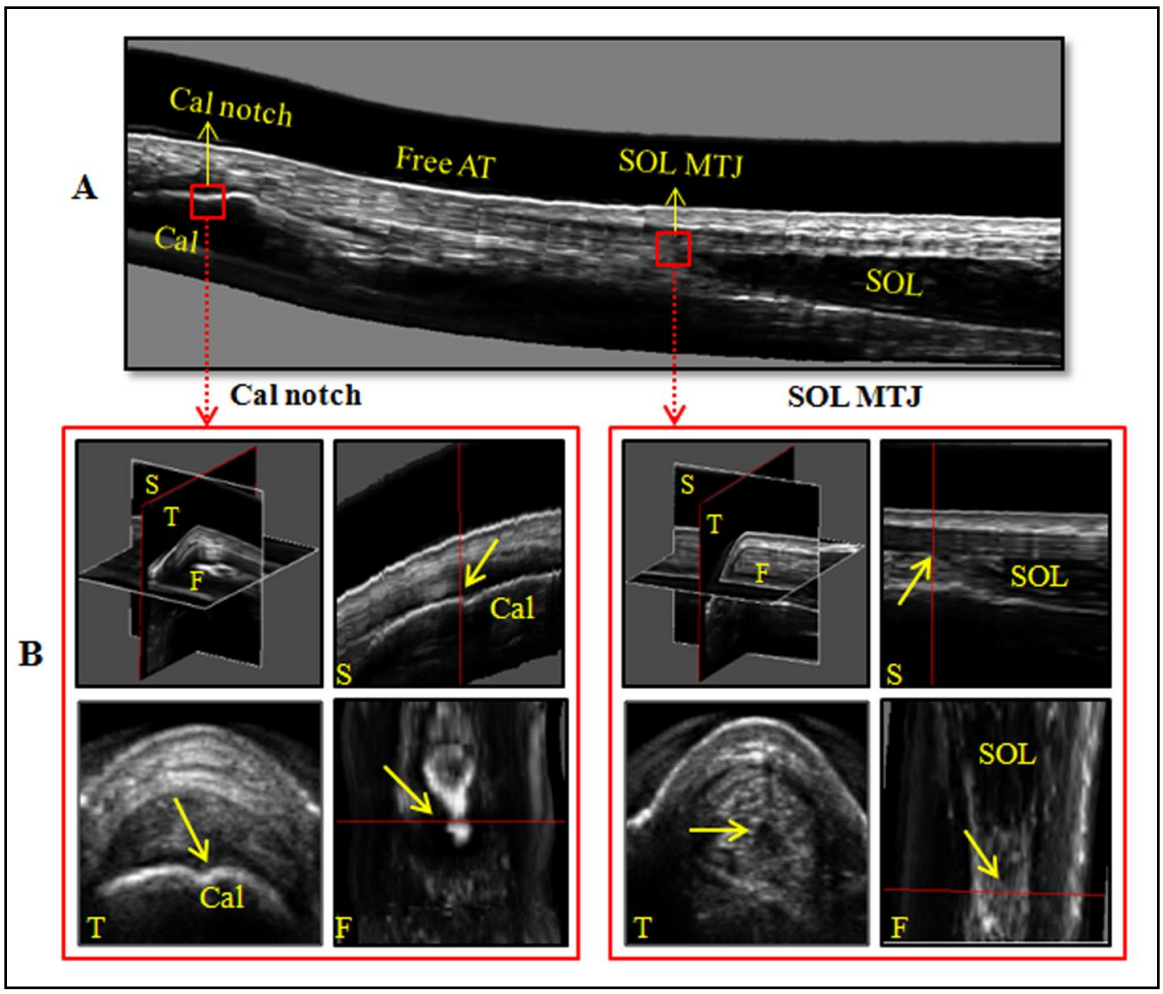

Figure 24: *(A) Sagittal plane re-slices of a reconstructed three-dimensional (3D) ultrasound image of the free Achilles tendon (AT). Two anatomical landmarks [calcaneal (Cal) notch, and soleus muscle-tendon junction (SOL MTJ)] were segmented on 3D AT images for calculation of AT length. (B) The exact 3D anatomical location of each landmark was determined using sagittal (S), frontal (F), and transverse (T) image planes.*

5.3.5 Statistical analysis

A two-way (3 by 10), repeated measures General Linear Model (GLM) was used to examine the main effects and interactions of the tendon type (tendinopathy, contralateral, and healthy) and the tendon region (10-100% of the normalised tendon length) for: (1) tendon transverse morphology (CSA, AP diameter, and ML diameter) at rest, and (2) tendon transverse strain (CSA, AP diameter and ML diameter) under load. A two-way repeated measures GLM was also used to assess the effect of tendon type and loading condition (Rest versus loaded) on tendon volume. The effect of tendon type on free AT length at rest, free AT longitudinal strain under load, and ankle plantarflexion torque under load was assessed using a between factor GLM. Bonferroni post hoc comparisons were used to identify differences amongst all tendon types and loading condition. All statistical analyses were performed using the Statistical Package for the Social Sciences version 22 (SPSS Inc, Chicago, IL, USA) and the level of significance was set at $\alpha = 0.05$. Data are reported as mean ± standard deviation (SD) in the text and the table and as mean ± standard error of mean (SEM) in the figures.

5.4 Results

5.4.1 Tendon morphology at rest

There were no significant differences in free tendon resting length between the tendon types (MAT: 72 ± 22 mm, contralateral: 71 ± 21 mm, healthy: 70 ± 19 mm) ($F_{2,27} = 0.06$, $P = 0.94$). The resting dimensions for each tendon in the transverse plane are displayed in figure 25. A significant main effect of tendon type ($F_{2,16} = 12.35$, $P = 0.001$) and a

significant tendon type-by-region interaction ($F_{18,144}$ = 1.91, P = 0.01) were also detected for tendon CSA at rest (Figure 25A). Significant main effects for tendon type ($F_{2,16}$ = 21.41, P < 0.001) and the tendon type-by-region interaction ($F_{18,144}$ = 2.95, P < 0.001) were similarly detected for tendon AP diameter at rest (Figure 25B). Post-hoc comparisons revealed that tendon CSA and AP diameter in MAT were significantly greater than those of the contralateral and healthy tendons at all increments from 20% to 90% of the normalized tendon length (P < 0.05). No significant main or interaction effects were detected for tendon ML diameter (P > 0.05) (Figure 25C). Pairwise comparisons revealed a trend toward a significantly higher CSA and AP diameter in contralateral versus healthy tendons from 40% to 100% of the tendon length (P = ~0.06).

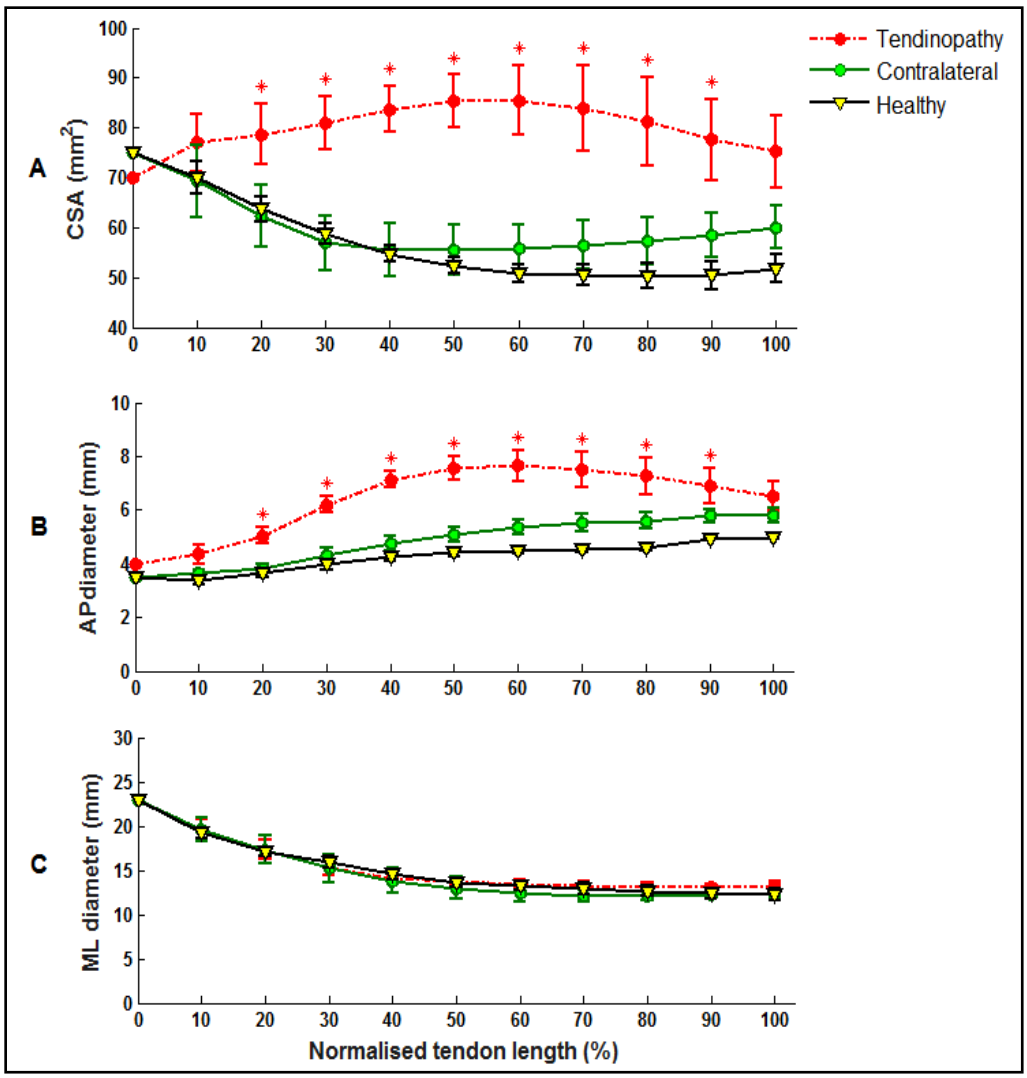

Figure 25: *The mean group free Achilles tendon (AT) cross-sectional area (CSA) (A), antero-posterior (AP) diameter (B), and medio-lateral (ML) diameter (C) at rest, expressed relative to the normalized tendon length (0% = calcaneal notch; 100% = soleus muscle-tendon junction) in tendinopathic (red circles), contralateral (green circles), and healthy (yellow triangles) control tendons. Post hoc comparisons revealed significantly higher values for CSA and AP diameter in tendinopathic tendon compared to the contralateral and healthy control tendons at 20-90% of the normalized tendon length. Asterisk (*) indicates significant difference between tendinopathic and contralateral and/or healthy tendons. Data are expressed as mean ± SEM (N = 20).*

5.4.2 Tendon longitudinal and transverse strains under load

There was a significant main effect of tendon type on tendon longitudinal strain under load ($F_{2,27}$ = 15.54, P < 0.001). Post-hoc comparisons revealed that free tendon underwent significantly greater longitudinal strain in the tendinopathic leg (10.8 ± 3.1%) compared to those of the contralateral and healthy legs (6.7 ± 1.4% and 6.3 ± 0.8%, respectively). The deformations and corresponding strains experienced by the CSA, AP diameter, and ML diameter are presented in figure 26. A significant main effect of tendon type was detected for CSA strain ($F_{2,16}$ = 29.51, P < 0.001) (Figure 26A), and AP diameter strain ($F_{2,16}$ = 27.89, P < 0.001) (Figure 26B). A significant tendon type-by-region interaction ($F_{18,144}$ = 4.88, P < 0.001) was also detected for AP diameter strain. No significant main or interaction effects were detected for tendon ML diameter strain (P > 0.05) (Figure 26C). Pairwise comparisons revealed that tendon CSA and AP diameter strains were significantly higher for MAT compared to the contralateral and healthy tendons across all the tendon regions (P < 0.05). No significant differences in tendon ML diameter strain were found between tendon types in any of the tendon regions (P > 0.05). Furthermore, no significant differences in tendon longitudinal and transverse morphology (CSA, AP diameter, and ML diameter) strains were detected at any of the tendon regions between the contralateral and healthy control tendons (P > 0.05).

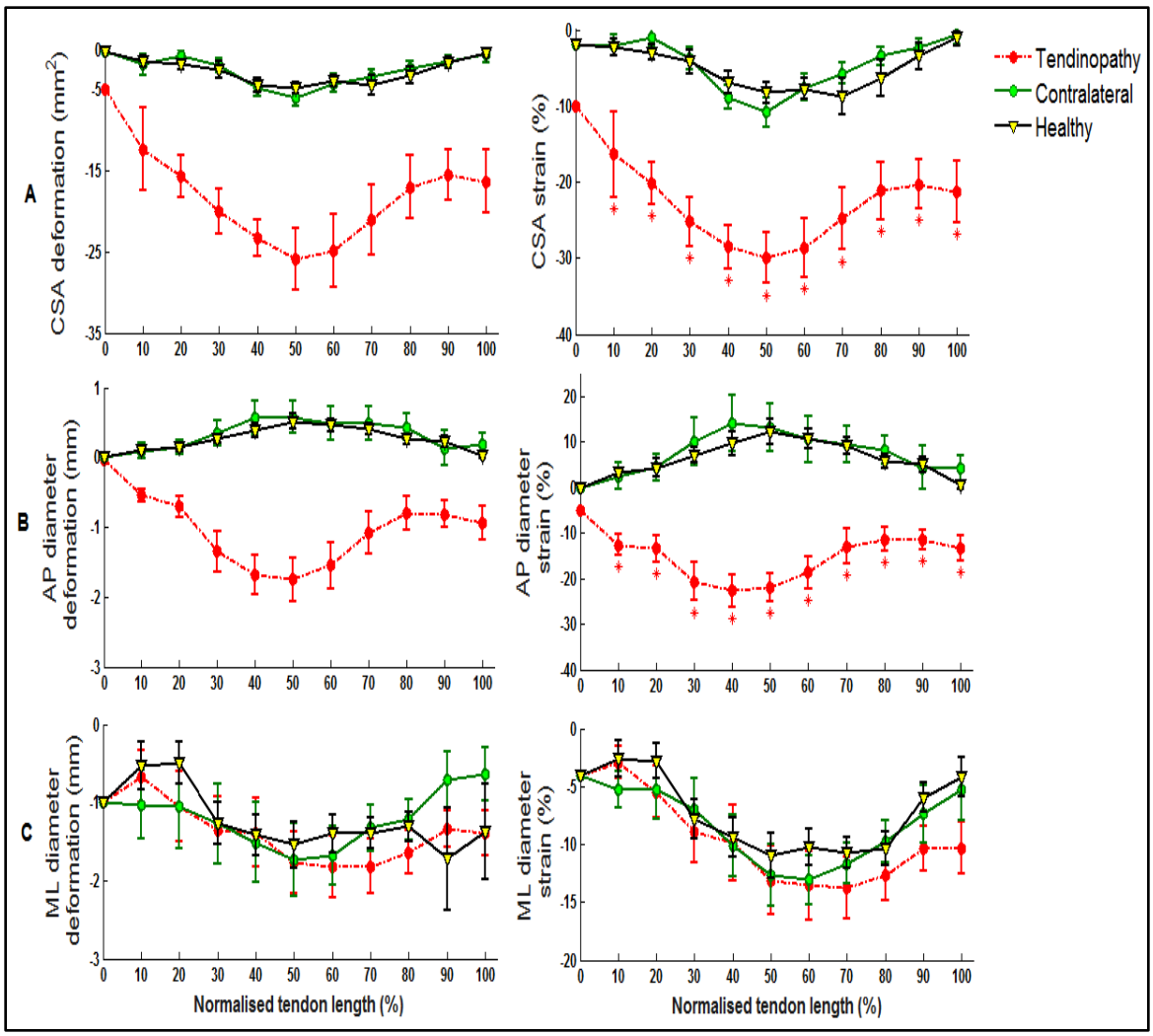

Figure 26: *The mean group deformation and the corresponding mean group strain of free Achilles tendon (AT) cross-sectional area (CSA) (A), antero-posterior (AP) diameter (B),and medio-lateral (ML) diameter (C) during load (50% maximal voluntary isometric plantarflexion contraction), expressed relative to the normalized tendon length (0% = calcaneal notch; 100% = soleus muscle-tendon junction) in tendinopathic (red circles), contralateral (green circles), and healthy (yellow triangles) tendons. Post hoc comparisons revealed that the tendinopathic free AT underwent significantly greater CSA and AP diameter strains relative to the contralateral and healthy control matched tendons*

across all the tendon regions. Asterisk (*) indicates significant difference between the tendinopathic and contralateral and/or healthy tendons. Data are expressed as mean ± SEM (N = 20).

The reconstructed free AT and the corresponding transverse ultrasound images along the tendon length for representative participants are depicted in figure 27, which illustrates the changes in tendon 3D morphology from rest to load in tendinopathic, contralateral, and healthy control tendons.

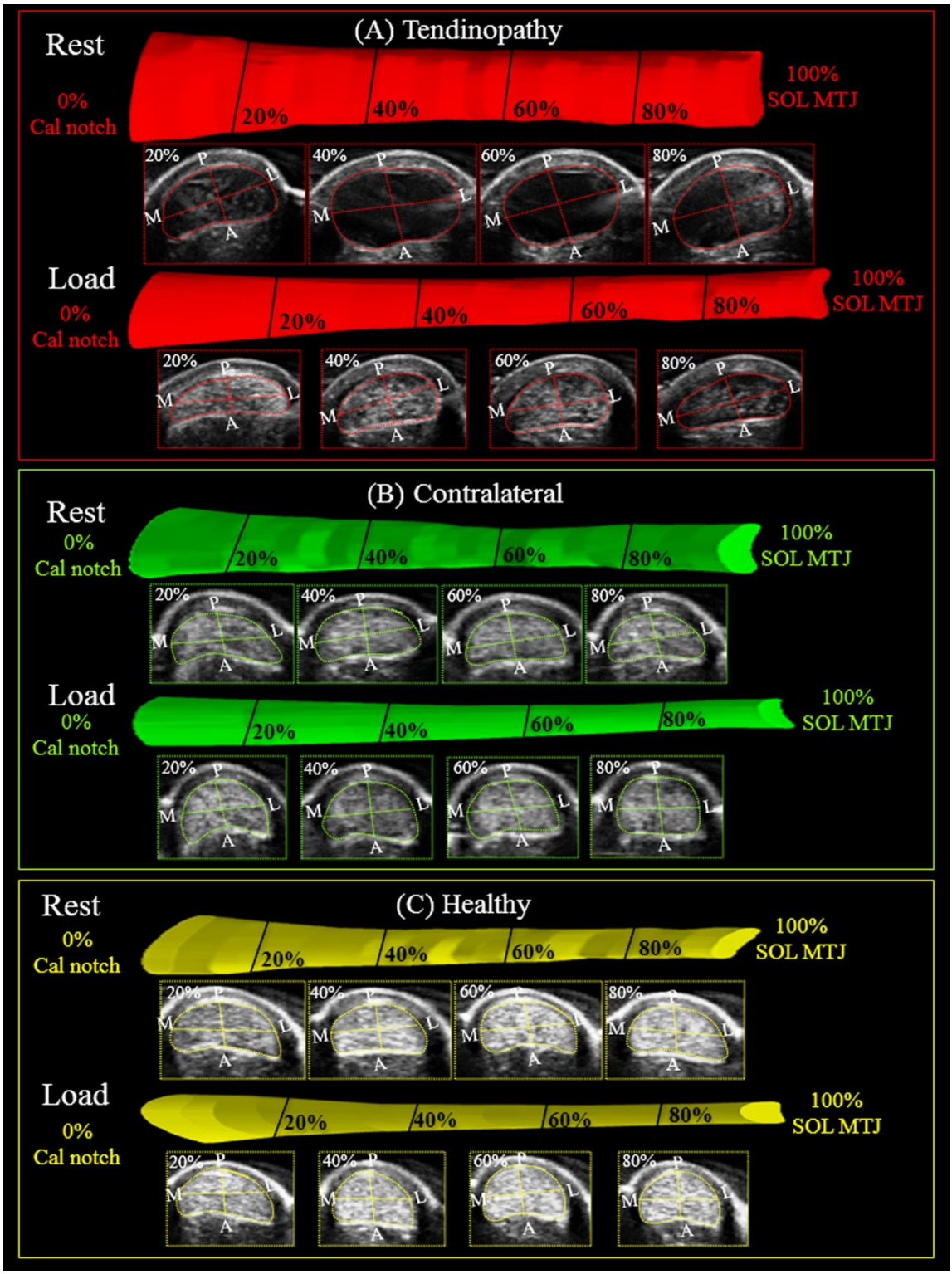

Figure 27: *Changes in the morphology of the three-dimensional (3D) surface-rendered free Achilles tendon (AT) and the corresponding transverse ultrasound images at 20, 40,*

60, and 80% of the tendon length [0% = calcaneal notch (Cal notch); 100% = soleus muscle-tendon junction (SOL MTJ)] from rest to load in tendinopathy (A), contralateral (B), and healthy control matched (C) tendons. Data is from a single participant as depicted in figure 23 for (A) and (B) and the healthy control matched participant (C). P, posterior; A, anterior; M, medial; L, lateral.

5.4.3 Tendon volume at rest and under load

A significant main effect of tendon type and tendon loading condition ($F_{2,18}$ = 26.68, P < 0.001; $F_{1,9}$ = 26.90, P = 0.001) and a significant tendon type-by-tendon loading condition interaction ($F_{2,18}$ = 29.06, P < 0.001) were detected for tendon volume (Figure 28). Post-hoc comparisons revealed that tendon volume in MAT at rest and under load were significantly greater than those of the contralateral and healthy tendons. Furthermore, a significant reduction in tendon volume under load in MAT was observed (P < 0.001).

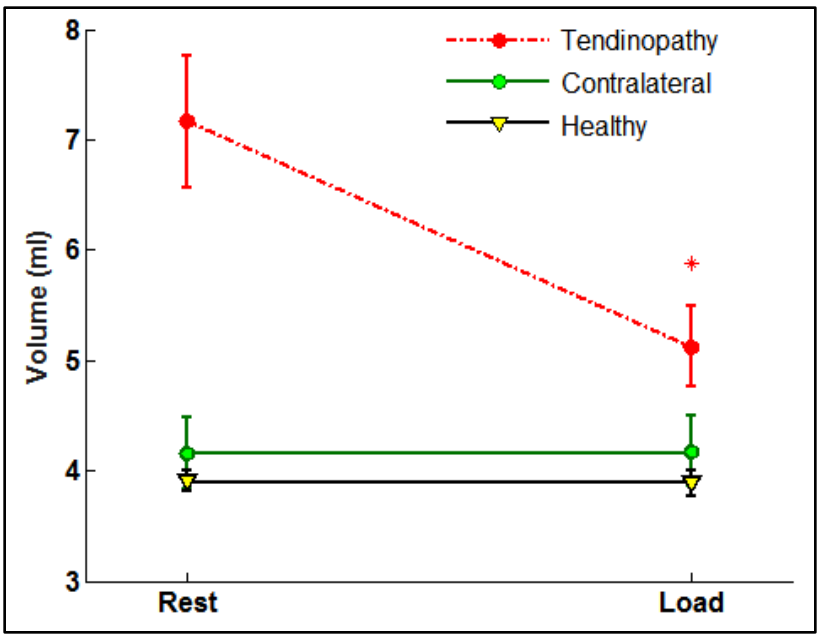

Figure 28: *Change in the mean group free Achilles tendon (AT) volume from resting to the loading states (50% maximal voluntary isometric plantarflexion contraction) in tendinopathic (red circles), contralateral (green circles), and healthy (yellow triangles) tendons. Post hoc comparisons revealed that the tendinopathic free AT experienced a significant reduction in tendon volume from resting to the loading states. Asterisk (*) indicates significant difference in free AT volume between resting and loading states ($P < 0.05$). Data are expressed as mean ± SEM ($N = 20$).*

5.5 Discussion

This *in vivo* study demonstrated that the tendinopathic free tendon had a larger CSA than contralateral and healthy tendons throughout the entire tendon length at rest, which was primarily driven by a greater tendon AP diameter. When loaded, the tendinopathic free tendon underwent a longitudinal strain, which was accompanied by a reduction in tendon transverse morphology (i.e., CSA, AP diameter, and ML diameter) along the entire tendon

length, resulting in a tendon volume reduction. In contrast, the contralateral and healthy tendons remained iso-volumetric and bulged along the AP axis during tensile loading. The tendinopathic free tendon also experienced greater longitudinal and transverse strains (i.e., CSA and AP diameter) relative to the contralateral and healthy tendons across all the tendon regions under the same external ankle torque. Overall, these findings suggest that the MAT changes the normal 3D morphology of the tendon at rest and under load throughout the entire tendon length. The findings of the present study could have important implications for our understanding of the tendinopathic AT physiology and mechanobiology during load, the frameworks for computational models of the tendinopathic tendon, the mechanisms associated with the therapeutic effect of tendon loading via ankle exercise in reducing tendon pain and restoration of function in people with tendinopathy, and also the characterization of pathologies of AT in people with MAT in clinical settings.

5.5.1 Tendon morphology at rest

Mean tendon CSA was on average approximately 40% larger in tendinopathic tendon than the contralateral and healthy tendons across all tendon regions at rest, which was explained by a corresponding larger mean AP diameter in tendinopathic tendon. These differences in tendon CSA and AP diameter were most pronounced in the tendon mid-portion, and were not evident along the ML diameter at any of the tendon regions. These findings provide the first *in vivo* data that describe free tendon morphological characteristics across all tendon regions in both tendinopathic and contralateral healthy tendons. Our finding that the free tendon with MAT has a larger CSA and AP diameter throughout the entire tendon length at

rest supports prior studies that have shown an increase in tendon thickness and area at a single site (Alfredson et al., 2014; Cassel et al., 2015; Docking et al., 2015; Grigg et al., 2012; Lind et al., 2006; Van Schie et al., 2010) in tendon mid-portion as a result of pathological alterations in tendon structure and composition in individuals with MAT. The widespread alteration in tendon morphology of the tendinopathic tendon (i.e., increase in tendon CSA and AP diameter) across the length of tendon is consistent with animal models that demonstrate localized tendon injury affects the entire tendon histology, gene expression, composition, and mechanical and morphological properties (Choi et al., 2016; Jacobsen et al., 2015; Smith et al., 2008). This finding suggests that the treatment strategies in people with MAT should aim to improve and monitor pathology in the entire tendon to minimize the risk of poor functional outcomes and potential recurrent AT injuries (Gajhede-Knudsen et al., 2013; Hägglund et al., 2007).

Further, based on our data, the increase in tendon CSA in the tendinopathic side seems to be primarily driven by increase in tendon AP, but not ML, diameter. To our knowledge, this is the first study to show that tendon ML diameter is not affected by the pathological changes associated with the tendinopathy. This finding could be explained by three potential reasons. First, previous studies have provided evidence that the anterior and posterior surfaces of the AT paratenon sheath undergoes degenerative process such as marked degenerative vascular changes, proliferation of loose connective tissue, increased number of elastic microfibrils, and widespread fat necrosis in tendinopathic AT (Harris and Peduto, 2006; Kvist et al., 1988; Ostlere, 2003; Paavola et al., 2002), leading to a more compliant tendon sheath (Leung and Griffith, 2008; Stecco et al., 2015; Stecco et al., 2014). As paratenon shapes the tendon core morphology (Carmont et al., 2011), it is

reasonable to speculate that the disruption and disorganization of the collagen fibers (Pingel et al., 2014), hypercellularity (Andersson et al., 2011a; Åström and Rausing, 1995), and increase in ground substance (Józsa and Kannus, 1997) and water content (de Mos et al., 2007) in tendon core in chronic Achilles tendinopathy may stretch the paratenon from anterior and posterior surfaces, resulting in bulging of tendon core in AP direction. Additionally, the mechanisms regulating tendon healing response following injury may contribute to the increase in tendon core AP diameter. Previous studies investigating the location and phenotype of cells that mediate tendon injury response have established that following tendon injury, paratenon cells proliferate, express tenogenic markers, and produce collagen fibers. These cells migrate toward the anterior and posterior surfaces of the injury site and bridge the injury site by assembling the collagen fibers in tendon core AP direction (Dyment et al., 2013; Yoshida et al., 2016). Lastly, it has been shown that a thicker tendon reduces the average stress (i.e. force/area) across the tendon cross section and provides a greater safety margin (Shim et al., 2014). It therefore seems plausible to assume that the increase in tendinopathic tendon AP diameter and the resulting increase in tendon CSA may be an important adaptation to compensate for the tendon lower mechanical and material properties (Arya and Kulig, 2010; Chang and Kulig, 2015; Child et al., 2010; Kulig et al., 2016) and structural disorganization (Docking and Cook, 2015; Docking et al., 2015) in response to mechanical loading in order to reduce the risk of tendon rupture (Hess, 2009). Irrespective of the mechanisms explaining this, our findings confirm the use of tendon AP diameter at tendon resting state as an important ultrasound diagnostic criterion in people with chronic MAT (Leung and Griffith, 2008; McAuliffe et al., 2016).

Free AT volume in tendinopathy, contralateral, and healthy legs at resting state were 7.16, 4.15, and 3.91 ml, respectively in the present study that falls well within the range reported in previous *in vivo* studies for free AT volume [tendinopathic free AT volume: ~6-8 ml (Gärdin et al., 2006; Gärdin et al., 2010; Shalabi et al., 2004a; Shalabi et al., 2004b; Shalabi et al., 2005); contralateral and healthy free AT volume: ~3-5 ml (Gärdin et al., 2006; Gärdin et al., 2010; Nuri et al., 2016; Obst et al., 2015b; Obst et al., 2014b)]. As no significant differences in free AT length were found between the three tendons at r**e**st (~70 mm), the higher volume of the tendon in tendinopathy leg observed here reflects the larger CSA of the tendinopathic tendon as a result of pathological alterations in tendon structure and composition accompanying chronic MAT (Andersson et al., 2011b; Corps et al., 2006; de Mos et al., 2007; Docking and Cook, 2015; Docking et al., 2015; Józsa and Kannus, 1997; Pingel et al., 2014).

5.5.2 Tendon longitudinal strain under load

The tendinopathic free tendon underwent a greater longitudinal strain, which was approximately two-thirds greater than healthy and contralateral healthy free tendons under the same tensile load (50% MVIC). The strains for the contralateral and healthy control tendons from the present study (~6.5%) were in close agreement (~5-6.8%) with prior studies of normal tendon using the same approach (Farris et al., 2013a; Finni et al., 2003; Nuri et al., 2016; Obst et al., 2015b; Obst et al., 2014b). Two prior studies reported 25% greater longitudinal whole AT strain in MAT compared to healthy control tendons at 100% MVIC (Arya and Kulig, 2010; Child et al., 2010). The higher strains in the present study at the level of the free AT (~10.7%) compared to prior studies of whole AT strain (~5%) (Arya and Kulig, 2010; Child et al., 2010) is in part because measures of whole AT strain

underestimate the strain at the level of the free AT, because the whole AT includes a portion of aponeurosis, which experiences low strains compared to the free AT (Farris et al., 2013a; Finni et al., 2003; Lichtwark et al., 2013a; Nuri et al., 2016; Obst et al., 2015a). This raises the possibility that longitudinal strain at the level of the pathological free AT may have been underestimated in previous *in vivo* studies that reported AT strain only at the level of whole AT complex in people with MAT (Arya and Kulig, 2010; Child et al., 2010). This may indicate that only free AT in the tendinopathic side is more susceptible to higher risk of further injury and acute rupture during athletic and recreational activities that subject the tendon to repetitive loading without sufficient recovery time (Fung et al., 2010; Fung et al., 2009; Wren et al., 2001) and the treatment protocols designed for people with MAT should specifically target and monitor free tendon. Overall, these findings suggest that tendinopathic AT due to the pathological alterations in tendon structure and composition (Andersson et al., 2011b; de Mos et al., 2007; Docking and Cook, 2015; Docking et al., 2015; Józsa and Kannus, 1997; Pingel et al., 2014) and the resultant lower material properties (Arya and Kulig, 2010; Chang and Kulig, 2015; Child et al., 2010; Kulig et al., 2016) is more compliant, which could lead to higher risk of further injuries and pathological changes and diminished capacity to store and utilize energy during functional activities.

5.5.3 Tendon transverse strain under load

During a submaximal isometric plantarflexion contraction (50% MVIC), the MAT, contralateral, and healthy tendons experienced a reduction in tendon CSA and ML diameter across all the tendon regions that was accompanied by a reduction in tendon AP

diameter in tendinopathic tendon and an increase in tendon AP diameter in contralateral and healthy tendons along the entire tendon length. The mean CSA strain along the length of the tendon was substantially larger in MAT (-24.6%) compared to contralateral (-4.6%) and healthy control tendons (-5.2%). The larger negative CSA strain in MAT was primarily driven by a greater negative strain along the AP diameter in MAT (-15.9%) compared to the positive strain of AP diameter in contralateral (8.1%) and healthy control tendons (7.0%), with no differences in tendon negative strain along the ML diameter (~ -9%). The polarity AP strain for contralateral and healthy tendons was positive, indicating tendon bulging along the AP axis under tensile load so that the tendon CSA becomes more cylindrical under load (Obst et al., 2015b; Obst et al., 2014b). The thickening of the healthy tendon along the AP axis and thinning along the ML axis under load likely occur due to the internal reorganization of the healthy tendon matrix components, which may be critical to accommodate asymmetrical force production by activation of the triceps surae muscles (Arndt et al., 1998; Bojsen-Møller and Magnusson, 2015) and minimize areas of stress and strain concentration within the tendon matrix (Haraldsson et al., 2008). Whereas, the AP strain for MAT was negative, indicating thinning of the tendon along the AP axis as reported in prior *in vivo* studies for tendinopathic tendon in response to an acute bout of exercise (Fahlström and Alfredson, 2010; Grigg et al., 2012; Wearing et al., 2015). The tendinopathic tendon also underwent a non-uniform tendon transverse morphology strain along its length under load, with the tendon mid-portion undergoing greater reduction in tendon CSA (-28.4%), AP diameter (-20.0%), and ML diameter (-12.0%) relative to the tendon distal and proximal portions. This could be explained by the combination effects of the most pronounced pathological changes in tendon structure and composition at tendon

mid-portion in the tendinopathic side as evidenced by a larger tendon CSA and AP diameter in the present study and the unique structural and/or mechanical factors of free tendon mid-portion, such as the site of AT twist (Edama et al., 2015a; Obst et al., 2014b). This indicates that the tendinopathic tendon mid-portion is more susceptible to further pathological changes and higher risk of strain-related injuries (e.g., rupture) (Hess, 2009).

5.5.4 Tendon volume under load

The tendinopathic tendon experienced a volume reduction of 28% relative to resting volume, whereas volume was conserved under load in the contralateral and healthy tendons. One prior study has similarly reported a volume reduction in MAT following a prolonged bout of exercise (Shalabi et al., 2004b). As alterations in tendinopathic free tendon transverse and longitudinal morphologies under load were accompanied by tendon volumetric changes, the load-inducted alterations in tendinopathic tendon 3D morphology are not only indicative of change in tendon matrix shape but also change in tendon matrix fluid content. These findings suggest that, unlike the healthy free AT, the tendinopathic free tendon does not behave iso-volumetrically and undergoes a volume reduction during tensile loading. The most plausible explanation for this volume reduction in MAT under load is radial fluid redistribution from tendon core to the peri-tendinous space (Ahmadzadeh et al., 2015; Han et al., 2000; Hannafin and Arnoczky, 1994; Helmer et al., 2006; Helmer et al., 2004; Wellen et al., 2004; Wellen et al., 2005) or/and vascular mechanisms (Åström and Westlin, 1994; Öhberg et al., 2001). Fluid extrusion from the tendinopathic tendon core to the periphery of the tendon in response to tensile loading could be caused by several factors. Firstly, it is well known that increased amounts of interfibrillar GAGs is a major histopathological feature in Achilles tendinopathy (Corps et

al., 2006; Movin et al., 1998a). In a resting state, GAGs are highly polarized, negatively charged molecules, which attract water molecules, resulting in a hydrated and negatively charged tendon matrix shielded by the positive ions (Scott, 2001; Yoon and Halper, 2005). During mechanical loading, an electric potential, known as streaming potential (Gu et al., 1993; Lai et al., 1991), may be created as positive ions enter and leave the matrix, which, in turn, may lead to tendon matrix ionic disturbance and subsequent release of water molecules from GAG molecules. Further, the altered tendon loading pattern as a result of the impaired triceps surae muscles activities in the tendinopathic side (Azevedo et al., 2009) and the ineffective tendon loading transfer mechanisms due to the disorganized and disrupted collagen fibers and interfascicular matrix (Pingel et al., 2014) coupled with the high concentration of the free and bound water molecules (de Mos et al., 2007) in tendinopathic tendon matrix may create a high positive fluid pressure in tendon core during mechanical loading (Ahmadzadeh et al., 2015). The impairment in tendinopathic tendon membrane permeability (i.e., porosity and voids ratio) (Chen et al., 1998; Van der Voet, 1997) likely as a result of the pathological changes in tendon membrane material properties, thickness, and pore architecture (size and orientation) (Arora et al., 2015; Caliari et al., 2011) could also increase the fluid exudation from tendon core during mechanical loading and exacerbate the aforementioned mechanisms. In addition, the contraction-induced decrease in tendinopathic tendon blood flow volume (Åström and Westlin, 1994; Öhberg et al., 2001) may also contribute to the overall tendon volume loss under load. Such volume loss of the tendinopathic tendon resulting from the fluid exudation during mechanical loading may play an important role in regulating tendon hydrostatic pressure, homeostasis, mechanotransduction, and remodeling (Archambault et

al., 2002; Lavagnino et al., 2008; Lavagnino et al., 2015; Maeda et al., 2013), providing a basis for understanding why cyclically loading the tendinopathic tendon is an effective treatment option in people with Achilles tendinopathy (O'Neill et al., 2015). A reduction in tendinopathic tendon water content has been reported in response to an acute bout of exercise (Ho and Kulig, 2016b). However, further studies are needed to investigate the fluid exudation mechanisms associated with tendinopathy and their potential roles in tendinopathic tendon mechanobiology during mechanical loading. Nevertheless, the findings of this study appear to contradict the previous suggestion that tendinopathy may restrict the load-induced fluid movement due to the pathological changes in tendon structure and composition accompanying tendinopathy (Grigg et al., 2012; Wearing et al., 2015).

5.5.5 Contralateral versus control healthy tendons at rest and under load

The observed trend toward statistical significant difference (P = ~0.06) in tendon CSA and AP diameter between contralateral and healthy tendons in the mid-proximal tendon region (40-100% of the normalized tendon length) at rest supports previous *in vivo* and *in vitro* studies that have reported evidence of pathological changes in contralateral tendon morphology (Docking et al., 2015; Grigg et al., 2012), histology (Andersson et al., 2011b; Williams et al., 1984), and structural integrity (Docking et al., 2013; Docking et al., 2015) in the presence of unilateral Achilles tendinopathy, highlighting the bilateral characteristics of the tendinopathy. A number of possible reasons for the frequent progression of unilateral Achilles tendinopathy to bilateral tendinopathy have been proposed in the literature such as mechanical overloading of the contralateral tendon as a result of altered

biomechanical and neuromuscular characteristics associated with Achilles tendinopathy (Azevedo et al., 2009; Munteanu and Barton, 2011), the involvement of systemic and central neuronal mechanisms (Andersson et al., 2011a; Cetti et al., 2003; Williams et al., 1984), and genetic and demographic factors (Franceschi et al., 2014; Gaida et al., 2009; Nell et al., 2012; September et al., 2016). Regardless of underlying cause, our data suggests that caution should be taken when using the contralateral tendon as a reference to quantify the alterations of tendon CSA and AP diameter in the tendinopathic side in the mid-proximal tendon region at resting state. The lack of difference in the magnitude and direction of the tendon transverse morphology and longitudinal strains between the contralateral and healthy tendons under load is in accordance with previous *in vivo* studies reporting that despite the presence of pathological symptoms associated with tendinopathy in contralateral tendon in patients with unilateral MAT, the mechanical properties of the contralateral tendon do not seem to be affected by tendinopathy (Chang and Kulig, 2015; Grigg et al., 2012; Kulig et al., 2016).

5.5.6 Limitations

There are a number of limitations that should be considered when interpreting the findings of the present study. First, although the small sample of individuals with MAT included in the present study (N = 10) with our inclusion criteria (mean symptom duration > 3 months; VISA-A score < 80 points) is representative of patients seen in clinical practice, it is heterogeneous in terms of the duration of symptoms (3.5 ± 2.9 y) and severity of MAT symptoms (mean VISA-A score = 54.2 ± 16.52). Further study with specific inclusion criteria is needed to examine whether there is a relationship between the stage of

tendinopathy and tendon 3D morphology at rest and under load in the tendinopathic and contralateral healthy sides in a larger population of patients with MAT. Second, the findings of the tendon transverse and longitudinal morphologies at rest and under load in the present study are limited to only free AT (i.e., soleus MTJ to calcaneus) and thus do not reflect the 3D morphology of proximal AT (i.e., gastrocnemius MTJ to soleus MTJ) and the whole AT complex (i.e., gastrocnemius MTJ to calcaneus). Caution is therefore warranted in generalizing the present findings to the AT aponeurotic sheath and the global tendon level. Third, as the transverse morphological measurements using 3DUS in the present study were restricted to tendon core, we were unable to measure the thickness of the peri-tendinous space and paratenon at rest and under load. Quantifying these tendon parameters could have provided an evidence of the possible fluid redistribution mechanism from the tendon core to the peri-tendinous space during loading *in vivo* condition. Further study is required to determine these tendon parameters at rest and under load using imaging techniques such as MRI that have greater resolution than ultrasound in order to identify the fluid exudation mechanism from the tendon core into the peri-tendinous space under load. Finally, the present study was conducted on male adults with MAT so caution should be taken when generalizing these findings to other AT disorders (e.g., insertional Achilles tendinopathy), females, and other tendons (e.g., patellar tendon).

5.6 Conclusion

The free tendon with mid-portion Achilles tendinopathy is associated with larger resting tendon CSA and AP diameter along the entire tendon length relative to the contralateral and healthy control tendons, suggesting the widespread development of tendon injury.

During a sub-maximal isometric plantarflexion contraction, the increase in tendon longitudinal strain and the corresponding reduction in tendon transverse morphology (i.e., CSA, AP diameter, and ML diameter) strain and volume of the tendinopathic free tendon may not only reflect the reorganization of the tendon matrix components but also a change in matrix fluid content and distribution. This finding could have an important implication for understanding the potential mechanisms associated with the therapeutic effect of tendon loading via ankle exercise in reducing tendon pain and restoration of function in people with tendinopathy. Further, the finding that the tendinopathic free tendon undergoes greater longitudinal and transverse strains than contralateral and healthy free tendons under the same tensile load further highlights the compliant nature of the tendinopathic tendon, which could lead to higher risk of strain-related injuries (e.g., rupture).

Chapter 6: Tendinopathic Achilles Tendon 3D Deformation During Repeated Loading

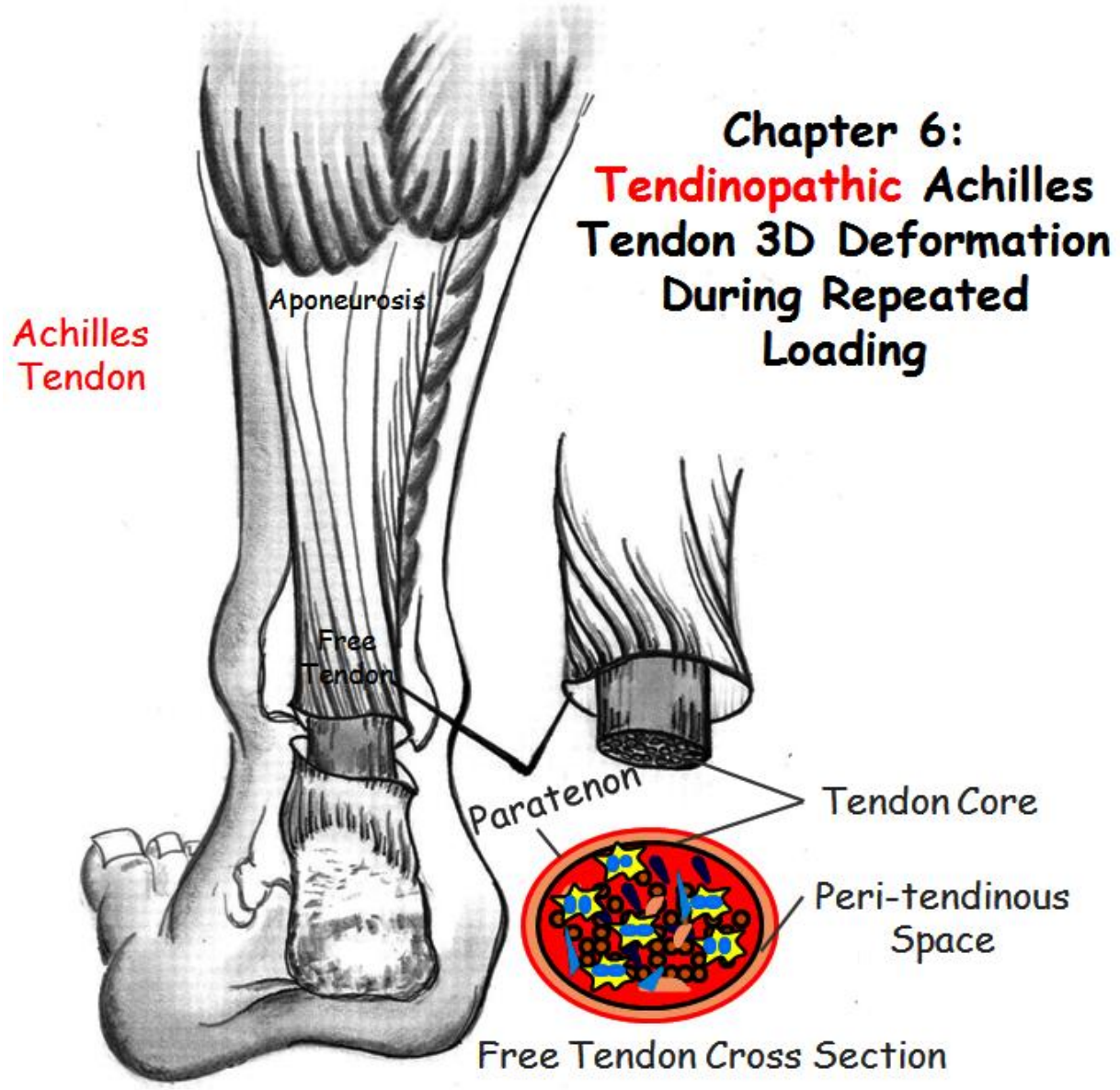

Chapter 6. The tendinopathic Achilles tendon does not remain iso-volumetric upon repeated loading: insights from 3D ultrasound

Acknowledgement of co-authorship:

This chapter includes a co-authored paper that has been re-formatted for this thesis. The bibliographic details/status of the co-authored paper, including all authors, are:

L. Nuri, S. J. Obst, R. Newsham-West, R. S. Barrett (2017). "The tendinopathic Achilles tendon does not remain iso-volumetric upon repeated loading: insights from 3D ultrasound". Journal of Experimental Biology (JEB). **DOI: 10.1242/jeb.159764.**

I have made a substantial contribution in the conception and design of this study, analysis and interpretation of the research data, and the drafting and critical revising of the final manuscript.

(Signed) Leila Nuri (Date) 10th March 2017

Student/corresponding author: Leila Nuri

(Countersigned) _____ (Date) _____

Principal Supervisor: Rod Barrett

(Countersigned) _____ (Date) _____

Principal Supervisor: Richard New-sham West

6.1 Abstract

Mid-portion Achilles tendinopathy (MAT) alters the normal three-dimensional (3D) morphology of the Achilles tendon (AT) at rest and under a single tensile load. However, how MAT changes the 3D morphology of AT during repeated loading remains unclear. This study compared the AT longitudinal, transverse and volume strains during repeated loading in MAT with those of the contralateral tendon in people with unilateral MAT. Ten adults with unilateral MAT performed 10 successive 25-s submaximal (50%) voluntary isometric plantarflexion contractions with both legs. Freehand 3D ultrasound scans were recorded and used to measure whole AT, free AT, and proximal AT longitudinal strains and free AT cross-sectional area (CSA) and volume strains. The free AT experienced higher longitudinal and CSA strain and reached steady state following a greater number of contractions (five contractions) in MAT compared to the contralateral tendon (third contractions). Further, free tendon CSA and volume strained more in MAT than contralateral tendon from the first contraction, whereas free AT longitudinal strain was not greater than the contralateral tendon until the fourth contraction. Volume loss from the tendon core therefore preceded the greater longitudinal strain in MAT. Overall, these findings suggest that the tendinopathic free AT experiences an exaggerated longitudinal and transverse strain response under repeated loading that is underpinned by an altered interaction between solid and fluid tendon matrix components. These alterations are indicative of accentuated poroelasticity and an altered local stress-strain environment within the tendinopathic free tendon matrix, which could affect tendon remodelling via mechanobiological pathways.

6.2 Introduction

Mid-portion Achilles tendinopathy (MAT) is a common pathology of the lower extremity that is characterized by pain, swelling, and thickening of the Achilles tendon (AT) mid-portion (Maffulli, 1998; Van Dijk et al., 2011). MAT affects sporting and general populations, causing disability, functional impairment, and compromised performance (de Jonge et al., 2011; Kvist, 1994). MAT has been shown to result in altered tendon composition, structure, and morphology including an increase in tendon cross-sectional area (CSA), thickness, and volume (Arya and Kulig, 2010; Child et al., 2010; Docking et al., 2015; Grigg et al., 2012; Shalabi et al., 2004b). The tendinopathic AT also exhibits lower stiffness and Young's modulus as well as greater longitudinal and transverse strains and higher hysteresis compared to healthy tendon under the same tensile load (Arya and Kulig, 2010; Chang and Kulig, 2015; Child et al., 2010; Wang et al., 2012). Alterations in AT geometry and material properties in MAT are important because of their potential to change the stress-strain patterns experienced by the AT during muscle contraction (Hansen et al., 2017). It has also been shown that in contrast to healthy tendon, which bulges along the antero-posterior diameter (Obst et al., 2015b; Obst et al., 2014b) and experiences a reduction in CSA and behaves iso-volumetrically (Nuri et al., 2016; Obst et al., 2015b; Obst et al., 2014b) during a single tensile load, the tendinopathic tendon undergoes a reduction in antero-posterior diameter and CSA and a corresponding reduction in volume of the tendon core. This observation is suggestive of fluid exudation from tendon core (i.e., the whole tendon, covered by epitenon layer) to the peri-tendinous space (i.e., the space between tendon epitenon and paratenon layers) and tendon matrix re-organization under load in MAT. To our knowledge no *in vivo* studies to date have examined the time-

dependent visco-poroelastic properties of MAT during repeated loading. Such studies could provide an insight into the time scale of interaction and involvement of tendon load-bearing components [solid (i.e., collagen fibrillar network and proteoglycans) and fluid (i.e., water)] within the tendinopathic tendon matrix during repeated loading.

In *vivo* studies of the time-dependent viscoelastic properties of the AT to date have been confined to normal tendon. In general, these studies show that during repeated application of the same force, the normal AT experiences gradual 3D deformation (i.e. creep) until steady-state behavior is reached (Fung, 2013). For example, Maganaris (2003) reported that high intensity (80%) successive maximal voluntary isometric plantarflexion contractions (MVIC) induced ~5 mm increase in whole AT (e.g., gastrocnemius muscle-tendon-junction (MTJ) to calcaneus) longitudinal elongation that reached steady state behavior after five contractions. Similarly, Hawkins et al. (2009) showed that low intensity repeated isometric contractions (25-35% MVIC) resulted in ~3% increase in whole AT longitudinal strain that plateaued after 270 contractions. More recently, Nuri et al. (2016) reported that whole AT longitudinal and transverse deformation during repeated loading were primarily driven from free AT (e.g., soleus MTJ to calcaneus), with little or no contribution from proximal AT (e.g., gastrocnemius MTJ to soleus MTJ) in healthy people and that both longitudinal and transverse deformation of the free AT reached steady state after three repetitions of a 25-s submaximal (50% MVIC) isometric plantarflexion contractions. As healthy free AT behaved iso-volumetrically during repetitive contractions, the alterations in tendon longitudinal and transverse morphologies during the first three contractions were indicative of a change in tendon matrix shape, with increased tendon length coupled to the reduction in tendon CSA (Nuri et al., 2016).

In contrast to healthy tendon, the loss of free AT volume during acute loading in MAT suggests that the normal interaction between solid and fluid matrix components may be interrupted. A continued loss of free tendon volume in MAT with repeated loading might be expected to increase loading on the solid component of the tendon matrix and adversely affect the ability of the tendon to resist ongoing loading. A loss of tendon volume with repeated loading could therefore be an important factor that limits tendon function and repair in tendinopathy due to the effect on the local tendon mechanobiology. Assessing changes in tendinopathic tendon morphology and volume during repeated loading may also provide an indication of the temporal relations between collagen creep and fluid exudation from the tendon core in MAT. This knowledge could also inform computational models of poroelastic tendon behavior in tendinopathy (Smith et al., 2013) and be useful for establishing a standardized conditioning protocol for individuals with MAT prior to performing mechanical tests, treatment protocols and physical activity. A greater number of contractions to reach steady state behavior might be expected in MAT because of the dual and interacting effects of changes in solid and fluid matrix component behavior.

The purpose of the present study was therefore to investigate the effect of repeated submaximal isometric plantarflexion contractions on the longitudinal deformation of the whole AT and the corresponding free tendon transverse and volume deformation in the tendinopathic side relative to those of the contralateral side in people with unilateral MAT. We hypothesised that longitudinal, transverse and volume strains would reach steady state at a higher magnitude and following a greater number of contractions in MAT compared to contralateral tendon. We also sought to determine whether the time-dependent viscoelastic

properties in MAT are mainly driven from the free AT as in normal tendon (Nuri et al., 2016), or whether the proximal AT exhibits altered behavior in MAT.

6.3 Materials and Methods

6.3.1 Participants

Ten individuals with MAT participated in the study. The inclusion criteria were: male adults, 18-60 years of age with unilateral MAT, duration of pain for more than 3 months, and Victorian Institute of Sports Assessment-Achilles tendon (VISA-A) score (0-100) of less than 80 points (Alfredson et al., 1998; Debenham et al., 2016). The exclusion criteria were: insertional tendinopathy, bilateral tendinopathy, history of AT rupture or surgery, inflammatory or degenerative ankle joint condition, and any musculoskeletal injuries thought to interfere with the participation in the study. All clinical examinations were performed by the same physiotherapist (L.N). Participant characteristics were age: 42.2±11.5 y, height: 176.6±7.5 cm, mass: 79.8±7.8 kg, VISA-A score: 54.2±16.5, and duration of symptoms: 3.5±2 y. The study was approved by the local university human research ethics committee and was performed in accordance with the principles of the Declaration of Helsinki.

6.3.2 Experimental protocol

Following the clinical examination, participants completed a familiarisation session on the same day and a testing session 3-5 days later. In the familiarization session, each participant performed 3 repetitions of a 4-s MVIC of the plantarflexors and dorsiflexors separately for each leg on the apparatus described below. A rest period of 60 s was

provided between contractions. The contraction with the highest torque in the tendinopathic side was chosen to determine the target torque (50% MVIC) for both legs in the subsequent testing session. Participants were then asked to practice holding contractions at 50% MVIC until they became familiarized with the testing procedure.

Participants were instructed to refrain from any form of training or vigorous physical activities for at least 48 h prior to the subsequent testing session and to use motorized transportation to travel to the laboratory. Upon arrival participants rested on a chair for 45 min (Nuri et al., 2016) and were subsequently asked to lie prone on an examination plinth with their knee and hip fully extended, and the ankle joint in neutral position. Their foot was then firmly secured to a footplate connected to a fixed torque transducer (Futek TFF600, Irvine, California, USA) using a custom-made adjustable ratchet system to minimize heel lift from the footplate during contractions (Obst et al., 2014a; Obst et al., 2014b). The rotational axis of the torque transducer was carefully aligned with the axis of rotation of the ankle joint. The visual feedback of the torque exerted by the foot was provided on a computer monitor, positioned one meter directly in front of the participants at eye level. The output from the torque transducer was recorded at a sampling frequency of 1000 Hz through the LabVIEW software (LabVIEW 9.9, National Instruments, Austin, Texas, USA). Participants performed 10 successive isometric plantarflexion contractions at 50% MVIC with their both legs separately. The order of testing the legs (tendinopathic, or contralateral side) was randomly decided for each participant. Verbal encouragement was provided to participants during each contraction. Pain was assessed during each contraction using a 10-cm visual analogue scale (VAS), with 0 indicating no pain and 10 indicating worst possible pain for each leg separately. Prior to testing, all participants were

familiarized with the use of VAS scoring system and were instructed to circle a number on the scale that corresponded to the pain in AT following each contraction.

6.3.3 Freehand three-dimensional ultrasound

Ultrasound scans was acquired at two resting states (e.g., immediately before the first contraction and immediately after completing the tenth contraction) and during each of ten contractions using a freehand three-dimensional ultrasound system (3DUS) consisting of a conventional ultrasound machine (SonixTouch, Ultrasonix, Richmond, BC, Canada) and a five camera optical tracking system (V100:R2, Tracking Tools v 2.5.2, Natural Point, Corvallis, Oregon, USA) (Obst et al., 2014a). The 3D position and orientation of the ultrasound transducer were determined from four reflective markers rigidly attached to the transducer using an optical tracking system. A coordinate transformation was then used to map the 2D brightness-mode (B-mode) ultrasound images into global coordinate system and a 3D reconstruction of AT was created using the Stradwin software package (Version 5.1, Mechanical Engineering, Cambridge University, UK; http://mi.eng.cam.ac.uk/~rwp/stradwin/). Before data collection, the temporal and spatial calibration of ultrasound transducer was performed in a water bath (~25° C) using a single-wall phantom calibration protocol recommended by Stradwin software developers (Prager et al., 1998). After calibration, pixel coordinates in any recorded 2D ultrasound images were transformed into 3D space with an approximate error of ±0.4 mm (Prager et al., 1998).

One investigator (L.N) performed all the AT ultrasound scans using a 58-mm linear transducer (L14-5 W/60 linear, Ultrasonix, Richmond, BC, Canada) with standardized

ultrasound image settings (depth 40 mm, gain 50%, dynamic range 65 dB, map 4, power 0). To ensure a consistent scanning area for all the contractions, the ultrasound scanning area was drawn on the skin according to the AT anatomical location seen on 2D real-time ultrasound (Fig. 29A). A rectangular shaped commercially available stand-off pad was attached to the end of the transducer using a custom-made ultrasound stand-off holder to maximize the image quality. A thick layer of ultrasound gel was then applied over the AT scanning area in order to provide appropriate ultrasound wave conductance and minimize the pressure exerted by the transducer on the skin. A stack of 2D B-mode images was then acquired by moving the transducer manually from the base of the heel to medial gastrocnemius (MG) MTJ in a transverse orientation at a steady speed (~9 mm s^{-1}). Each ultrasound scan took approximately 25 s to complete and the finalized stacks of 2D B-mode images consisted of 1350 frames with an average distance frame of 0.1 mm. The 3D US approach is limited to evaluating tendon morphology under static loading condition and the accuracy of measurement, particularly for tendon length, depends on the scanning time and the number of 2D B-mode images acquired during scanning (Lichtwark et al., 2013; Obst et al., 2014a). Therefore, the tendon loading condition under which the AT ultrasound scanning was performed in the present study (i.e. ~25s isometric plantarflexion contraction at 50% MVIC) was a compromise between allowing sufficient scan time to capture a sufficiently dense ultrasound image stack, and ensuring that participants were able to maintain the target contraction intensity over the scan period (Nuri et al., 2016).

Three main anatomical point landmarks (calcaneal notch, soleus (SOL) MTJ, and MG MTJ) were selected manually on 3D AT images using 3D landmark tool in Stradwin software. Sagittal and frontal image re-slices were used to start the manual segmentation

and were corrected where necessary by viewing the corresponding 3D transverse image slices (Fig. 29B,C). The whole AT length was defined as the distance between the calcaneal notch and MG MTJ; the free AT length was defined as the distance between the calcaneal notch and SOL MTJ; and proximal AT length was defined as the distance between MG MTJ and SOL MTJ. Tendon deformation was determined by subtracting tendon resting length from the corresponding length during each contraction. Sagittal and transversal images of free tendon were used to digitize tendon CSA at 2 mm intervals along the length of the free tendon. The free AT volume reconstruction was then obtained from the 3D location of the digitized CSAs using 3D rendering algorithms in Stradwin (Treece et al., 1999) (Fig. 30A,B). The accuracy of our 3DUS for free AT volume measurement compared to phantoms of similar size and the minimal detectable change for *in vivo* free AT volume at rest have been estimated to be ±0.5 ml and ±0.2 ml, respectively (Obst et al., 2014a). Further, 3DUS provides a high level of within-session reliability (ICC≥0.98) for the measures of AT morphological properties (i.e., AT length, mean free AT CSA, and free AT volume) at rest and during sub-maximal voluntary isometric plantarflexion contraction (Obst et al., 2014a; Nuri et al., 2016). The mean free tendon CSA (mm^2) was obtained by dividing free tendon volume by free tendon length (×1000). Tendon length, CSA and volume strains were computed by dividing the tendon deformation by the corresponding resting values. The measurement of free AT transverse strain during tensile loading could have important implications for our understanding of the AT elastic energy storage and release action (Lichtwark and Wilson, 2006), triceps surae muscle bulging characteristics (Aziz et al., 2008), and AT in vivo mechanobiology (Wang et al., 2012).

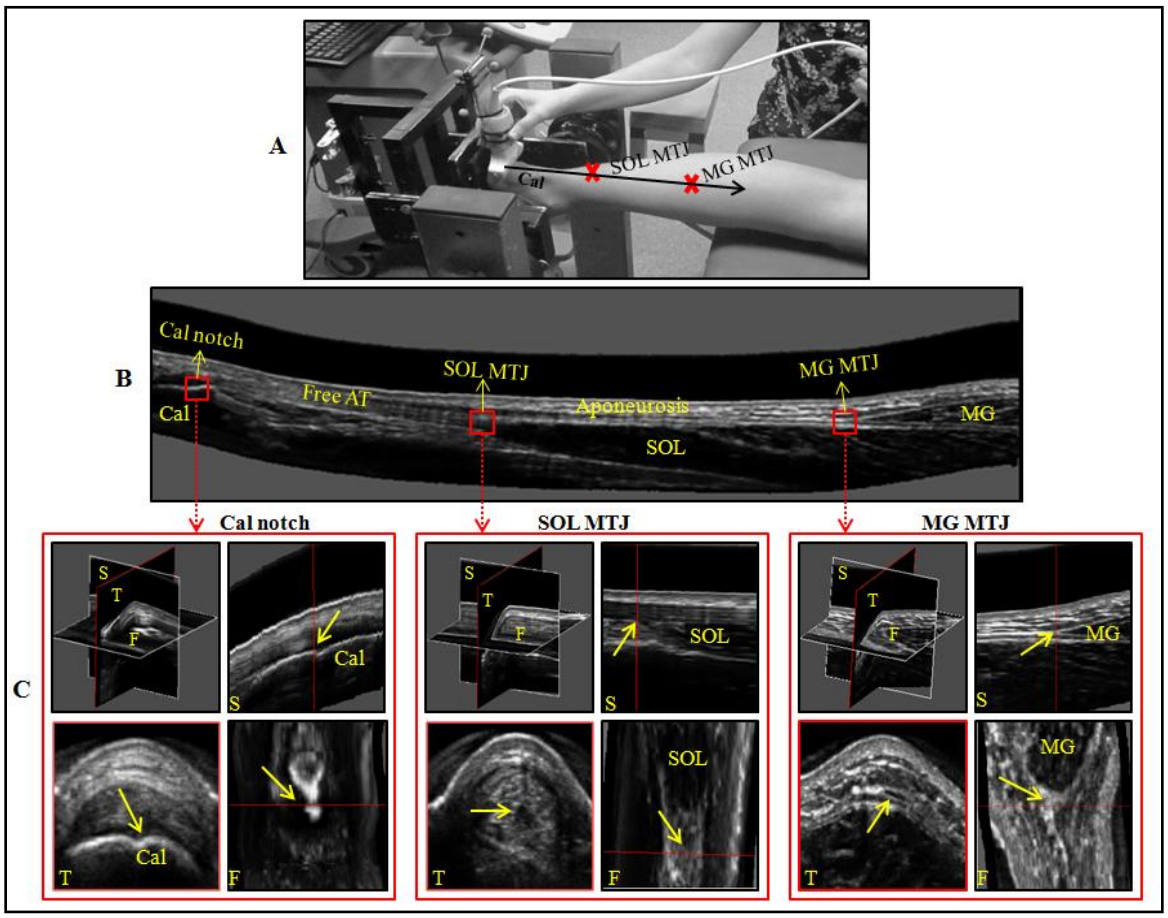

Figure 29: *Experimental set-up and three dimensional (3D) Achilles tendon (AT) image reconstruction and segmentation. (A) Participant positioned prone in testing apparatus with the ankle joint in 90° (neutral position). The ultrasound scan was performed by sweeping the ultrasound transducer from the base of the heel to the medial gastrocnemius (MG) muscle-tendon junction (MTJ) as indicated by the arrow. The black crosses denote MTJ for the soleus (SOL) and MG. (B) Sagittal plane re-slices of the reconstructed 3D ultrasound image of the AT. (C) Sagittal (S), transverse (T), and frontal (F) image re-slices used to identify the anatomical location of the calcaneal (Cal) notch, SOL MTJ, and MG MTJ.*

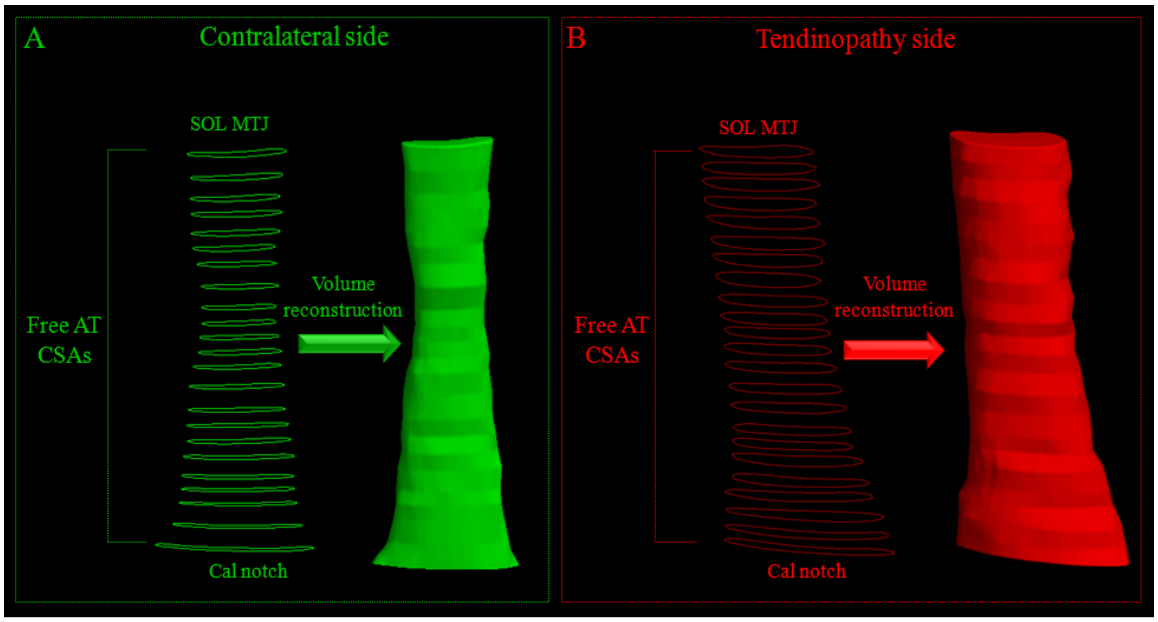

Figure 29: *Free Achilles tendon (AT) cross-sectional area (CSA) segmentation and volume reconstruction for contralateral (A) and tendinopathic (B) sides of a single representative participant. The free AT CSAs were manually digitized from the transverse images at ~2-3 mm intervals from the calcaneal (Cal) notch to the soleus muscle-tendon-junction (SOL MTJ) and the free AT 3D volume was rendered from the segmented CSAs using the surface interpolation algorithm in Stradwin software.*

6.3.4 Electromyography (EMG)

Following skin preparation, pre-gelled and self-adhesive surface electrodes (model H124SG, Covidien Kendall, 24 mm, Germany) with a fixed center-to-center interelectrode distance of 20 mm were placed over the belly of the MG, lateral gastrocnemius (LG), SOL and tibialis anterior (TA) muscles according to SENIAM recommendations by Hermens et al. (2000). A ground reference electrode was placed over the fibular head. Muscle activity was recorded using a four channel double differential EMG system (Bagnoli-8 EMG, DELSYS, USA). EMG signals were sampled at a frequency of 1000 Hz and bandpass

filtered between 20 and 400 Hz using a fourth-order zero lag Butterworth filter in Matlab software (The Mathworks, Natick, Massachusetts, USA) and converted to Root Mean Square (RMS) values using a 20-ms non-overlapping window. The RMS value was then normalized relative to the measured MVIC values (%MVIC). EMG activity for MG, LG, and SOL were also expressed as a ratio of total triceps surae (TS) muscle activation to investigate the effects of each contraction on the synergetic activations. Furthermore, the co-activation index was calculated from the ratio of normalized EMG activity for TA to the sum of normalized EMG activities for the SOL and TA (Hammond et al., 1988).

6.3.5 Statistical analysis

Paired t-tests were used to compare the resting dimensions of the tendon (whole AT, free AT and proximal AT lengths, and free AT CSA and volume) between sides (tendinopathy and contralateral). A full factorial two-way repeated measures Analysis of Variance (ANOVA) was used to evaluate the effects of side and contraction number (ten contractions) on tendon longitudinal strain for each tendon region (whole AT, free AT, and proximal AT), free tendon CSA strain, and free tendon volume strain separately. Planned contrasts (SPSS CONTRAST syntax) were subsequently used to determine differences in tendon longitudinal strain, CSA strain, and volume strain between sides for each contraction and between consecutive contractions for each side. Furthermore, a one-way repeated measures ANOVA was used to determine the effect of contraction number on ankle joint torque, pain score, EMG activity of MG, LG, SOL, and TA muscles, the ratios of normalized EMG activity, and co-activation index for each side separately. The level of significance was set at $\alpha=0.05$. All analyses were performed using the Statistical Package for the Social Sciences version 22 (SPSS, Chicago, Illinois, USA). In the text, data are

expressed as mean±standard deviation (s.d.) and in the figures they are presented as mean±standard error of mean (s.e.m.).

6.4 Results

6.4.1 Effect of tendon side on tendon dimensions at rest

No differences in resting lengths of tendon regions were detected between the tendinopathic side (whole AT: 203±29 mm; free AT: 74±23 mm; proximal AT: 129±23 mm) and the contralateral side (whole AT: 206±23 mm; free AT: 72±22 mm; proximal AT: 134±21 mm) ($t\ (9)$=-0.04, P=0.96; $t\ (9)$=-0.84, P=0.41; $t\ (9)$=1.02, P=0.33, respectively). However the mean resting free AT CSA was significantly higher in the tendinopathic side (97±17 mm^2) compared to the contralateral side (60±13 mm^2) ($t\ (9)$=-8.63, P<0.001). Similarly, the mean resting free AT volume was significantly higher in the tendinopathic side (7.16±1.89 ml) compared to the contralateral side (4.15±1.01 ml) ($t\ (9)$=-8.84, P<0.001).

6.4.2 Effect of tendon side and contraction number on tendon longitudinal strain

The whole AT, free AT, and proximal AT longitudinal elongations and the corresponding strains are displayed in figure 31. Significant main effects of side and contraction number were detected for whole AT longitudinal strain ($F_{1,\ 9}$=7.37, P=0.02 and $F_{9,\ 81}$=49.04, P<0.001, respectively) and free AT longitudinal strain ($F_{1,\ 9}$=25.61, P=0.001 and $F_{9,\ 81}$=74.76, P<0.001, respectively). Significant side-by-contraction number interaction effects were also detected for whole and free AT longitudinal strain ($F_{9,\ 81}$=15.21, P<0.001 and $F_{9,\ 81}$=25.35, P<0.001, respectively). Planned contrasts revealed greater whole and free

AT longitudinal strain in the tendinopathic versus the contralateral side from the fourth contraction. Planned contrasts also revealed that whole and free AT longitudinal strain values increased as a function of contraction number up to the fifth contraction in the tendinopathic side and the third contraction in contralateral side for both regions (Fig. 31A,B). No significant differences in proximal AT strain were found between contractions in both sides (Fig. 31C).

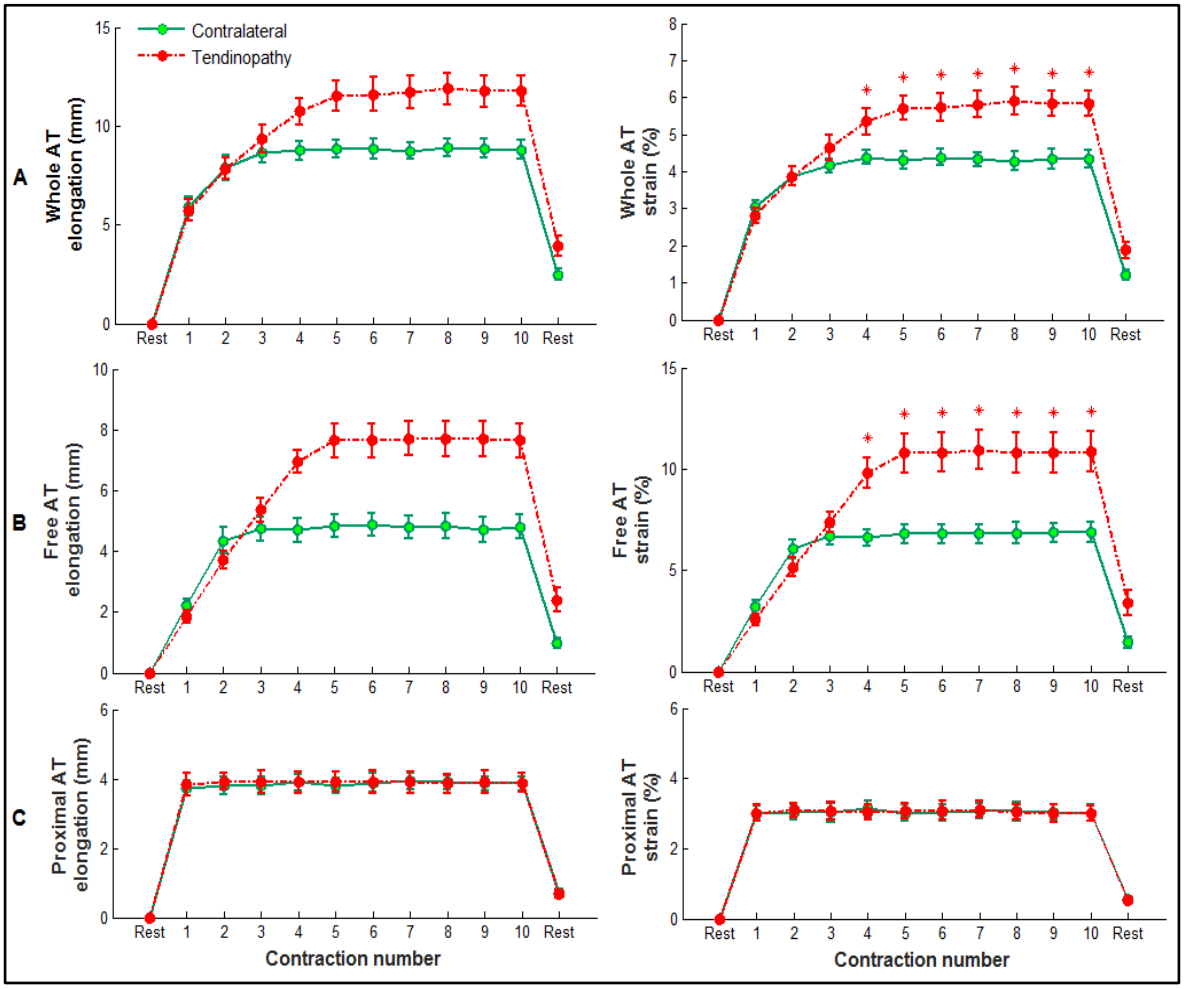

Figure 30: *Change in Achilles tendon (AT) longitudinal elongation and strain during repeated loading. The mean group whole AT (A), free AT (B), and proximal AT (C) longitudinal elongation and strain in tendinopathy (red circles) and contralateral (green circles) sides during 10 successive isometric plantarflexion contractions at 50% MVIC.*

Data are expressed as mean ± SEM (N = 10). Asterisks (*) indicate significant differences between the tendinopathic and contralateral sides during each contraction (P < 0.05). Planned contrasts revealed that the whole and free AT in the tendinopathic side experienced greater longitudinal strain than those of the contralateral side during contractions 4-10.

6.4.3 Effect of tendon side and contraction number on free tendon transverse strain

The free AT CSA deformation and the corresponding strain are presented in figure 32. Side and contraction number had a significant main effect on mean free AT CSA strain ($F_{1, 9}$=11.05, P=0.009 and $F_{9, 81}$=23.73, P<0.001, respectively). A significant side-by-contraction number interaction for free AT CSA strain was also detected ($F_{9, 81}$=6.79, P<0.001). Planned contrasts revealed that free AT CSA strained significantly more in the tendinopathic side compared with the contralateral side during all 10 contractions. Planned contrasts also revealed that free AT CSA strain values significantly decreased with contraction number up to the fifth contraction in the tendinopathic side and the third contraction in the contralateral side (Fig. 32A,B).

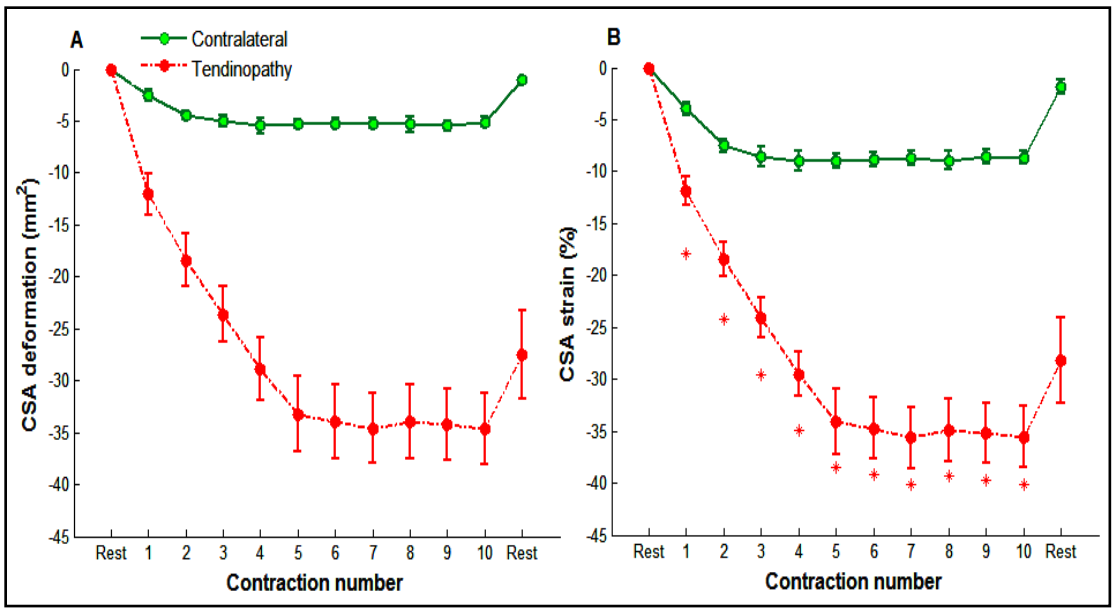

Figure 31: *Change in free Achilles tendon (AT) cross-sectional area (CSA) deformation and strain during repeated loading. The mean group free AT CSA deformation (A) and strain (B) during 10 successive isometric plantarflexion contractions at 50% MVIC in the tendinopathic (red circles) and contralateral (green circles) sides. Data are expressed as mean ± SEM (N = 10). Asterisks (*) indicate significant differences between the tendinopathic and contralateral sides during each contraction (P < 0.05). Planned contrasts revealed that the free tendon CSA in the tendinopathic side strained greater than that of the contralateral side during contractions 1-10.*

6.4.4 Effect of tendon side and contraction number on free tendon volume strain

The free AT volume deformation and the corresponding strain are displayed in figure 33. Side and contraction number had a significant main effect on mean free AT volume ($F_{1, 9}$=94.36, P<0.001 and $F_{9, 81}$=19.59, P<0.001, respectively). There was a significant side-by-contraction number interaction for free AT volume strain ($F_{9, 81}$=18.11, P<0.001). Planned contrasts revealed that free AT volume strained significantly more in the

tendinopathic side compared with the contralateral side during all 10 contractions. Planned contrasts also revealed that free AT volume strain values significantly decreased with contraction number up to the fifth contraction in the tendinopathic side (Fig. 33A,B).

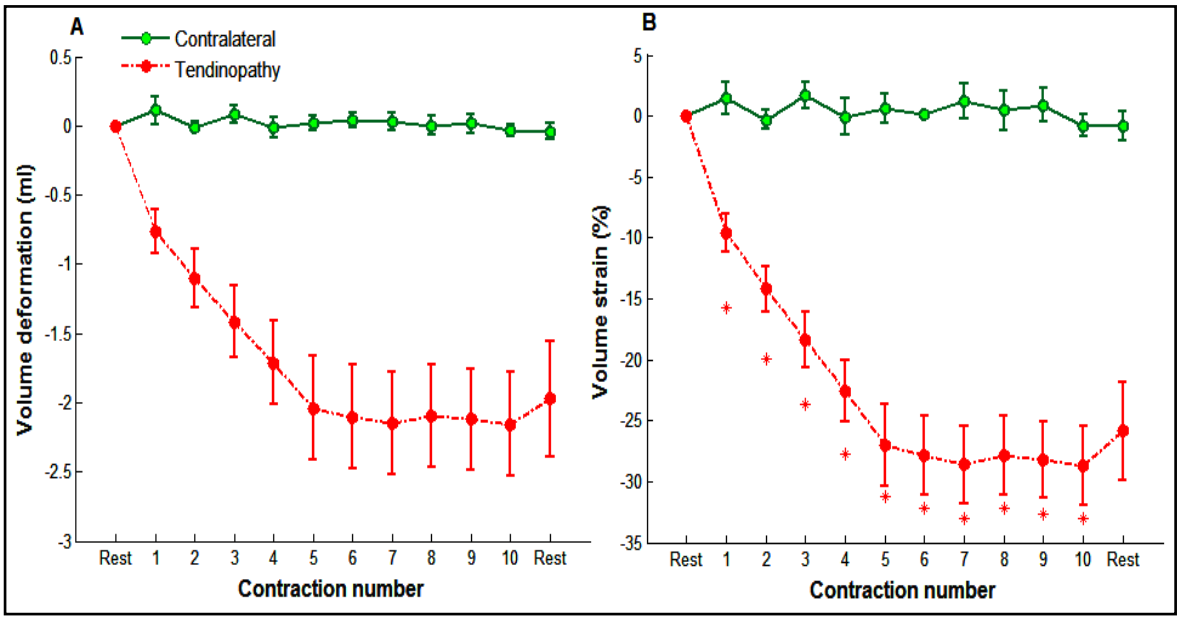

Figure 32: *Change in free Achilles tendon (AT) volume deformation and strain during repeated loading. The mean group free AT volume deformation (A) and strain (B) during 10 successive isometric plantarflexion contractions at 50% MVIC in the tendinopathic (red circles) and contralateral (green circles) sides. Data are expressed as mean ± SEM (N = 10). Asterisks (*) indicate significant differences between the tendinopathic and contralateral sides during each contraction (P < 0.05). Planned contrasts revealed that the free tendon volume in the tendinopathic side strained greater than that of the contralateral side during contractions 1-10.*

6.4.5 Effect of contraction number on ankle joint torque, EMG, and pain score

Ankle plantarflexion torque for MVIC in the tendinopathic side was 90.5±10.35 N.m and for submaximal contractions in the tendinopathic and contralateral sides were 45.77±4.22

N.m and 44.52±5.25 N.m, respectively. Normalized EMG activities for MG, LG, SOL, and TA for the tendinopathic side were 38.34±3.81%, 21.93±2.21%, 36.34±1.23%, and 5.55±0.32%, respectively and for contralateral side were 39.23±0.76%, 25.11±1.58%, 38.61±0.79%, and 5.42±0.85%, respectively. The co-activation index for the tendinopathic and contralateral sides were 0.12±0.008 and 0.11±0.006, respectively. No significant main effects of contraction number or differences in ankle joint torque, normalized EMG activity of MG, LG, SOL and TA, ratios of normalized EMG activity (MG/TS, LG/TS, SOL/TS), and co-activation index between contractions were detected for both sides. The group mean pain score during 10 contractions for the tendinopathic and contralateral sides were 1.5±0.46 and 0.02±0.03, respectively. There was a significant difference in tendon pain score between contractions for the tendinopathic side ($F_{9, 81}$=12.32, p<0.001). Planned contrast revealed that tendon pain decreased from contraction 1 (2.6±1.5) to 2 (1.82±1.14) and 2 to 3 (1.35±0.85). No significant difference in tendon pain score was found between contractions for the contralateral side.

6.5 Discussion

This study examined the time course of longitudinal deformation of the whole AT, free AT and proximal AT, and the transverse and volume deformation of the free AT in people with unilateral MAT during repeated submaximal isometric plantarflexion contractions. Our hypothesis that AT longitudinal, transverse and volume strains would be greater and require a greater number of contractions to reach steady state in MAT compared to contralateral tendon was supported. The volume reduction due to repeated loading preceded the exaggerated longitudinal strain response in MAT, and is suggestive of fluid

loss from the tendon core. The observed rapid volume loss coupled with the aberrant 3D strain behavior of the free AT in MAT are indicative of accentuated poroelasticity and an altered local stress-strain environment within the free tendon in tendinopathy, which could alter tendon remodelling via mechanobiological pathways.

6.5.1 Resting CSA and volume of the tendinopathic and contralateral free AT

Consistent with previous *in vivo* studies, the MAT had a larger mean resting free AT CSA than contralateral tendon (97 mm^2 and 60 mm^2, respectively) (Leung and Griffith, 2007; Arya and Kulig, 2010; Docking and Cook, 2016), reflecting the pathological alterations in tendon structure and composition within MAT. The mean resting free tendon CSA value reported here for MAT (97 mm^2) lies within the range of values reported in previous studies for free AT in individuals with MAT (90-100 mm^2) (Leung and Griffith, 2007; Arya and Kulig, 2010; Docking and Cook, 2016). The mean resting contralateral free tendon CSA value in the present study (60 mm^2) was also in close agreement (56-75 mm^2) with prior studies using the same approach (Obst et al., 2015; Nuri et al., 2016), but were lower than for several prior studies (80-90 mm^2) (Maganaris and Paul, 2002; Magnusson and Kjaer, 2003; Reeves and Cooper, 2017). We believe this discrepancy in normal tendon CSA between studies could be due to the differences in imaging methods [MRI **(**Magnusson and Kjaer, 2003; Reeves and Cooper, 2017); 2D US (Maganaris and Paul, 2002); 3D US (present study)], tendon CSA segmentation methods [(tendon core + tendon paratenon (Maganaris and Paul, 2002; Magnusson and Kjaer, 2003; Reeves and Cooper, 2017); only tendon core (present study)] and tendon region from which the measurement of tendon CSA was made [free AT insertion (Maganaris and Paul, 2002); whole free AT length (present study)]. Further, resting free AT volume in the tendinopathy and

contralateral legs were 7.16 and 4.15 ml, respectively. These values fall within the range reported in previous *in vivo* studies for free AT volume [tendinopathic free AT volume: ~6-8 ml (Shalabi et al., 2004; Gärdin et al., 2010); healthy free AT volume: ~3-5 ml (Obst et al., 2014a,b; Nuri et al., 2016)]. As no significant differences in free AT length were found between the tendinopathy and contralateral legs at rest (~72 mm), the higher volume of the free tendon in tendinopathy leg observed here reflects the larger CSA of the tendinopathic tendon as a result of pathological alterations in tendon structure and composition accompanying chronic MAT (Åström and Rausing, 1995; Docking et al., 2015).

6.5.2 Longitudinal and transverse strain of the Achilles tendon during repeated loading

AT longitudinal and transverse strains from the first to tenth contraction were three and five times greater in MAT compared to the contralateral tendon. The longitudinal creep of whole AT was primarily driven by elongation of the free AT in MAT and contralateral tendons, with no differences in tendon proximal AT strain observed between contractions and between tendons during repeated loads. This finding adds to previous studies that reported a higher longitudinal strain at the level of whole (Arya and Kulig, 2010; Child et al., 2010) and free tendon in MAT relative to the healthy control tendon, by showing that the strain behavior of the proximal AT is not affected in MAT and does not experience longitudinal creep in response to repeated loading. The proximal AT therefore does not appear to be vulnerable to strain-related injuries during repeated loading in MAT. Differences in tendon anatomical structure, [fascicle/fibre orientation (Szaro et al., 2009),

fluid content (Grosse et al., 2015; Syha et al., 2014), and crimp angle (Magnusson et al., 2002)], the magnitude and direction of load exerted, and loading distribution pattern (Iwanuma et al., 2011; Farris et al., 2013; Reeves and Cooper, 2017) between proximal AT and free AT have been proposed as possible mechanisms underpinning the isolated creep behavior of the free AT during repeated loading (Nuri et al., 2016).

6.5.3 Volumetric changes in the free Achilles tendon during repeated loading

In contrast to normal tendon, which is known to behave iso-volumetrically in response to repeated loads (Nuri et al., 2016), the present study revealed that the free AT core experienced a volume reduction of 29% by the 10th contraction in MAT. This finding is consistent with studies that report reduction in tendinopathic tendon water content (Ho and Kulig, 2016), volume (Shalabi et al., 2004), and thickness (Fahlstrom and Alfredson, 2010; Grigg et al., 2012; Wearing et al., 2015) following exercise. The gradual increase in tendinopathic free AT length and the corresponding reduction in tendon CSA and volume observed here suggests that repeated loading not only changes a tendinopathic free AT matrix shape, but also alters tendon fluid content until a steady state is reached. We also noted that despite the volume and CSA reduction loss in the tendinopathic tendon during repeated loading, the free AT volume and CSA remained higher in the MAT (5.12 ml and 67 mm^2, respectively) compared to the contralateral tendon (4.15 ml and 55 mm^2, respectively) following repeated loading. The volume reduction in MAT under load therefore does not fully account for the extra volume in the resting tendon due to pathology. From an injury prevention perspective, the larger CSA in MAT would be expected to protect the tendon from experiencing high stress and compensate at least in

part for the lower tendon material properties in MAT (Arya and Kulig, 2010; Chang and Kulig, 2015; Child et al., 2010; Wang et al., 2012).

The load-induced volume reduction of tendinopathic free tendon during repeated loads as observed here could be due to the fluid movement from tendon core to peri-tendinous space (Hannafin and Arnoczky, 1994; Helmer et al., 2004) and/or vascular mechanism (i.e., the contraction-induced decrease in tendinopathic tendon blood volume) (Åström and Westlin, 1994). The fluid movement from tendon core to peri-tendinous space during mechanical loading could be explained by a combination of factors such as the release of water molecules from glycosaminoglycans as a result of the induced electric potential, known as streaming potential (Gu et al., 1993) in tendinopathic tendon matrix and high positive fluid pressure in tendinopathic tendon core (Ahmadzadeh et al., 2015) resulting from the high concentration of free and bound water molecules (De Mos et al., 2007) and ineffective tendon loading transfer mechanisms due to the disorganized and disrupted collagen fibers (Pingel et al., 2014) within the tendinopathic tendon matrix. The impairment in tendinopathic tendon core sheath (i.e., epitenon) permeability (i.e., porosity and voids ratio) (Chen et al., 1998) could also exacerbate the effect of the aformentioned mechanisms.

6.5.4 Number of contractions required to achieve steady state Achilles tendon strain behavior

Steady state behavior was achieved simultaneously for longitudinal and transverse AT strains following five contractions in MAT compared to three contractions in the contralateral tendon. More contractions were likely required in the tendinopathic side due

to a combination of more longitudinal and transverse creep coupled with the volume reduction in MAT. We also observed a reduction in self-reported pain score up to the third contraction in MAT, which likely reflects changes in local mechanical environment within the tendinopathic tendon matrix during repeated loading. A practical implication of these findings is that more contractions are required to condition a tendon with MAT relative to healthy tendon, and that tendon conditioning in MAT has the added benefit of decreasing pain perception (Rio et al., 2015).

Although the tendinopathic tendon underwent significantly greater CSA and the corresponding volume reduction than contralateral tendon from the first contraction, the whole and free AT longitudinal strains in the tendinopathic side were not greater than those of the contralateral tendon until the fourth contraction. This observation could be attributed to the involvement of different load-bearing mechanisms at different time scales within the tendinopathic tendon matrix in response to repetitive tensile loading. It is well known that the load support mechanisms of the tendon derive from the simultaneous interaction of the solid and fluid phases of the tissue (Fung, 2013) and that the tendinopathic tendon has a degraded solid structure (Docking et al., 2015; Pingel et al., 2014) and contains more free and bound water molecules (de Mos et al., 2007). The normal fluid–solid interaction pattern within the tendon in response to load in the presence of tendinopathy appears to be altered, with the rapid volume reduction from the free AT core observed in MAT being suggestive of a decreasing support from the fluid component and corresponding increase in load bearing to the solid component until steady state is reached. The specific reason for the lack of statistical difference in free AT longitudinal strain between the MAT and contralateral tendon in the first three contractions is unclear,

but could be caused by a stiffening effect of fluid flow on the more compliant collagen fibrillar network in MAT (Buckley et al., 2013). These alterations in solid and fluid behavior in MAT would also be expected to alter the local mechanical environment of the tissue. A non-optimal mechanical environment within the free tendon in MAT could be an important factor limiting tendon regeneration, and may need to be considered when designing interventions for treating MAT.

6.5.5 Limitations and future directions

In the present study only the mean whole free AT transverse strain was assessed due to large variation in tendon injury location along the length of the free AT in participants with MAT. Studies in the field of tendon mechanobiology suggest that there is an optimal strain environment for positive tendon adaptation (Wang, 2006), with either higher or lower than optimal strains resulting in a catabolic effect. It therefore follows that targeted rehabilitation strategies, perhaps combining biological and exercise-based therapies, could be developed in the future to create an optimal mechanical environment for tendon regeneration. In future studies it will be important to better characterise the local strains in the region of the tendinopathic lesion. Secondly, we were not able to visualize the whole tendon CSA along the proximal AT during a single transverse ultrasound sweep in the present study. Such information could be obtained in future using other imaging approaches such as MRI (Iwanuma et al., 2011; Reeves and Cooper, 2017). Thirdly, 3D US is limited by its inability to detect the thickness of tendon paratenon, epitenon, and peri-tendinous space, and thus the tendon CSA measurement in the present study was confined to the tendon core. Further studies are required to determine these tendon parameters at rest and during repeated loading using imaging techniques such as MRI that

have greater resolution than ultrasound in order to identify the fluid exudation mechanism from the tendon core into the peri-tendinous space as well as the time course of recovery of tendinopathic tendon volume following a standardized AT repeated loading protocol. Further, although all measurements were made at the same relative ankle joint plantarflexion torque (50% MVIC), we cannot be certain that the force applied to the free tendon and proximal AT were equal or whether longitudinal and/or transverse force distribution changed as a function of contraction number. It is however important to note that the activation level of TA muscle during repeated isometric plantarflexion contractions was small (~5%) and no changes in EMG activity of the triceps surae and TA muscles and the co-activation index were detected between contractions. Finally, the present study was conducted using a specific repeated loading protocol (25 s at 50% MVIC per contraction) (Nuri et al., 2016) in male adults with unilateral MAT so caution should be taken when generalizing these findings to other loading protocols (high intensity-short duration loading), females, other AT disorders (e.g., insertional Achilles tendinopathy), and other tendons (e.g., patellar tendon).

6.6 Conclusion

Tendinopathic free Achilles tendon underwent higher longitudinal, transverse, and volume strains relative to the contralateral tendon and reached steady state strain behavior after a greater number of contractions. The loss of free AT volume in MAT preceded the greater longitudinal strain in MAT relative to the contralateral tendon. Taken together these findings suggest the 3D strain behavior and normal temporal pattern of interaction between the solid and fluid phases of the tissue within the tendinopathic tendon matrix is altered in response to repeated loading.

Chapter 7: General Discussion

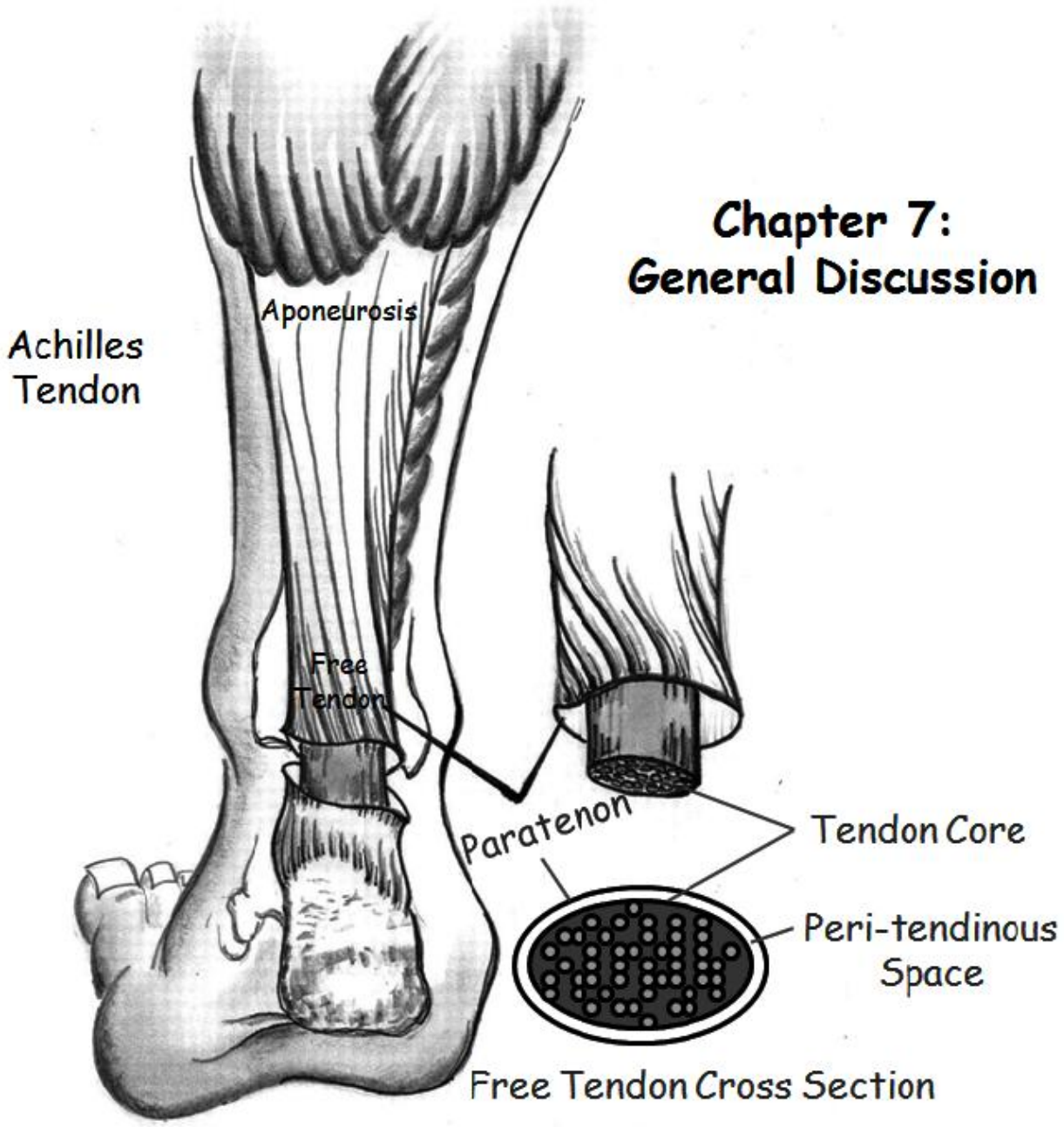

Chapter 7. General Discussion

The general purpose of this thesis was to investigate the three-dimensional (3D) morphology of the healthy Achilles tendon (AT) at the regional level during conditioning (Chapter 3) and its time course of recovery from the conditioning effects (Chapter 4) and to assess the effect of unilateral mid-portion Achilles tendinopathy (MAT) on AT 3D morphology and volume at rest, under a single tensile load, and during repeated loading at the regional level (Chapters 5 and 6). This chapter summarises and synthesizes the unique findings of the thesis in the context of the current literature. The main limitations of all the studies, recommendations for future research, and the general conclusions of the thesis are also presented.

7.1 Conditioning and recovery of healthy human Achilles tendon

Despite the importance of tendon conditioning in the measurement of tendon mechanical properties (Seynnes et al., 2015), the healthy AT conditioning process has been only investigated in two previous *in vivo* studies, which reported only the changes in whole AT longitudinal elongation and strain in response to successive tensile loading (Hawkins et al., 2009; Maganaris, 2003). However, the whole AT (i.e., gastrocnemius muscle-tendon junction (MTJ) to calcaneus) is not a single elastic structure. The distal AT (free AT: i.e, soleus MTJ to calcaneus) and the proximal AT (i.e., gastrocnemius MTJ to soleus MTJ) have distinctly different structures that leads to different mechanical properties. For example, it has been shown that the free AT undergoes a greater longitudinal strain than proximal AT during the same tensile load before and after fatiguing exercise (Farris et al.,

2013a; Finni et al., 2003; Lichtwark et al., 2013a; Magnusson et al., 2003; Obst et al., 2015a). Furthermore, it has been demonstrated that the load-induced alterations in free AT longitudinal deformation is associated with the corresponding region-specific changes in tendon transverse morphology (i.e., tendon CSA), with the tendon mid portion undergoing greater transverse deformation and strain compared to the proximal and distal portions (Obst et al., 2015b; Obst et al., 2014b). Therefore, the longitudinal conditioning effects of whole AT reported in previous studies (Hawkins et al., 2009; Maganaris, 2003) may not represent the longitudinal conditioning of free AT and proximal AT and the corresponding regional transverse conditioning of free AT.

Chapter 3 examined the regional 3D deformation of human Achilles tendon during conditioning consisting of 10 successive 25-s submaximal (50%) voluntary isometric plantarflexion contractions. The longitudinal conditioning of whole AT was primarily driven from the creep response of the free AT and was accompanied by a corresponding reduction in free tendon CSA that was most pronounced within the tendon mid-portion. As free AT volume remained unaltered throughout conditioning, the alterations in tendon morphological deformation during conditioning were indicative of a change in only tendon matrix shape, likely due to the reorganization of the collagenous and non-collagenous tendon matrix components. The isolated creep response of the free AT observed in chapter 3 is supported by two previous studies reporting that the acute effects of fatiguing exercise such as, running and eccentric heel drop exercise (i.e., increase in tendon length and strain) are only confined to the free AT, with no changes evident at the level of proximal AT (Lichtwark et al., 2013a; Obst et al., 2015a). This observation could be due to the possible differences in fascicle/fibre orientation (Szaro et al., 2009), crimp angle (Magnusson et al.,

2002), fluid content (Grosse et al., 2015), and loading characteristics (Farris et al., 2013) between AT regions that likely underpin the microstructural alterations associated with conditioning within free AT (Houssen et al., 2011; Miller et al., 2012a). Further, the finding that free tendon mid portion underwent greater transverse strain relative to the proximal and distal portions supports previous studies demonstrating that alterations in tendon transverse morphology during load both before and after acute bout of exercise are localized to the free tendon mid-portion (Obst et al., 2015b; Obst et al., 2014b), indicating the unique structure and mechanical behavior of this region. Overall, the findings of chapter 3 highlight the vulnerable nature of the free AT mid-portion to the strain-related injuries (e.g., tendinopathy and rupture) when it is subjected to the repeated loads.

Chapter 4 examined the time course of recovery of 3D AT deformation from the conditioning effects reported in chapter 3 during a 50% MVIC of the plantarflexors immediately prior to conditioning, immediately following conditioning, and at 5 further time points following conditioning (15, 30, 60, 90, and 120 min). During the time course of recovery, the whole and free AT longitudinal strains and the free AT transverse strain remained at the steady state for 60 min and returned to pre-conditioned strain values after 2 h. These findings indicate that the recovery from conditioning effects was complete for the whole and free AT strain in both longitudinal and transverse dimensions. The full recovery of AT following conditioning observed in chapter 4 is consistent with previous *in vitro* studies demonstrating that the conditioning effects on tendon mechanical and morphological properties are non-damaging, transient, and recoverable (Fung, 2013; Lanir and Fung, 1974; McPherson et al., 1992; Nurmi et al., 2004; O'Brien et al., 1989; Pilia et al., 2015; Thorpe et al., 2014). However, the time required for the full recovery of AT

morphological deformation from conditioning effects reported in chapter 4 (2 h) is shorter than those reported by previous studies examining the free AT morphological changes following the application of an acute bout of fatiguing exercise (days) (Grigg et al., 2009; Grigg et al., 2012; Grosse et al., 2015; Rosengarten et al., 2014; Wearing et al., 2013). This discrepancy between the findings of chapter 4 and those of the previous studies may be explained by the fact that fatigue loading applied in previous studies may have induced microstructural damage to the tendon (Fung et al., 2010; Fung et al., 2009; Thorpe et al., 2014), leading to a long-term tendon recovery (Gardner et al., 2012; Lavagnino et al., 2014). This finding indicates that the confounding effects of free AT recovery following conditioning can be large and need to be considered in the design of experiments that assess AT mechanical properties.

7.2 Response of the pathological Achilles tendon to loading

Chapter 5 examined the effect of unilateral mid-portion Achilles tendinopathy (MAT) on free AT 3D morphology at rest and under a single tensile load. In the tendinopathic side, tendon CSA and AP diameter were larger than those of the contralateral and healthy tendons across all tendon regions at rest that were peaked in tendon mid-region, with no significant difference in tendon ML diameter found between the three tendons at any of the tendon regions. This finding supports previous studies that reported an increase in tendon thickness and area at a single site of tendon mid-portion in people with MAT (Alfredson et al., 2014; Docking and Cook, 2015; Grigg et al., 2012; Van Schie et al., 2010) and studies, which demonstrated a widespread development of tendinopathic symptoms throughout the entire length of the tendon (Choi et al., 2016; Jacobsen et al., 2015; Smith et al., 2008).

The finding that the increase in tendinopathic tendon CSA is mainly driven from increase in tendon AP diameter could be explained by the degenerative alterations in anterior and posterior surfaces of the paratenon sheath (Harris and Peduto, 2006; Kvist et al., 1988; Paavola et al., 2002), the mechanisms regulating tendon healing response following injury (Dyment et al., 2013; Yoshida et al., 2016), and pathological adaptation response of tendinopathic tendon for providing a greater safety margin (Shim et al., 2014). Under the same tensile load (50% MVIC), the tendinopathic tendon experienced greater longitudinal and transverse strains than control tendons and experienced a reduction in tendon CSA, AP diameter, and ML diameter along the entire tendon length, resulting in a tendon volume reduction. However, the contralateral and healthy tendons behaved iso-volumetrically and experienced a reduction in tendon CSA and ML diameter and an increase in tendon AP diameter. The finding that the tendinopathic tendon becomes thinner in AP direction and undergoes a volume reduction under load supports previous studies that demonstrated an immediate decrease in tendon thickness, water content, and volume following exercise (Fahlström and Alfredson, 2010; Grigg et al., 2012; Ho and Kulig, 2016b; Shalabi et al., 2004b; Wearing et al., 2015). Factors such as fluid movement from tendon core to peri-tendinous space resulting from release of water molecules from glycosaminoglycans (Gu et al., 1993; Lai et al., 1991), high positive fluid pressure in tendon core (Ahmadzadeh et al., 2015; Altiero, 1997), and the impairment of tendon membrane permeability (Chen et al., 1998; Prendergast et al., 1996) or/and vascular mechanisms (Åström and Westlin, 1994; Öhberg et al., 2001) could contribute to the load-induced reduction of the tendinopathic tendon.

Chapter 6 further examined the effect of unilateral MAT on AT 3D morphological deformation during 10 successive 25-s isometric plantarflexion contractions at 50% MVIC. The whole AT creep response was confined to the free AT in both the tendinopathic and contralateral sides, with no changes in proximal AT elongation and the corresponding strain in both sides observed. The magnitude of creep for the whole and free AT longitudinal strains and free AT CSA and volume strains in the tendinopathic side were greater than those of the contralateral side and reached steady state at higher strain values and following a greater number of contractions in the tendinopathic side. This finding is in agreement with previous studies that demonstrated a higher longitudinal strain at the whole and free AT levels in tendinopathic tendon relative to the healthy control tendons during load (Arya and Kulig, 2010; Child et al., 2010), and explains why the pathologic free tendon in individuals with MAT is at greater risk of further strain-induced injury (e.g., rupture) in response to repeated loads (Hess, 2009). Further, the tendinopathic tendon's whole and free AT longitudinal strains were not greater than those of the contralateral tendon until the tendinopathic tendon experienced a volume reduction of 25% (fourth contraction) during repeated loads. This observation may indicate that due to the gradual fluid exudation from tendon core from the first contraction, there may have been a transition in tendinopathic tendon load-bearing mechanism from a fluid-dominated phase to the solid one, exposing the solid phase to higher stress at the same level of force, resulting in higher longitudinal strain in tendinopathic tendon. Aside from making the tendinopathic tendon more vulnerable to further tendon injuries, these changes likely also alter the local mechanical environment within the tendinopathic tendon matrix, and are therefore likely to be a barrier to tendon repair.

7.3 General limitations and future directions

The limitations of each individual study that comprises this thesis have been discussed in detail within the relevant chapters. However, there are a number of general limitations that must be acknowledged when interpreting the main findings of this thesis and should be considered in future studies. First, only a small sample of male adults with heterogeneous duration, symptoms, and the injury location of unilateral MAT in Chapters 5 and 6 were included. The findings of this thesis, therefore, should not be generalized to different population groups, females, other Achilles tendon disorders (e.g., insertional Achilles tendinopathy), and other human tendons (e.g., patellar tendon). Further, while 3DUS is able to measure the tendon morphology along the entire tendon length at rest and under load, the accuracy of measurement, particularly for tendon length, depends on the scanning time and the number of 2D images acquired during scanning. This approach is also limited to evaluating tendon morphology under static loading conditions (Lichtwark et al., 2013a; Obst et al., 2014a). The restriction of 3DUS measurement to isometric contraction limits the findings to static strain measurement, where the static loading may itself contribute to tendon creep. Further, as the free AT scanning was completed before the proximal AT in Chapter 3, 4, and 6, the different time course of scanning time may have also affected the interpretation of our data. Therefore, the tendon loading condition under which the AT ultrasound scanning was performed in all the studies of this thesis (i.e. ~25s isometric plantarflexion contraction at 50% MVIC) were a compromise between allowing sufficient scan time to capture a sufficiently dense ultrasound image stack, and ensuring that participants were able to maintain the target contraction intensity over the scan period. The restriction of 3DUS measurement to isometric contraction limits the findings to static

strain measurement, where the static loading may itself contribute to tendon creep. Further, as the free AT scanning was completed before the proximal AT in Chapter 3, 4, and 6, the different time course of scanning time may have also affected the interpretation of our data. Future studies are warranted to examine the effects of different loading modes on 3D deformation of healthy and pathologic AT during a single load and repeated loads (as reported for static loading in Chapter 3, 5, and 6) and the 3D recovery of AT under load following repeated loads (as reported for static loading in Chapter 4). 3DUS is also limited by its inability to detect the thickness of tendon paratenon, epitenon, and peri-tendinous space, and thus all the tendon transverse morphology measurements (i.e., CSA) in this thesis were confined to the tendon core. Further study is required to determine these tendon parameters at rest and under load using imaging techniques such as MRI that have greater resolution than ultrasound in order to identify the fluid exudation mechanism from the tendon core into the peri-tendinous space under load.

From studies 5 and 6 it was clear that the response of the AT to loading is dramatically altered in tendinopathy. It therefore follows that the local mechanical environment of the tendon solid and fluid components within the AT are also different to healthy tendon. In future it will be necessary to better characterize this local mechanical environment through the use of multi-scale modelling techniques (Smith et al., 2013) that could be informed by the present findings. Studies in the field of tendon mechanobiology suggest that an optimal strain environment for positive tendon adaptation exists (Wang, 2006), with either higher or lower than optimal strains resulting in a catabolic effect. It therefore follows that targeted rehabilitation strategies, perhaps combining biological and exercise-based therapies, could be developed in the future to create an optimal environment for tendon

regeneration. This approach will require identifying the strain fields that best promote tendon recovery from future mechanobiology experiments, and then developing biofeedback mechanisms that ensure that the appropriate mechanical stimulus is provided in training.

7.4 General conclusions

The healthy AT experiences creep in response to repeated loads that occur primarily in the free AT mid-portion, and is recoverable within 2 h. In contrast to healthy tendon, which experiences a reduction in tendon CSA and ML diameter, and bulges along the AP diameter and behaves iso-volumetrically under load, tendinopathic tendon undergoes a reduction in tendon CSA, AP diameter, ML diameter, and volume. The likely mechanism of this volume reduction is fluid exudation from the tendon core to the peri-tendinous space or/and vascular mechanisms. During repeated loading, the loss of free AT volume in MAT preceded the greater longitudinal strain relative to the contralateral tendon. Overall these findings are indicative of substantial internal reorganization of tendinopathic tendon fascicles and fluid content under load which have likely implications for tendon injury risk and repair.

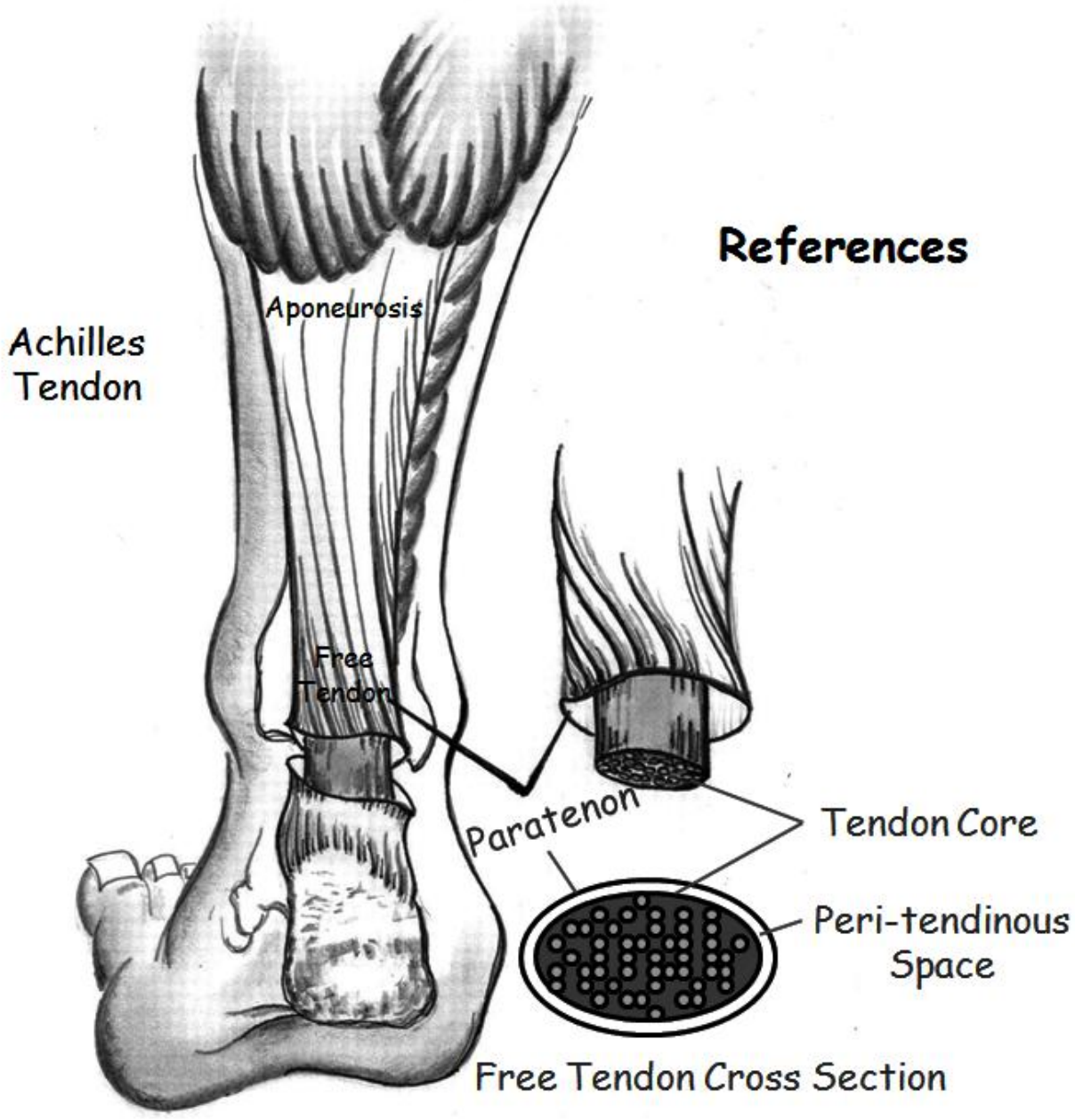
References
Aponeurosis
Achilles
Tendon
Free
Tendon
Paratenon
Tendon Core
Peri-tendinous
Space
Free Tendon Cross Section

References

Abate M, Silbernagel KG, Siljeholm C, Di Iorio A, De Amicis D, Salini V, Werner S, Paganelli R. (2009). Pathogenesis of tendinopathies: inflammation or degeneration? *Arthritis Res Ther* **11**, 235-238.

Ahmadzadeh H, Freedman BR, Connizzo BK, Soslowsky LJ, Shenoy VB. (2015). Micromechanical poroelastic finite element and shear-lag models of tendon predict large strain dependent Poisson's ratios and fluid expulsion under tensile loading. *Acta biomater* **22**, 83-91.

Aiyegbusi AI, Okafor UA, Leke OP. (2016). Prevalence of Achilles tendinopathy and its association with physical characteristics in recreational sport participants in Lagos, Nigeria. *J Clin Sci* **13**, 163-166.

Alfredson H, Spang C, Forsgren S. (2014). Unilateral surgical treatment for patients with midportion Achilles tendinopathy may result in bilateral recovery. *Br J Sports Med* **48**, 1421-1424.

Alfredson H, Pietilä T, Jonsson P, Lorentzon R. (1998). Heavy-load eccentric calf muscle training for the treatment of chronic Achilles tendinosis. *Am J Sports Med* **26**, 360-366.

Andersson G, Backman LJ, Scott A, Lorentzon R, Forsgren S, Danielson P. (2011a). Substance P accelerates hypercellularity and angiogenesis in tendon tissue and enhances paratendinitis in response to Achilles tendon overuse in a tendinopathy model. *Br J Sports Med* **45**, 1017-1022.

Andersson G, Forsgren S, Scott A, Gaida JE, Stjernfeldt JE, Lorentzon R, Alfredson, H, Backman C, Danielson P. (2011b). Tenocyte hypercellularity and vascular proliferation in a rabbit model of tendinopathy: contralateral effects suggest the involvement of central neuronal mechanisms. *Br J Sports Med* **45**, 399-406.

Andrew G, Jonathan S. (2014). Comparison of Achilles tendon loading between male and female recreational runners. *J Hum Kinet* **44**, 155-159.

Arampatzis A, Karamanidis K, Albracht K. (2007). Adaptational responses of the human Achilles tendon by modulation of the applied cyclic strain magnitude. *J Exp Biol* **210**, 2743- 2753.

Archambault JM, Elfervig-Wall MK, Tsuzaki M, Herzog W, Banes AJ. (2002). Rabbit tendon cells produce MMP-3 in response to fluid flow without significant calcium transients. *J Biomech* **35**, 303-309.

Arndt AN, Komi PV, Brüggemann GP, Lukkariniemi J. (1998). Individual muscle contributions to the in vivo Achilles tendon force. *Clin Biomech* **13**, 532-541.

Arnoczky SP, Tian T, Lavagnino M, Gardner K. (2004). Ex vivo static tensile loading inhibits MMP-1 expression in rat tail tendon cells through a cytoskeletally based mechanotransduction mechanism. *J Orthop Res* **22**, 328-333.

Arora A, Kothari A, Katti DS. (2015). Pore orientation mediated control of mechanical behavior of scaffolds and its application in cartilage-mimetic scaffold design. *J Mech Behav Biomed Mater* **51**, 169-183.

Arya S, Kulig K. (2010). Tendinopathy alters mechanical and material properties of the Achilles tendon. *J Appl Physiol* **108**, 670-675.

Asplund CA, Best TM. (2013). Achilles tendon disorders. *BMJ* **346**, f1262.

Åström M. (1998). Partial rupture in chronic Achilles tendinopathy: a retrospective analysis of 342 cases. *Acta Orthop Scand* **69**, 404-407.

Åström M. (1997). On the nature and etiology of chronic achilles tendinopathy: Lund University.

Åström M, Rausing A. (1995). Chronic Achilles tendinopathy: A survey of surgical and histopathologic findings. *Clin Orthop Relat Res* **316**, 151-164.

Åström M, Westlin N. (1994). Blood flow in chronic Achilles tendinopathy. *Clin Orthop Relat Res* **308**, 166-172.

Atkinson TS, Haut RC, Altiero NJ. (1997). A poroelastic model that predicts some phenomenological responses of ligaments and tendons. *J Biomech Eng* **119**, 400-405.

Azevedo LB, Lambert MI, Vaughan CL, O'Connor CM, Schwellnus MP. (2009). Biomechanical variables associated with Achilles tendinopathy in runners. *Br J Sports Med* **43**, 288-292.

Barber L, Barrett R, Lichtwark G. (2009). Validation of a freehand 3D ultrasound system for morphological measures of the medial gastrocnemius muscle. *J Biomech* **42**, 1313-1319.

Baur H, Müller S, Hirschmüller A, Cassel M, Weber J, Mayer F. (2011). Comparison in lower leg neuromuscular activity between runners with unilateral mid-portion Achilles tendinopathy and healthy individuals. *J Electromyogr Kinesiol* **21**, 499-505.

Benazzo F, Zanon G, Maffulli N. (2000). An Operative Approach to Achilles Tendinopathy. *Sports Med Arthrosc* **8**, 96-101.

Benjamin M, Kaiser E, Milz S. (2008). Structure-function relationships in tendons: a review. *J Anat* **212**, 211-228.

Blankstein A, Cohen I, Diamant L, Heim M, Dudkiewicz I, Israeli A, Ganel A, Chechick A. (2001). Achilles tendon pain and related pathologies: diagnosis by ultrasonography. *Isr Med Assoc J* **3**, 575-578.

Bojsen-Møller J, Magnusson SP. (2015). Heterogeneous Loading of the Human Achilles Tendon In Vivo. *Exerc Sport Sci Rev* **43**, 190-197.

Bojsen-Møller J, Hansen P, Aagaard P, Svantesson U, Kjaer M, Magnusson SP. (2004). Differential displacement of the human soleus and medial gastrocnemius aponeuroses during isometric plantar flexor contractions in vivo. *J Appl Physiol* **97**, 1908-1914.

Booth ML, Ainsworth BE, Pratt M, Ekelund U, Yngve A, Sallis JF, Oja P. (2003). International physical activity questionnaire: 12-country reliability and validity. *Med Sci Sports Exerc* **35**, 1381-1395.

Caliari SR, Ramirez MA, Harley BA. (2011). The development of collagen-GAG scaffold-membrane composites for tendon tissue engineering. *Biomaterials* **32**, 8990-8998.

Carew EO, Barber JE, Vesely I. (2000). Role of preconditioning and recovery time in repeated testing of aortic valve tissues: validation through quasilinear viscoelastic theory. *Ann Biomed Eng* **28**, 1093-1100.

Carlstedt CA, Nordin M. (1989). Biomechanics of tendons and ligaments. In: Nordin M, Frankel VH, editors. Basic biomechanics of the musculoskeletal system. 2nd ed. Philadelphia: Lea and Febiger, 59-74.

Carmont MR, Highland AM, Rochester JR, Paling EM, Davies MB. (2011). An anatomical and radiological study of the fascia cruris and paratenon of the Achilles tendon. *Foot Ankle Surg* **17**, 186-192

Cassel M, Baur H, Hirschmüller A, Carlsohn A, Fröhlich K, Mayer F. (2015). Prevalence of Achilles and patellar tendinopathy and their association to intratendinous changes in adolescent athletes. *Scand J Med Sci Sports* **25**, 310-318.

Cetti R, Junge J, Vyberg M. (2003). Spontaneous rupture of the Achilles tendon is preceded by widespread and bilateral tendon damage and ipsilateral inflammation: a clinical and histopathologic study of 60 patients. *Acta Orthop Scand* **74**, 78-84.

Chang YJ, Kulig K. (2015). The neuromechanical adaptations to Achilles tendinosis. *J Physiol* **593**, 3373-3387.

Cheng VW, Screen HR. (2007). The micro-structural strain response of tendon. *J Mater Sci* **42**, 8957-8965.

Chen CT, Malkus DS, Vanderby R Jr. (1998). A fiber matrix model for interstitial fluid flow and permeability in ligaments and tendons. *Biorheology* **35**, 103-118.

Child S, Bryant AL, Clark RA, Crossley KM. (2010). Mechanical properties of the Achilles tendon aponeurosis are altered in athletes with achilles tendinopathy. *Am J Sports Med* **38**, 1885-1893.

Chimenti RL, Bucklin M, Kelly M, Ketz J, Flemister AS, Richards MS, Buckley MR. (2016). Insertional Achilles tendinopathy associated with altered transverse compressive and axial tensile strain during ankle dorsiflexion. *J Orthop Res. doi:* 10.1002/jor.23338.

Choi RK, Smith MM, Martin JH, Clarke JL, Dart AJ, Little CB, Clarke EC. (2016). Chondroitin sulfate glycosaminoglycans contribute to widespread inferior biomechanics in tendon after focal injury. *J Biomech* **49**, 2694-2701.

Connizzo BK, Adams SM, Adams TH, Birk DE, Soslowsky LJ. (2016). Collagen V expression is crucial in regional development of the supraspinatus tendon. *J Orthop Res* **34**, 2154-2161.

Cook JL, Khan KM, Purdam C. (2002). Achilles tendinopathy. *Man Ther* **7**, 121-130.

Corps AN, Robinson AH, Movin T, Costa ML, Hazleman BL, Riley GP. (2006). Increased expression of aggrecan and biglycan mRNA in Achilles tendinopathy. *Rheumatology* **45**, 291-294.

Cousineau-Pelletier P, Langelier E. (2010). Relative contributions of mechanical degradation, enzymatic degradation, and repair of the extracellular matrix on the response of tendons when subjected to under-and over-mechanical stimulations in vitro. *J Orthop Res* **28**, 204-210.

Cronin NJ, Lichtwark G. (2013). The use of ultrasound to study muscle–tendon function in human posture and locomotion. *Gait posture* **37**, 305-312.

Cronin NJ, Af Klint R, Grey MJ, Sinkjaer T. (2011). Ultrasonography as a tool to study afferent feedback from the muscle–tendon complex during human walking. *J Electromyogr Kinesiol* **21**, 197-207.

Debenham JR, Travers MJ, Gibson W, Campbell A, Allison GT. (2016). Achilles tendinopathy alters stretch shortening cycle behaviour during a sub-maximal hopping task. *J Sci Med Sport* **19**, 69-73.

De Jonge S, Warnaars JL, De Vos RJ, Weir A, Van Schie HT, Bierma-Zeinstra SM, Verhaar JA, Tol JL. (2014). Relationship between neovascularization and clinical severity in Achilles tendinopathy in 556 paired measurements. *Scand J Med Sci Sports* **24**, 773-778.

De Jonge S, Van den Berg C, De Vos RJ, Van Der Heide HJ, Weir A, Verhaar JA, Bierma-Zeinstra SM, Tol JL. (2011). Incidence of midportion Achilles tendinopathy in the general population. *Br J Sports Med* **45**, 1026-1028.

De Mos M, Van El B, DeGroot J, Jahr H, Van Schie HT, Van Arkel ER, Tol H, Heijboer R, Van Osch GJ, Verhaar JA. (2007). Achilles tendinosis changes in biochemical composition and collagen turnover rate. *Am J Sports Med* **35**, 1549-1556.

Docking SI, Cook J. (2015). Pathological tendons maintain sufficient aligned fibrillar structure on ultrasound tissue characterization (UTC). *Scand J Med Sci Sports* **26**, 675-683.

Docking SI, Rosengarten SD, Daffy J, Cook J. (2015). Structural integrity is decreased in both Achilles tendons in people with unilateral Achilles tendinopathy. *J Sci Med Sport* **18**, 383-387.

Docking SI, Van Schie J, Daffy J, Rosengarten SD, Cook J. (2013). Bilateral changes in unilateral Achilles tendinopathy quantified using ultrasound tissue characterisation. *Br J Sports Med* **47**, e2.

Doral MN, Alam M, Bozkurt M, Turhan E, Atay OA, Dönmez G, Maffulli N. (2010). Functional anatomy of the Achilles tendon. *Knee Surg Sports Traumatol Arthrosc* **18**, 638-643.

Dourte LM, Pathmanathan L, Mienaltowski MJ, Jawad AF, Birk DE, Soslowsky LJ. (2013). Mechanical, compositional, and structural properties of the mouse patellar tendon with changes in biglycan gene expression. *J Orthop Res* **31**, 1430-1437.

Dyment NA, Liu CF, Kazemi N, Aschbacher-Smith LE, Kenter K, Breidenbach AP, Shearn JT, Wylie C, Rowe DW, Butler DL. (2013). The paratenon contributes to scleraxis-expressing cells during patellar tendon healing. *PloS one* **8**, e59944.

Edama M, Kubo M, Onishi H, Takabayashi T, Inai T, Yokoyama E, Hiroshi W, Satoshi N, Kageyama I. (2015). The twisted structure of the human Achilles tendon. *Scand J Med Sci Sports* **25**, 497-503.

El Hawary R, Stanish WD, Curwin SL. (1997). Rehabilitation of tendon injuries in sport. *Sports Med* **24**, 347-358.

El Khoury L, Ribbans WJ, Raleigh SM. (2016). MMP3 and TIMP2 gene variants as predisposing factors for Achilles tendon pathologies: Attempted replication study in a British case-control cohort. *Meta gene* **9**, 52-55.

Elias JJ, Kilambi S, Ciccone WJ. (2009). Tension level during preconditioning influences hamstring tendon graft properties. *Am J Sports Med* **37**, 334-338.

Elliott DM, Robinson PS, Gimbel JA, Sarver JJ, Abboud JA, Iozzo RV, Soslowsky LJ. (2003). Effect of altered matrix proteins on quasilinear viscoelastic properties in transgenic mouse tail tendons. *Ann Biomed Eng* **31**, 599-605.

Emerson C, Morrissey D, Perry M, Jalan R. (2010). Ultrasonographically detected changes in Achilles tendons and self reported symptoms in elite gymnasts compared with controls-An observational study. *Man Ther* **15**, 37-42.

Esposito F, Limonta E, Cè E. (2011). Passive stretching effects on electromechanical delay and time course of recovery in human skeletal muscle: new insights from an electromyographic and mechanomyographic combined approach. *Eur J Appl Physiol* **111**, 485-495.

Fahlström M, Alfredson H. (2010). Ultrasound and Doppler findings in the Achilles tendon among middle-aged recreational floor-ball players in direct relation to a match. *Br J Sports Med* **44**, 140-143.

Fahlström M, Lorentzon R, Alfredson H. (2002). Painful conditions in the Achilles tendon region: a common problem in middle-aged competitive badminton players. *Knee Surg Sports Traumatol Arthrosc* **10**, 57-60.

Fang F, Lake SP. (2016). Experimental evaluation of multiscale tendon mechanics. *J Orthop Res. doi:* 10.1002/jor.23488.

Farris DJ, Trewartha G, McGuigan MP, Lichtwark GA. (2013). Differential strain patterns of the human Achilles tendon determined in vivo with freehand three-dimensional ultrasound imaging. *J Exp Biol* **216**, 594-600.

Figueroa D, Calvo R, Vaisman A, Meleán P, Figueroa F. (2010). Effect of tendon tensioning: an in vitro study in porcine extensor tendons. *Knee* **17**, 245-248.

Finni T, Hodgson JA, Lai AM, Edgerton VR, Sinha S. (2003). Nonuniform strain of human soleus aponeurosis-tendon complex during submaximal voluntary contractions in vivo. *J Appl Physiol* **95**, 829-837.

Fornage BD. (1986). Achilles tendon: US examination. *Radiology* **159**, 759-764.

Franceschi F, Papalia R, Paciotti M, Franceschetti E, Di Martino A, Maffulli N, Denaro V. (2014). Obesity as a risk factor for tendinopathy: a systematic review. *Int J Endocrinol*. doi: 10.1155/2014/670262.

Franchi M, De Pasquale V, Martini D, Quaranta M, Macciocca M, Dionisi A, Ottani V. (2010). Contribution of glycosaminoglycans to the microstructural integrity of fibrillar and fiber crimps in tendons and ligaments. *Scientific World Journal* **10**, 1932-1940.

Franz JR, Slane LC, Rasske K, Thelen DG. (2015). Non-uniform in vivo deformations of the human Achilles tendon during walking. *Gait Posture* **41**, 192-197.

Fredberg U, Bolvig L, Andersen NT, Stengaard-Pedersen K. (2008). Ultrasonography in evaluation of Achilles and patella tendon thickness. *Ultraschall Med* **29**, 60-65.

Fredberg U, Stengaard-Pedersen K. (2008). Chronic tendinopathy tissue pathology, pain mechanisms, and etiology with a special focus on inflammation. *Scand J Med Sci Sports* **18**, 3-15.

Fujii M, Furumatsu T, Miyazawa S, Tanaka T, Inoue H, Kodama Y, Masuda K, Seno N, Ozaki T. (2016). Features of human autologous hamstring graft elongation after pre-tensioning in anterior cruciate ligament reconstruction. *Int Orthop* **40**, 2553-2558.

Fukashiro S, Komi PV, Järvinen M, Miyashita M. (1995). In vivo Achilles tendon loading during jumping in humans. *Eur J Appl Physiol Occup Physiol* **71**, 453-458.

Fukunaga T, Roy RR, Shellock FG, Hodgson JA, Day MK, Lee PL, Kwong-Fu H, Edgerton VR. (1992). Physiological cross-sectional area of human leg muscles based on magnetic resonance imaging. *J Orthop Res* **10**, 928-934.

Fung YC. (2013) Biomechanics: mechanical properties of living tissues: New York: Springer-Verlag.

Fung DT, Wang VM, Andarawis-Puri N, Basta-Pljakic J, Li Y, Laudier DM, Sun HB, Jepsen KJ, Schaffler MB, Flatow EL. (2010). Early response to tendon fatigue damage accumulation in a novel in vivo model. *J Biomech* **43**, 274-279.

Fung DT, Wang VM, Laudier DM, Shine JH, Basta-Pljakic J, Jepsen KJ, Schaffler MB, Flatow EL. (2009). Subrupture tendon fatigue damage. *J Orthop Res* **27**, 264-273.

Gaida JE, Ashe MC, Bass SL, Cook JL. (2009). Is adiposity an under-recognized risk factor for tendinopathy? A systematic review. *Arthritis Rheum* **61**, 840-849.

Gajhede-Knudsen M, Ekstrand J, Magnusson H, Maffulli N. (2013). Recurrence of Achilles tendon injuries in elite male football players is more common after early return to play: an 11-year follow-up of the UEFA Champions League injury study. *Br J Sports Med* **47**, 763-768.

Gärdin A, Movin T, Svensson L, Shalabi A. (2010). The long-term clinical and MRI results following eccentric calf muscle training in chronic Achilles tendinosis. *Skeletal Radiol* **39**, 435-442.

Gärdin A, Bruno J, Movin T, Kristoffersen-Wiberg M, Shalabi A. (2006). Magnetic resonance signal, rather than tendon volume, correlates to pain and functional impairment in chronic Achilles tendinopathy. *Acta Radiol* **47**, 718-724.

Gardner K, Lavagnino M, Egerbacher M, Arnoczky SP. (2012). Re-establishment of cytoskeletal tensional homeostasis in lax tendons occurs through an actin-mediated cellular contraction of the extracellular matrix. *J Orthop Res* **30**, 1695-1701.

Gatt R, Wood MV, Gatt A, Zarb F, Formosa C, Azzopardi KM, Casha A, Agius TP, Schembri-Wismayer P, Attard L. (2015). Negative Poisson's ratios in tendons: An unexpected mechanical response. *Acta Biomater* **24**, 201-208.

Giddings VL, Beaupre GS, Whalen RT, Carter DR. (2000). Calcaneal loading during walking and running. *Med Sci Sports Exerc* **32**, 627-634.

Graf BK, Vanderby R Jr, Ulm MJ, Rogalski RP, Thielke RJ. (1994). Effect of preconditioning on the viscoelastic response of primate patellar tendon. *Arthroscopy* **10**, 90-96.

Grigg NL, Wearing SC, Smeathers JE. (2012). Achilles tendinopathy has an aberrant strain response to eccentric exercise. *Med Sci Sports Exerc* **44**, 12-17.

Grigg NL, Stevenson NJ, Wearing SC, Smeathers JE. (2010). Incidental walking activity is sufficient to induce time-dependent conditioning of the Achilles tendon. *Gait Posture* **31**, 64-67.

Grigg NL, Wearing SC, Smeathers JE. (2009). Eccentric calf muscle exercise produces a greater acute reduction in Achilles tendon thickness than concentric exercise. *Br J Sports Med* **43**, 280-283.

Grosse U, Syha R, Gatidis S, Grözinger G, Martirosian P, Partovi S, Nikolaou K, Robbin MR, Schick F, Springer F. (2016). MR-based in vivo follow-up study of Achilles tendon volume and hydration state after ankle-loading activity. *Scand J Med Sci Sports* **26**, 1200-1208.

Gu WY, Lai WM, Mow VC. (1993). Transport of fluid and ions through a porous-permeable charged-hydrated tissue, and streaming potential data on normal bovine articular cartilage. *J Biomech* **26**, 709-723.

Gupta HS, Screen HR. (2017). Structural Building Blocks of Soft Tissues: Tendons and Heart Valves. In Material Parameter Identification and Inverse Problems in Soft Tissue Biomechanics, pp. 1-35: Springer.

Hägglund M, Waldén M, Ekstrand J. (2007). Lower reinjury rate with a coach-controlled rehabilitation program in amateur male soccer: a randomized controlled trial. *Am J Sports Med* **35**, 1433-1442.

Han S, Gemmell SJ, Helmer KG, Grigg P, Wellen JW, Hoffman AH, Sotak CH. (2000). Changes in ADC caused by tensile loading of rabbit Achilles tendon: evidence for water transport. *J Magn Reson* **144**, 217-227.

Hannafin JA, Arnoczky SP. (1994). Effect of cyclic and static tensile loading on water content and solute diffusion in canine flexor tendons: an in vitro study. *J Orthop Res* **12**, 350-356.

Harris CA, Peduto AJ. (2006). Achilles tendon imaging. *Australas Radiol* **50**, 513-525.

Hawkins D, Lum C, Gaydos D, Dunning R. (2009). Dynamic creep and pre-conditioning of the Achilles tendon in-vivo. *J Biomech* **42**, 2813-2817.

Helmer KG, Nair G, Cannella M, Grigg P. (2006). Water movement in tendon in response to a repeated static tensile load using one-dimensional magnetic resonance imaging. *J Biomech Eng* **128**, 733-741.

Helmer KG, Wellen J, Grigg P, Sotak CH. (2004). Measurement of the spatial redistribution of water in rabbit Achilles tendon in response to static tensile loading. *J Biomech Eng* **126**, 651-656.

Hermens HJ, Freriks B, Disselhorst-Klug C, Rau G. (2000). Development of recommendations for SEMG sensors and sensor placement procedures. *J Electromyogr Kinesiol* **10**, 361-374.

Hess GW. (2009). Achilles tendon rupture: a review of etiology, population, anatomy, risk factors, and injury prevention. *Foot Ankle Spec* **3**, 29-32.

Ho KY, Kulig K. (2016). Changes in water content in response to an acute bout of eccentric loading in a patellar tendon with a history of tendinopathy: A case report. *Physiother Theory Pract* **32**, 566-570.

Holzapfel GA, Ogden RW. (2006). Mechanics of biological tissue: Springer Science & Business Media.

Hopkins C, Fu SC, Chua E, Hu X, Rolf C, Mattila VM, Qin L, Yung PS, Chan KM. (2016). Critical review on the socio-economic impact of tendinopathy. *Sports Med Arthrosc Rehabil Ther Technol* **4**, 9-20.

Hosseini SM, Wilson W, Ito K, Van Donkelaar CC. (2014). How preconditioning affects the measurement of poro-viscoelastic mechanical properties in biological tissues. *Biomech Model Mechanobiol* **13**, 503-513.

Houssen YG, Gusachenko I, Schanne-Klein MC, Allain JM. (2011). Monitoring micrometer-scale collagen organization in rat-tail tendon upon mechanical strain using second harmonic microscopy. *J Biomech* **44**, 2047-2052.

Howard ME, Cawley PW, Losse GM, Johnston RB. (1996). Bone-patellar tendon-bone grafts for anterior cruciate ligament reconstruction: the effects of graft pretensioning. *Arthroscopy* **12**, 287-292.

Humphrey JD, Dufresne ER, Schwartz MA. (2014). Mechanotransduction and extracellular matrix homeostasis. *Nat Rev Mol Cell Biol* **15**, 802-812.

Iwanuma S, Akagi R, KuriharaT, Ikegawa S, Kanehisa H, Fukunaga T, Kawakami Y. (2011). Longitudinal and transverse deformation of human Achilles tendon induced by isometric plantar flexion at different intensities. *J Appl Physiol* **110**, 1615-1621.

Jacobsen E, Dart AJ, Mondori T, Horadogoda N, Jeffcott LB, Little CB, Smith MM. (2015). Focal Experimental Injury Leads to Widespread Gene Expression and Histologic Changes in Equine Flexor Tendons. *PloS one* **10**, e0122220.

Jaglowski JR, Williams BT, Turnbull TL, LaPrade RF, Wijdicks CA. (2016). High-load preconditioning of soft tissue grafts: an in vitro biomechanical bovine tendon model. *Knee Surg Sports Traumatol Arthrosc* **24**, 895-902.

Järvinen TA, Kannus P, Maffulli N, Khan KM. (2005). Achilles tendon disorders: etiology and epidemiology. *Foot Ankle Clin* **10**, 255-266.

Jhingan S, Perry M, O'Driscoll G, Lewin C, Teatino R, Malliaras P, Maffulli N, Morrissey D. (2011). Thicker Achilles tendons are a risk factor to develop Achilles tendinopathy in elite professional soccer players. *Muscles Ligaments Tendons J* **29**, 51-56.

Józsa LG, Kannus P. (1997). Human tendons: anatomy, physiology, and pathology. Champaign, IL: Human Kinetics Publishers.

Kader D, Saxena A, Movin T, Maffulli N. (2002). Achilles tendinopathy: some aspects of basic science and clinical management. *Br J Sports Med* **36**, 239-249.

Kannus P. (2000). Structure of the tendon connective tissue. *Scand J Med Sci Sports* **10**, 312-320.

Ker RF, Alexander RM, Bennett MB. (1988). Why are mammalian tendons so thick? *J Zool* **216**, 309-324.

Khan KM, Cook JL, Bonar F, Harcourt P, Åstrom M. (1999). Histopathology of common tendinopathies. *Sports Med* **27**, 393-408.

Kleiner DM. (1998). Human Tendons: Anatomy, Physiology and Pathology. *J Athl Train* **33**, 185-186.

Komi PV, Fukashiro S, Järvinen M. (1992). Biomechanical loading of Achilles tendon during normal locomotion. *Clin Sports Med* **11**, 521-531.

Kubo K, Kanehisa H, Fukunaga T. (2003). Gender differences in the viscoelastic properties of tendon structures. *Eur J Appl Physiol* **88**, 520-526.

Kubo K, Kanehisa H, Kawakami Y, Fukunaga T. (2001). Influences of repetitive muscle contractions with different modes on tendon elasticity in vivo. *J Appl Physiol* **91**, 277-282.

Kulig K, Chang YJ, Winiarski S, Bashford GR. (2016). Ultrasound-Based Tendon Micromorphology Predicts Mechanical Characteristics of Degenerated Tendons. *Ultrasound Med Biol* **42**, 664-673.

Kvist MH, Lehto MU, Jozsa L, Järvinen M, Kvist HT. (1988). Chronic Achilles paratenonitis An immunohistologic study of fibronectin and fibrinogen. *Am J Sports Med* **16**, 616-623.

Kvist M. (1994). Achilles tendon injuries in athletes. *Sports medicine* **18**, 173-201.

Kvist M. (1991). Achilles tendon injuries in athletes. *Ann Chir Gynaecol* **80,** 188-201.

Lai WM, Hou JS, Mow VC. (1991). A triphasic theory for the swelling and deformation behaviors of articular cartilage. *J Biomech Eng* **113**, 245-258.

Lanir Y, Fung YC. (1974). Two-dimensional mechanical properties of rabbit skin. II. Experimental results. *J Biomech* **7**, 171-182.

Lavagnino M, Wall ME, Little D, Banes AJ, Guilak F, Arnoczky SP. (2015). Tendon mechanobiology: Current knowledge and future research opportunities. *J Orthop Res* **33**, 813-822.

Lavagnino M, Bedi A, Walsh CP, Enselman ER, Sheibani-Rad S, Arnoczky SP. (2014). Tendon Contraction After Cyclic Elongation Is an Age-Dependent PhenomenonL: In Vitro and In Vivo Comparisons. *Am J Sports Med* **42**, 1471-1477.

Lavagnino M, Arnoczky SP, Kepich E, Caballero O, Haut RC. (2008). A finite element model predicts the mechanotransduction response of tendon cells to cyclic tensile loading. *Biomech Model Mechanobiol* **7**, 405-416.

Lersch C, Grötsch A, Segesser B, Koebke J, Brüggemann GP, Potthast W. (2012). Influence of calcaneus angle and muscle forces on strain distribution in the human Achilles tendon. *Clin Biomech* **27**, 955-961.

Leung JL, Griffith JF. (2008). Sonography of chronic Achilles tendinopathy: a case-control study. *J Clin Ultrasound* **36**, 27-32.

Lichtwark GA, Cresswell AG, Newsham-West RJ. (2013). Effects of running on human Achilles tendon length–tension properties in the free and gastrocnemius components. *J Exp Biol* **216**, 4388-4394.

Lichtwark GA, Wilson AM. (2007). Is Achilles tendon compliance optimised for maximum muscle efficiency during locomotion? *J Biomech* **40**, 1768-1775.

Lichtwark GA, Bougoulias K, Wilson AM. (2007). Muscle fascicle and series elastic element length changes along the length of the human gastrocnemius during walking and running. *J Biomech* **40**, 157-164.

Lichtwark GA, Wilson AM. (2006). Interactions between the human gastrocnemius muscle and the Achilles tendon during incline, level and decline locomotion. *J Exp Biol* **209**, 4379-4388.

Lichtwark GA, Wilson AM. (2005). In vivo mechanical properties of the human Achilles tendon during one-legged hopping. *J Exp Biol* **208**, 4715-4725.

Lind B, Öhberg L, Alfredson H. (2006). Sclerosing polidocanol injections in mid-portion Achilles tendinosis: remaining good clinical results and decreased tendon thickness at 2-year follow-up. *Knee Surg Sports Traumatol Arthrosc* **14**, 1327-1332.

Longo UG, Ronga M, Maffulli N. (2009). Achilles tendinopathy. *Sports Med Arthrosc* **17**, 112-126.

Lopes AD, Hespanhol JL, Yeung SS, Costa LO. (2012). What are the main running-related musculoskeletal injuries? *Sports Med* **42**, 891-905.

Lorimer AV, Hume PA. (2014). Achilles tendon injury risk factors associated with running. *Sports Med* **44**, 1459-1472.

Maeda E, Hagiwara Y, Wang JH, Ohashi T. (2013). A new experimental system for simultaneous application of cyclic tensile strain and fluid shear stress to tenocytes in vitro. *Biomed Microdevices* **15**, 1067-1075.

Maffulli N, Khan KM, Puddu G. (1998). Overuse tendon conditions: time to change a confusing terminology. *Arthroscopy* **14**, 840-843.

Maffulli N, Ewen SW, Waterston SW, Reaper J, Barrass V. (2000). Tenocytes from ruptured and tendinopathic Achilles tendons produce greater quantities of type III collagen than tenocytes from normal Achilles tendons. An in vitro model of human tendon healing. *Am J Sports Med* **28**, 499-505.

Maffulli N, Kenward MG, Testa V, Capasso G, Regine R, King JB. (2003). Clinical diagnosis of Achilles tendinopathy with tendinosis. *Clin J Sport Med* **13**, 11-15.

Maffulli N, Sharma P, Luscombe KL. (2004). Achilles tendinopathy: aetiology and management. *J R Soc Med* **97**, 472-476.

Maganaris CN, Narici MV, Maffulli N. (2008). Biomechanics of the Achilles tendon. *Disabil Rehabil* **30**, 1542-1547.

Maganaris CN, Narici MV, Almekinders LC, Maffulli N. (2004). Biomechanics and pathophysiology of overuse tendon injuries. *Sports Med* **34**, 1005-1017.

Maganaris CN. (2003). Tendon conditioning: artefact or property? *Proc Biol Sci* **270**, 39-42.

Magnusson SP, Hansen P, Aagaard P, Brønd J, Dyhre-Poulsen P, Bojsen-Moller J, Kjaer M. (2003). Differential strain patterns of the human gastrocnemius aponeurosis and free tendon in vivo. *Acta Physiol Scand* **177**, 185-195.

Magnusson SP, Kjaer M. (2003). Region-specific differences in Achilles tendon cross-sectional area in runners and non-runners. *Eur J Appl Physiol* **90**, 549-553.

Magnusson SP, Qvortrup K, Larsen JO, Rosager S, Hanson P, Aagaard P, Krogsgaard M, Kjaer M. (2002). Collagen fibril size and crimp morphology in ruptured and intact Achilles tendons. *Matrix Biol* **21**, 369-377.

McAuliffe S, McCreesh K, Culloty F, Purtill H, O'sullivan K. (2016). Can ultrasound imaging predict the development of Achilles and patellar tendinopathy? A systematic review and meta-analysis. *Br J Sports Med **50***, 1516-1523.

McPherson R, King G, Shrive N. (1992). Extension rate alters load relaxation in the rabbit MCL. In *38th Annual Meeting, Orthopaedic Research Society*, February 17–20.

Mercier L, Langø T, Lindseth F, Collins LD. (2005). A review of calibration techniques for freehand 3D ultrasound systems. *Ultrasound Med Biol* **31**, 143-165.

Miller KS, Connizzo BK, Feeney E, Soslowsky LJ. (2012a). Characterizing local collagen fiber re-alignment and crimp behavior throughout mechanical testing in a mature mouse supraspinatus tendon model. *J Biomech* **45**, 2061-2065.

Miller KS, Edelstein L, Connizzo BK, Soslowsky LJ. (2012b). Effect of preconditioning and stress relaxation on local collagen fiber re-alignment: Inhomogeneous properties of rat supraspinatus tendon. *J Biomech Eng* **134**, 031007.

Morales-Orcajo E, De Bengoa Vallejo RB, Iglesias ML, Bayod J. (2016). Structural and material properties of human foot tendons. *Clin Biomech* **37**, 1-6.

Movin T, Kristoffersen-Wiberg M, Rolf C, Aspelin P. (1998a). MR imaging in chronic Achilles tendon disorder. *Acta Radio* **39**, 126-132.

Movin T, Kristoffersen-Wiberg M, Shalabi A, Gad A, Aspelin P, Rolf C. (1998b). Intratendinous alterations as imaged by ultrasound and contrast medium-enhanced magnetic resonance in chronic achillodynia. *Foot Ankle Int* **19**, 311-317.

Movin T, Gad A, Reinholt FP, Rolf C. (1997). Tendon pathology in long-standing Achillodynia: Biopsy findings in 40 patients. *Acta Orthop Scand* **68**, 170-175.

Munteanu SE, Barton CJ. (2011). Lower limb biomechanics during running in individuals with Achilles tendinopathy: a systematic review. *J Foot Ankle Res* **4**, 1146-1155.

Muraoka T, Muramatsu T, Fukunaga T, Kanehisa H. (2005). Geometric and elastic properties of in vivo human Achilles tendon in young adults. *Cells Tissues Organs* **178**, 197-203.

Nell EM, Van der Merwe L, Cook J, Handley CJ, Collins M, September AV. (2012). The apoptosis pathway and the genetic predisposition to Achilles tendinopathy. *J Orthop Res* **30**, 1719-1724.

Nielsen RO, Buist I, Srensen H, Lind M, Rasmussen S. (2012). Training errors and running related injuries: a systematic review. *Int J Sports Phys Ther* **7**, 58-75.

Nigg BM. (2001). The role of impact forces and foot pronation: a new paradigm. *Clin J Sport Med* **11**, 2-9.

Nourissat G, Berenbaum F, Duprez D. (2015). Tendon injury: from biology to tendon repair. *Nat Rev Rheumatol* **11**, 223-233.

Nuri L, Obst SJ, Newsham-West R, Barrett RS. (2016). Regional three-dimensional deformation of human Achilles tendon during conditioning. *Scand J Med Sci Sports.* doi: 10.1111/sms.12742.

Nurmi JT, Kannus P, Sievänen H, Järvelä T, Järvinen M, Järvinen TL. (2004). Interference Screw Fixation of Soft Tissue Grafts in Anterior Cruciate Ligament Reconstruction: Part 2 Effect of Preconditioning on Graft Tension During and After Screw Insertion. *Am J Sports Med* **32**, 418-424.

Obst SJ, Newsham-West R, Barrett RS. (2016). Changes in Achilles tendon mechanical properties following eccentric heel drop exercise are specific to the free tendon. *Scand J Med Sci Sports **26***, 421-431.

Obst SJ, Newsham-West R, Barrett RS. (2015). Three-dimensional morphology and strain of the human Achilles free tendon immediately following eccentric heel drop exercise. *J Exp Biol* **218**, 3894-3900.

Obst SJ, Newsham-West R, Barrett RS. (2014a). In vivo measurement of human Achilles tendon morphology using freehand 3-D ultrasound. *Ultrasound Med Biol* **40**, 62-70.

Obst SJ, Renault JB, Newsham-West R, Barrett RS. (2014b). Three-dimensional deformation and transverse rotation of the human free Achilles tendon in vivo during isometric plantarflexion contraction. *J Appl Physiol* **116**, 376-384.

Obst SJ, Barrett RS, Newsham-West R. (2013). Immediate effect of exercise on Achilles tendon properties: systematic review. *Med Sci Sports Exerc* **45**, 1534-1544.

O'Brien WR, Friederich NF, Muller W. (1989). The effects of stress relaxation on initial graft loads during anterior cruciate ligament reconstruction. *Orthop Trans* **13**, 316-317.

Öhberg L, Lorentzon R, Alfredson H. (2001). Neovascularisation in Achilles tendons with painful tendinosis but not in normal tendons: an ultrasonographic investigation. *Knee Surg Sports Traumatol Arthrosc* **9**, 233-238.

O'Neill S, Watson PJ, Barry S. (2015). Why are eccentric exercises effective for Achilles tendinopathy? *Int J Sports Phys Ther* **10**, 552-562.

O'Reilly MA, Massouh H. (1993). Pictorial review: the sonographic diagnosis of pathology in the Achilles tendon. *Clin Radiol* **48**, 202-206.

Ostlere S. (2003). Imaging the ankle and foot. *Imaging* **15**, 242-269.

Paavola M, Kannus P, Järvinen TA, Khan K, Józsa L, Järvinen M. (2002). Achilles tendinopathy. *J Bone Joint Surg Am* **84**, 2062-2076.

Paavola M, Kannus P, Paakkala T, Pasanen M, Järvinen M. (2000). Long-term prognosis of patients with Achilles tendinopathy. An observational 8-year follow-up study. *Am J Sports Med* **28**, 634-642.

Pang X, Wu JP, Allison GT, Xu J, Rubenson J, Zheng MH, Lloyd DG, Gardiner B, Wang A, Kirk TB. (2016). The three dimensional microstructural network of elastin, collagen and cells in Achilles tendons. *J Orthop Res.* doi: 10.1002/jor.23240.

Pearce CJ, Ismail M, Calder JD. (2009). Is apoptosis the cause of noninsertional Achilles tendinopathy? *Am J Sports Med* **37**, 2440-2444.

Peltonen J, Cronin NJ, Stenroth L, Finni T, Avela J. (2012). Achilles tendon stiffness is unchanged one hour after a marathon. *J Exp Biol* **215**, 3665-3671.

Piedade SR, Dal Fabbro IM, Mischan MM. (2006). Cyclic-loading of the Human Gracilis and Semitendinosus Muscle Tendons: Study of Young Adult Cadavers. *Artif Organs* **30**, 680-685.

Pierre-Jerome C, Moncayo V, Terk MR. (2010). MRI of the Achilles tendon: a comprehensive review of the anatomy, biomechanics, and imaging of overuse tendinopathies. *Acta Radiol* **51**, 438-454.

Pilia M, Murray M, Guda T, Heckman M, Appleford M. (2015). Pretensioning of soft tissue grafts in anterior cruciate ligament reconstruction. *Orthopedics* **38**, 582-587.

Pingel J, Lu Y, Starborg T, Fredberg U, Langberg H, Nedergaard A, Weis M, Eyre D, Kjaer M, Kadler KE. (2014). 3-D ultrastructure and collagen composition of healthy and overloaded human tendon: evidence of tenocyte and matrix buckling. *J Anat* **224**, 548-555.

Pollock CM, Shadwick RE. (1994). Relationship between body mass and biomechanical properties of limb tendons in adult mammals. *Am J Physiol* **266**, 1016-1021.

Prager RW, Rohling RN, Gee AH, Berman L. (1998). Rapid calibration for 3-D freehand ultrasound. *Ultrasound Med Biol* **24**, 855-869.

Prendergast PJ, Van Driel WD, Kuiper JH. (1996). A comparison of finite element codes for the solution of biphasic poroelastic problems. *Proc Inst Mech Eng H* **210**, 131-136.

Puxkandl R, Zizak I, Paris O, Keckes J, Tesch W, Bernstorff S, Purslow P, Fratzl P (2002). Viscoelastic properties of collagen: synchrotron radiation investigations and structural model. *Philos Trans R Soc Lond B Biol Sci* **357**, 191-197.

Quinn KP, Winkelstein BA. (2011). Preconditioning is correlated with altered collagen fiber alignment in ligament. *J Biomech Eng* **133**, 064506.

Reeves ND, Cooper G. (2017). Is human Achilles tendond deformation greater in regions where cross-sectional area is samller? *J Exp Biol* **220**, 1634-1642.

Reeves ND, Cooper G. (2014). Human Tendon Deformation: Is It Greatest At Regions Of Smallest Cross-sectional Area? *Br J Sport Med* **48**, 56-57.

Reeves ND, Maganaris CN, Ferretti G, Narici MV. (2005). Influence of 90-day simulated microgravity on human tendon mechanical properties and the effect of resistive countermeasures. *J Appl Physiol* **98**, 2278-2286.

Reyes AM, Jahr H, Van Schie HT, Weinans H, Zadpoor AA. (2014). Prediction of the elastic strain limit of tendons. *J Mech Behav Biomed Mater* **30**, 324-338.

Rio E, Kidgell D, Purdam C, Gaida J, Moseley GL, Pearce AJ, Cook J. (2015). Isometric exercise induces analgesia and reduces inhibition in patellar tendinopathy. *Br J Sports Med* **49**, 1277-1283.

Robinson JM, Cook JM, Purdam C, Visentini PJ, Ross J, Maffulli N, Taunton JE, Khan KM. (2001). The VISA-A questionnaire: a valid and reliable index of the clinical severity of Achilles tendinopathy. *Br J Sports Med* **35**, 335-341.

Rosengarten SD, Cook JL, Bryant AL, Cordy JT, Daffy J, Docking SI. (2015). Australian football players' Achilles tendons respond to game loads within 2 days: an ultrasound tissue characterisation (UTC) study. *Br J Sports Med* **49**, 183-187.

Ryan CN, Sorushanova A, Lomas AJ, Mullen AM, Pandit A, Zeugolis DI. (2015). Glycosaminoglycans in tendon physiology, pathophysiology, and therapy. *Bioconjug Chem* **26**, 1237-1251.

Ryan M, Wong A, Taunton J. (2010). Favorable outcomes after sonographically guided intratendinous injection of hyperosmolar dextrose for chronic insertional and midportion achilles tendinosis. *Am J Roentgenol* **194**, 1047-1053.

Santos ML, Rodrigues MT, Domingues RM, Reis RL, Gomes ME. (2017). Biomaterials as Tendon and Ligament Substitutes: Current Developments. *Reg Strat Knee Disable* **21**, 349-371.

Sasaki N, Odajima S. (1996). Stress-strain curve and Young's modulus of a collagen molecule as determined by the X-ray diffraction technique. *J Biomech* **29**, 655-658.

Schatzmann L, Brunner P, Stäubli HU. (1998). Effect of cyclic preconditioning on the tensile properties of human quadriceps tendons and patellar ligaments. *Knee Surg Sports Traumatol Arthrosc* **6**, 56-61.

Scott JE. (2001). Structure and function in extracellular matrices depend on interactions between anionic glycosaminoglycans. *Pathol Biol* **49**, 284-289.

Screen HR. (2008). Investigating load relaxation mechanics in tendon. *J Mech Behav Biomed Mater* **1**, 51-58.

Screen HR, Bader DL, Lee DA, Shelton JC. (2004). Local strain measurement within tendon. *Strain* **40**, 157-163.

Seebacher JR, Inglis AE, Marshall JL, Warren RF. (1982). The structure of the posterolateral aspect of the knee. *J Bone Joint Surg Am* **64**, 536-541.

Sellon JL, Wempe MK, Smith J. (2014). Sonographically guided distal biceps tendon injections: Techniques and validation. *J Ultrasound Med* **33**, 1461-1474.

September A, Rahim M, Collins M. (2016). Towards an understanding of the genetics of tendinopathy. *Adv Exp Med Biol* **920**, 109-116.

Seynnes OR, Bojsen-Møller J, Albracht K, Arndt A, Cronin NJ, Finni T, Magnusson SP. (2015). Ultrasound-based testing of tendon mechanical properties: a critical evaluation. *J Appl Physiol* **118**, 133-141.

Shalabi A, Movin T, Kristoffersen-Wiberg M, Aspelin P, Svensson L. (2005). Reliability in the assessment of tendon volume and intratendinous signal of the Achilles tendon on MRI: a methodological description. *Knee Surg Sports Traumatol Arthrosc* **13**, 492-498.

Shalabi A, Kristoffersen-Wiberg M, Aspelin P, Movin T. (2004a). Immediate Achilles tendon response after strength training evaluated by MRI. *Med Sci Sports Exerc* **36**, 1841-1846.

Shalabi A, Kristoffersen-Wilberg M, Svensson L, Aspelin P, Movin T. (2004b). Eccentric training of the gastrocnemius-soleus complex in chronic Achilles tendinopathy results in decreased tendon volume and intratendinous signal as evaluated by MRI. *Am J Sports Med* **32**, 1286-1296.

Shim VB, Fernandez JW, Gamage PB, Regnery C, Smith DW, Gardiner BS, Lloyd DG, Besier TF. (2014). Subject-specific finite element analysis to characterize the

influence of geometry and material properties in Achilles tendon rupture. *J Biomech* **47**, 3598-3604.

Skirven TM, Osterman AL, Fedorczy KJ, Amadio PC. (2011). Rehabilitation of the hand and upper extremity, 2-volume set: expert consult: Sixth Edition, United States: Elsevier Health Sciences. PP. 439-555.

Slane LC, DeWall R, Martin J, Lee K, Thelen DG. (2015). Middle-aged adults exhibit altered spatial variations in Achilles tendon wave speed. *Physiol Meas* **36**, 1485-1496.

Slane LC, Thelen DG. (2014). Non-uniform displacements within the Achilles tendon observed during passive and eccentric loading. *J Biomech* **47**, 2831-2835.

Smith DW, Rubenson J, Lloyd D, Zheng M, Fernandez J, Besier T, Xu J, Gardiner BS. (2013). A conceptual framework for computational models of Achilles tendon homeostasis. *Wiley Interdiscip Rev Syst Biol Med* **5**, 523-538.

Smith MM, Sakurai G, Smith SM, Young AA, Melrose J, Stewart CM, Appleyard RC, Peterson JL, Gillies RM, Dart AJ. (2008). Modulation of aggrecan and ADAMTS expression in ovine tendinopathy induced by altered strain. *Arthritis Rheum* **58**, 1055-1066.

Sopakayang R. (2013). A new viscoelastic model for preconditioning in ligaments and tendons. *Proc Cong Eng* **3**, 3-5.

Stecco A, Busoni F, Stecco C, Mattioli-Belmonte M, Soldani P, Condino S, Ermolao A, Zaccaria M, Gesi M. (2015). Comparative ultrasonographic evaluation of the

Achilles paratenon in symptomatic and asymptomatic subjects: an imaging study. *Surg Radiol Anat* **37**, 281-285.

Stecco C, Cappellari A, Macchi V, Porzionato A, Morra A, Berizzi A, De Caro R. (2014). The paratendineous tissues: an anatomical study of their role in the pathogenesis of tendinopathy. *Surg Radiol Anat* **36**, 561-572.

Stenroth L, Peltonen J, Cronin NJ, Sipilä S, Finni T. (2012). Age-related differences in Achilles tendon properties and triceps surae muscle architecture in vivo. *J Appl Physiol* **113**, 1537-1544.

Stephens PR, Nunamaker DM, Butterweck DM. (1989). Application of a Hall-effect transducer for measurement of tendon strains in horses. *Am J Vet Res* **50**, 1089-1095.

Sverdlik A, Lanir Y. (2002). Time-dependent mechanical behavior of sheep digital tendons, including the effects of preconditioning. *J Biomech Eng* **124**, 78-84.

Syha R, Springer F, Grözinger G, Würslin C, Ipach I, Ketelsen D, Schabel C, Gebhard H, Hein T, Martirosian P. (2014). Short-term exercise-induced changes in hydration state of healthy Achilles tendons can be visualized by effects of off-resonant radiofrequency saturation in a three-dimensional ultrashort echo time MRI sequence applied at 3 tesla. *J Magn Reson Imaging* **40**, 1400-1407.

Szaro P, Witkowski G, Smigielski R, Krajewski P, Ciszek B. (2009). Fascicles of the adult human Achilles tendon-an anatomical study. *Ann Anat* **191**, 586-593.

Teramoto A, Luo ZP. (2008). Temporary tendon strengthening by preconditioning. *Clin Biomech* **23,** 619-622.

Thorpe CT, Riley GP, Birch HL, Clegg PD, Screen HR. (2016). Fascicles and the interfascicular matrix show adaptation for fatigue resistance in energy storing tendons. *Acta Biomater* **42**, 308-315.

Thorpe CT, Godinho MS, Riley GP, Birch HL, Clegg PD, Screen HR. (2015a). The interfascicular matrix enables fascicle sliding and recovery in tendon, and behaves more elastically in energy storing tendons. *J Mech Behav Biomed Mater* **52**, 85-94.

Thorpe CT, Chaudhry S, Lei II, Varone A, Riley GP, Birch HL, Clegg PD, Screen HR. (2015b). Tendon overload results in alterations in cell shape and increased markers of inflammation and matrix degradation. *Scand J Med Sci sports* **25**, 381-391.

Thorpe CT, Riley GP, Birch HL, Clegg PD, Screen HR. (2014). Effect of fatigue loading on structure and functional behaviour of fascicles from energy-storing tendons. *Acta Biomater* **10**, 3217-3224.

Thorpe CT, Birch HL, Clegg PD, Screen HR. (2013a). The role of the non-collagenous matrix in tendon function. *Int J Exp Pathol* **94**, 248-259.

Thorpe CT, Klemt C, Riley GP, Birch HL, Clegg PD, Screen HR. (2013b). Helical sub-structures in energy-storing tendons provide a possible mechanism for efficient energy storage and return. *Acta Biomater* **9**, 7948-7956.

Treece GM, Gee AH, Prager RW, Cash CJ, Berman LH. (2003). High-definition freehand 3-D ultrasound. *Ultrasound Med Biol* **29**, 529-546.

Treece GM, Prager RW, Gee AH, Berman L. (2000). Surface interpolation from sparse cross sections using region correspondence. *IEEE Trans Med Imaging* **19**, 1106-1114.

Treece GM, Prager RW, Gee AH, Berman L. (1999). Fast surface and volume estimation from non-parallel cross-sections, for freehand three-dimensional ultrasound. *Med Image Anal* **3**, 141-173.

Van Der Voet A. (1997). A comparison of finite element codes for the solution of biphasic poroelastic problems. *Proc Inst Mech Eng H* **211**, 209-211.

Van Dijk CN, Van Sterkenburg MN, Wiegerinck JI, Karlsson J, Maffulli N. (2011). Terminology for Achilles tendon related disorders. *Knee Surg Sports Traumatol Arthrosc* **19**, 835-841.

Van Gils CC, Steed RH, Page JC. (1996). Torsion of the human Achilles tendon. *J Foot Ankle Surg* **35**, 41-48.

Van Schie HT, De Vos RJ, De Jonge S, Bakker EM, Heijboer MP, Verhaar JA, Tol JL, Weinans H. (2010). Ultrasonographic tissue characterisation of human Achilles tendons: quantification of tendon structure through a novel non-invasive approach. *Br J Sports Med* **44**, 1153-1159.

Van Snellenberg W, Wiley JP, Brunet G. (2007). Achilles tendon pain intensity and level of neovascularization in athletes as determined by color Doppler ultrasound. *Scand J Med Sci Sports* **17**, 530-534.

Van Sterkenburg MN, Van Dijk CN. (2011). Mid-portion Achilles tendinopathy: why painful? An evidence-based philosophy. *Knee Surg Sports Traumatol Arthrosc* **19**, 1367-1375.

Vergari C, Pourcelot P, Holden L, Ravary-Plumioën B, Gerard G, Laugier P, Mitton D, Crevier-Denoix N. (2011). True stress and Poisson's ratio of tendons during loading. *J Biomech* **44**, 719-724.

Wang YN, Galiotis C, Bader D. (2000). Determination of molecular changes in soft tissues under strain using laser Raman microscopy. *J Biomech* **33**, 483-486.

Wang HK, Lin KH, Su SC, Shih TT, Huang YC. (2012). Effects of tendon viscoelasticity in Achilles tendinosis on explosive performance and clinical severity in athletes. *Scand J Med Sci Sports* **22**, 147-155.

Wang JH. (2006). Mechanobiology of tendon. *J Biomech* **39**, 1563-1582.

Wang JH, Iosifidis MI, Fu FH. (2006). Biomechanical basis for tendinopathy. *Clin Orthop Relat Res* **443**, 320-332.

Wang XT, Ker RF. (1995). Creep rupture of wallaby tail tendons. *J Exp Biol* **198**, 831-845.

Watanabe Y, Moriya H, Takahashi K, Yamagata M, Sonoda M, Shimada Y, Tamaki T. (1993). Functional anatomy of the posterolateral structures of the knee. *Arthroscopy* **9**, 57-62.

Wearing SC, Locke S, Smeathers JE, Hooper SL. (2015). Tendinopathy alters cumulative transverse strain in the patellar tendon postexercise. *Med Sci Sports Exerc* **47**, 264-271.

Wearing SC, Smeathers JE, Hooper SL, Locke S, Purdam C, Cook JL. (2014). The time course of in vivo recovery of transverse strain in high-stress tendons following exercise. *Br J Sports Med* **48**, 383-387.

Wellen J, Helmer KG, Grigg P, Sotak CH. (2005). Spatial characterization of T1 and T2 relaxation times and the water apparent diffusion coefficient in rabbit Achilles tendon subjected to tensile loading. *Magn Reson Med* **53**, 535-544.

Wellen J, Helmer KG, Grigg P, Sotak CH. (2004). Application of porous-media theory to the investigation of water ADC changes in rabbit Achilles tendon caused by tensile loading. *J Magn Reson* **170**, 49-55.

White JW. (1943). Torsion of the Achilles tendon: its surgical significance. *Arch Surg* **46**, 784-787.

Williams IF, McCullagh KG, Goodship AE, Silver IA. (1984). Studies on the pathogenesis of equine tendonitis following collagenase injury. *Res Vet Sci* **36**, 326-338.

Wilmink J, Wilson AM, Goodship AE. (1992). Functional significance of the morphology and micromechanics of collagen fibres in relation to partial rupture of the superficial digital flexor tendon in racehorses. *Res Vet Sci* **53**, 354-359.

Woo SL, Gomez MA, Woo YK, Akeson WH. (1982). Mechanical properties of tendons and ligaments. II. The relationships of immobilization and exercise on tissue remodeling. *Biorheology* **19**, 397-408.

Wren TA, Yerby SA, Beaupré GS, Carter DR. (2001). Mechanical properties of the human Achilles tendon. *Clin Biomech* **16**, 245-251.

Wyndow N, Cowan SM, Wrigley TV, Crossley KM. (2013). Triceps surae activation is altered in male runners with Achilles tendinopathy. *J Electromyogr Kinesiol* **23**, 166-172.

Yang X, Coleman DP, Pugh ND, Nokes LD. (2012). The volume of the neovascularity and its clinical implications in Achilles tendinopathy. *Ultrasound Med Biol* **38**, 1887-1895

Yoon JH, Halper J. (2005). Tendon proteoglycans: biochemistry and function. *J Musculoskelet Neuronal Interact* **5**, 22-34.

Yoshida R, Alaee F, Dyrna F, Kronenberg MS, Maye P, Kalajzic I, Rowe DW, Mazzocca AD, Dyment NA. (2016). Murine supraspinatus tendon injury model to identify the cellular origins of rotator cuff healing. *Connect Tissue Res* **57**, 507-515.

Young SR, Gardiner B, Mehdizadeh A, Rubenson J, Umberger B, Smith DW. (2016). Adaptive remodeling of Achilles tendon: A Multi-scale computational model. *PLoS Comput Biol* **12**, e1005106.

Zajac FE. (1989). Muscle and tendon: properties, models, scaling and application to biomechanics and motor. *Crit Rev Biomed Eng* **17**, 359-411.